Adaptive Pre-Distortion for Laser Diodes with Direct Modulation Frequencies up to 1 GHz

A Thesis

Submitted to the College of Graduate Studies and Research

in Partial Fulfillment of the Requirements

for the Degree of

Master of Science

in the Department of Electrical Engineering

University of Saskatchewan

by

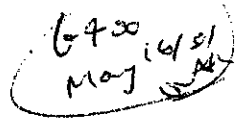

Russell G. Gutwin

Saskatoon, Saskatchewan

April 2001

Permission To Use

In presenting this thesis in partial fulfillment of the requirements for a Postgraduate degree from the University of Saskatchewan, the author has agreed that the Libraries of this University may make it freely available for inspection. The author further has agreed that permission for copying of this thesis in any manner, in whole or in part, for scholarly purposes may be granted by the professor who supervised this thesis work or, in his absence, by the Head of the Department or the Dean of the College in which this thesis work was done. It is understood that any copying or publication or use of this thesis or parts thereof for financial gain shall not be allowed without the author's written permission. It is also understood that due recognition shall be given to the author and to the University of Saskatchewan in any scholarly use which may be made of any material in this thesis.

Request for permission to copy or to make other use of material in this thesis in whole or part should be addressed to:

Head of the Department of Electrical Engineering
University of Saskatchewan
57 Campus Drive
Saskatoon, Saskatchewan, Canada
S7N 5A9

Abstract

The never ending demand for more information access presents a continuous challenge for most communication service providers. Although optical technologies have already played a significant role in providing for system growth and increased capabilities, the deployment of optical hardware is often dependent on electro-optic device limitations. One important challenge faced is in the provision of fiber–to–the–home (FTTH) services, which might include integrated cable television, telephone and internet access, without neglect for additional future broadband service possibilities. With hope to minimize changes to equipment, data formats, component availability and cost, an acceptable evolutionary answer involves improving the linearity of signal generating light sources.

Residential customers will gradually seek improvements to the broadband services that are presently offered by low-cost, analogue cable television. Unfortunately, device fabrication techniques that minimize the non-linear characteristics of a light source can increase per–unit costs and prohibit optical technologies from application in general distribution systems. It is, therefore, desirable to explore linearization techniques that work with inexpensive intensity–modulated laser systems so that any FTTH service can be economically delivered.

In this thesis, a previously developed model for a semiconductor laser has been simulated using a SPICE–based software tool. Also, for the purpose of achieving acceptable linear performance at frequencies up to 1 GHz, a third-order Volterra predistortion circuit has been added to the laser module studied. Manual optimization of the pre-distorter coefficients has reduced the optical 2nd and 3rd harmonic distortion between 600 and 1000 MHz to less than -69 dBc, an improvement from laser–only levels of -42 dBc. These results are especially meaningful in high channel-count common antenna television (CATV) systems where a single–channel optical modulation index of 4 % is required.

By extending the study of the linearized laser, a self–adaptive technique was developed that can appropriately adjust the pre-distorter to laser changes caused by temperature variation and aging. This adaptive scheme introduced a second, identical Volterra distortion circuit that was driven by a portion of the laser output and compared with the initial pre-distorter. Differences between distortion system signals in the two Volterra circuits were used to alter the pairs of coefficient settings and adapt the distortion compensation to the need. In this way, the enhanced electro-optic system has become capable of maintaining low distortion performances during circumstances where small changes to laser parameters can be expected. Also, the adaptive design holds promise for reducing certain network service costs, as well as simplifying the means to manufacture a linear light source component.

Acknowledgements

During my period of work on this project, I have experienced much support and assistance from the staff and affiliates of Telecommunications Research Laboratories. In addition to their research funding, I have appreciated their ongoing effort to provide professional development opportunities and a very people–friendly environment. I have especially appreciated the support, freedom, guidance and insight that David Dodds has provided me with as my research supervisor. The research and educational environment afforded me by the University of Saskatchewan and TRLabs has served me well, and for that I am very grateful.

Dedication

This thesis is dedicated to

Susan, Gail, Tom

and the loving memory of Glenn.

Thank you for your encouragement, support, love and prayers.

Table Of Contents

List of Tables

List of Figures

List of Abbreviations

AM-VSB	amplitude modulated vestigial sideband
BER	bit–error rate
CATV	common antenna television (cable TV)
CNR	carrier–to–noise ratio
CSO	composite second-order
CTB	composite triple beat
CW	continuous wave
DBR	distributed Bragg reflector
DFB	distributed feedback
DH	double–heterojunction
EHP	electron—hole pair
FDM	frequency–division multiplexing
FFT	fast–Fourier transform
FM	frequency modulated
FP	Fabry–Perot
FSK	frequency–shift keyed
FTTC	fiber–to–the–curb
FTTH	fiber–to–the–home
GRINSCH	graded index separate confinement heterostructure
HD	harmonic distortion
HD_2	second harmonic distortion
HD_3	third harmonic distortion

HRC	harmonically related carriers
ICC	incremental coherent carriers
IM	intensity modulated
IMD	intermodulation distortion
IMP	intermodulation products
IRC	incremental related carriers
ISI	inter–symbol interference
LED	light emitting diode
LD	laser diode
L-I	light—current
MQW	multiquantum well
MZ	Mach–Zehnder
OMI	optical modulation index
PSK	phase–shift keyed
QW	quantum well
RF	radio–frequency
RIN	relative intensity noise
rms	root–mean–square
R-O	relaxation–oscillation
SCM	sub-carrier multiplexing
SNR	signal–to–noise ratio
SPICE	simulation program with integrated circuit emphasis
TOC	trial–of–concept
TV	television
VCSEL	vertical-cavity surface-emitting laser
wrt	with respect to

List of Symbols

α	a per–unit–length optical loss or absorption for a LD cavity
β	the fraction of spontaneously emitted photons that are in-phase with lasing emissions
ϵ	a power gain compression factor for a LD cavity
$\eta_{ext}, \eta_i, \eta_{st}$	quantum efficiencies, external to a device, internal to a material and stimulated emission recombinations
λ, λ_{max}	wavelengths, arbitrary and maximum
ν_{min}	a material–specific minimum frequency for a photon
ρ	a substitution variable for simplifying an expression
σ	an optical modulation index or OMI value
τ_p, τ_s	lifetimes, for photons and for electrons producing spontaneous emissions
$\tau, \tau_1, \tau_2, \tau_u$	variables of time
υ	a substitution variable for simplifying an expression
φ	a substitution variable for simplifying an expression
$\omega, \omega_1, \omega_2, \omega_3, \omega_n$	signal frequencies in angular form
Γ	an optical confinement factor for a LD cavity
Ψ_1, Ψ_2, Ψ_3	first, second and third branch weighting factors for an adaptive distortion system
$a, \ldots h, k, \ldots n$	the distortion system coefficients
c	the speed of light (2.998E8 metres/second)
c_{d1}, c_{d2}, c_{d3}	the TOC distortion coefficients

c_0, c_1, c_2, c_3, c_4	Maclaurin series coefficients
d_c	the LD cavity depth or thickness (transverse dimension)
f_r	the relaxation–oscillation frequency for a LD
f, f_1, f_2, f_3	signal frequencies
g, g_o, g_{th}	the per–unit–length optical power gains or multipliers, at operating, unsaturated 'static' and threshold conditions
h	Planck's constant (6.626E-34 joule-seconds)
$h(t), h_a(t), h_b(t), h_c(t)$	impulse responses for linear systems
$h_1(t_1), h_n(t_1, \ldots t_n),$ $h_u(\tau_1, \ldots \tau_u)$	first-, n^{th}- and u^{th}-order impulse responses, or Volterra kernels, for an arbitrary non-linear system
$i, i(t), i_{distorted}$	time–varying signal currents, arbitrary and distorted
i_{pk}	the peak magnitude of an electrical (current) signal
k	Boltzmann's constant (1.381E-23 joules/kelvin)
m_{ch}	an OMI for one channel within a SCM system
n	a positive integer denoting system order
n	the ideality factor for the diode equation
q	electric charge (1.602E-19 coulombs)
s, s_1, s_2, s_3	Laplace transform parameters
$s, s(t)$	time–varying photon densities or optical signals
s_{pk}	the peak magnitude of an optical signal
t, t_1, t_n	variables of time
u	an arbitrary positive integer
$v(t)$	an arbitrary time–varying signal
$x, x(t), x_{V1}(t), \ldots$	input signals for an arbitrary system, or at a subscripted node
$y, y(t), y_{V13}(t), \ldots$	output signals for an arbitrary system, or at a subscripted node
$A, \ldots H, J, \ldots M, P$	substitution variables for simplifying expressions
A, A_1, A_2, A_3, A_4	magnitudes of sinusoidal components in a signal

$\boldsymbol{D_1}[\cdot], \boldsymbol{D_2}[\cdot], \boldsymbol{D_3}[\cdot]$	first-, second- and third-order distortion system operators
$D_1(j\omega_1), D_2(j\omega_1, j\omega_2),$ $D_3(j\omega_1, j\omega_2, j\omega_3)$	first-, second- and third-order Volterra transfer functions for the distortion systems
$D_{2'}(), D_{3'}()$	altered Laplace transforms of the second- and third-order non-linear transfer functions
$D_{A1}(j\omega_1),$ $D_{A2}(j\omega_1, j\omega_2),$ $D_{A3}(j\omega_1, j\omega_2, j\omega_3)$	adaptive first-, second- and third-order Volterra transfer functions for the distortion system
E$\pm u$	symbol representing $\times 10^{\pm u}$, as in 4.321E-5 = 0.00004321
E_c, E_f, E_g, E_v	conduction–band, Fermi, bandgap and valence–band quantum energies
$\boldsymbol{H_1}[\cdot], \boldsymbol{H_2}[\cdot], \boldsymbol{H_3}[\cdot],$ $\boldsymbol{H_u}[\cdot]$	first-, second-, third- and u^{th}-order arbitrary Laplace system operators
$H_a(), H_b(), H_c()$	linear system transfer functions for systems a, b and c
$H_1, H_2, H_3,$ $H_n(j\omega_1, \cdots j\omega_n)$	first-, second-, third- and n^{th}-order non-linear transfer functions for an arbitrary system
$I, I(t)$	total LD (drive) currents
I_b	a LD bias current (not time–varying)
I_{th}	a threshold current for a device
$J, J(t)$	device current densities
J_o	the current density at unsaturated 'static' conditions
J_{sat}	the reverse saturation current density for a device
J_{th}	the threshold current density for a device
L_c	the LD cavity length (longitudinal dimension)
M_s	the modulation sensitivity for a device
N	the density of conduction-band electrons in a cavity
N_{ch}	the number of channels within a SCM system

N_o	the density of conduction-band electrons in a cavity at threshold conditions (or initial transparency)
P_b	a LD optical bias power (not time–varying)
$P_o, P_o(t)$	arbitrary and time–varying optical output powers
R_1, R_2	the longitudinal 'end-face' reflectivities for a cavity
$S, S(t)$	total LD photon densities
S_b	a LD bias photon density (not time–varying)
T	an absolute temperature
V_c	the LD cavity volume
$V(t)$	a time–varying voltage
W_c	the cavity width (lateral dimension)
X, Y, Z	arbitrary, fixed–value coefficients

Chapter 1

Introduction

1.1 Optical Network Background

During recent decades, the access to information through networked terminal equipment has grown enormously. As a result, network designers have recommended that transmission and distribution systems use fiber optic technologies in order to meet high bandwidth expectations, and allow for further growth. Because these networks presently use electrical devices within their terminal and switching equipment, the optical transmission of information involves an opto-electronic transmitter and receiver at the ends of each transmission or distribution network segment. Typical systems use glass fibers for optical waveguides, photo diodes for receivers and laser diodes for transmitters.

Because an optical fiber has the potential to convey many high bandwidth channels within its spatially confined and low loss core, optical network technologies have encouraged the ongoing development of lower cost broadband information services. However, the effective exploitation of the benefits afforded by using optical waveguides must also involve consideration of photo detectors, light sources, and other necessary sub-system components.

Since the quantity of network segments increases significantly as a distribution network branches out toward its end–user applications (see Figure 1.1), a growing network size means an increase in the quantity of opto-electronic components used. Often the components used at each branch point are active and perhaps intelligent.

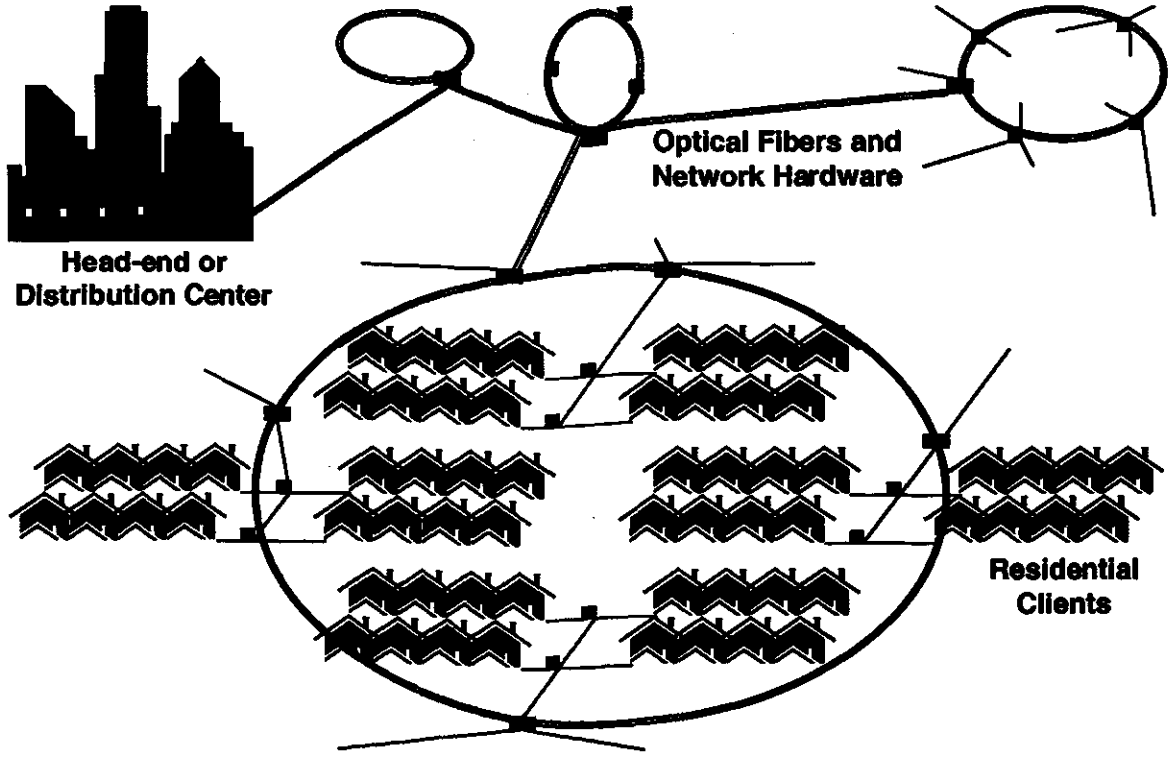

Figure 1.1: Representative Distribution Network

This implies that many branch points include sub-systems to detect, direct and regenerate the appropriate information signal back and forth along each adjoining network segment. Since the branched information content may be unique to a client or client group, each network drop must have a unique light source and detector if two–way communication and interactive services are desired.

As the commercial economics of a broadband optical network gradually permit it to expand outward from the 'head–end' of a distribution system, toward the primary consumers of the information, a greater quantity of inexpensive opto-electronic components will be required. In the future it may become necessary, if not very desirable, for each network client to have a broadband optical link into their home and office. This future network structure and its service features would require at least one laser diode (LD) per client, along with the other associated and necessary system components. Today some new homes are being constructed with built-in fiber networks, emphasizing the anticipation of expanding optical systems even within the

client's own domain. Because the deployment of the broadband lasers used in network trunks today would make future network services and growth unaffordable, light source alternatives must be found.

1.2 Fiber Optic Transmission Systems

Optical systems can handle information in either of the two basic forms: analogue or digital. The information simply uses an electromagnetic carrier in the optical spectrum, instead of a carrier having radio or microwave frequencies; the analogue or digital signal modulates an optical carrier before travelling, or propagating, through the waveguide.

As in other transmission technologies, noise and distortion may degrade the performance of an optical system. These factors present a unique challenge when an optical link uses an inexpensive LD at relatively high modulation frequencies. This difficulty stems from the lack of good linearity during the conversion of the electrical signal within the light source. The frequency dependent distortion will often limit transmission system bandwidth. There are some methods for control and minimization, but they may involve the use of an alternate and prohibitively expensive laser, or a more complex system design.

Digital systems use binary or multi–level symbol sequences to convey information. The performance of a digital channel depends on it conveying a timely representation of the original information, without exceeding a specific probability of error. Unfortunately, the inherent non-linearity of a LD operating at the frequencies required to achieve high bit–rates causes distortion to the optical signal. A distorted signal changes the shape and/or phase of the data symbol, creating inter–symbol interference (ISI) and errors at the decision gate of the receiver. This results in an increase to the bit–error rate (BER) for the channel, and may be a limiting factor for the information services the system can support.

A significant amount of networked information originates or exists in analogue form, and most terminal equipment is analogue in nature. As a result, optical transmission systems that use analogue modulation techniques have the potential to per-

mit end–users to avoid the replacement of their present devices. However, due to the affordability and benefits of digital technologies, the exchange of predominantly analogue information is rapidly changing throughout the world. Therefore, transmission systems that economically allow some flexibility in handling a migration from analogue to digital formats have become preferred assets to network operators. Broadband optical systems can provide this.

Although they are more bandwidth–efficient, analogue systems require the received signal waveform to represent the one transmitted much more accurately than the comparable data sequence in a digital system. Changes to a transmitted optical intensity/power, electric field, frequency, or phase must be proportional, or analogous, to corresponding input signal variations. Analogue transmission system performance is measured by determining the amount of noise and interference that is added to the signal waveform. Therefore, collectively, the transmitter, waveguide and receiver must deliver a linear response.

Within the bounds of their technologies, electrical and microwave systems have succeeded in handling analogue information. However, much of the potential in optical systems remains un-tapped. Most notably, the modulation of inexpensive LDs using analogue signals is presently restricted to low–frequency bands because the device non-linearities significantly degrade their optical performance at high frequencies. Most analogue systems face this problem when a bandwidth greater than 600 MHz is required.

Analogue systems often use a sub-carrier multiplexing (SCM) scheme so that many channels of information — amplitude, frequency and/or phase modulated — can simultaneously be transmitted without inflicting noticeable interference on each other. Sub-carrier multiplexing is simply frequency–division multiplexing (FDM) of many sub-channels of information prior to modulation of the system transmitter.

A simple SCM system, like that shown in Figure 1.2, could use a common antenna television (CATV) signal to directly modulate an optical carrier. In such a system, the radio–frequency (RF) carrier of each television signal is then referred to as a sub-carrier. Since the output signal from the laser includes quite a few modulated

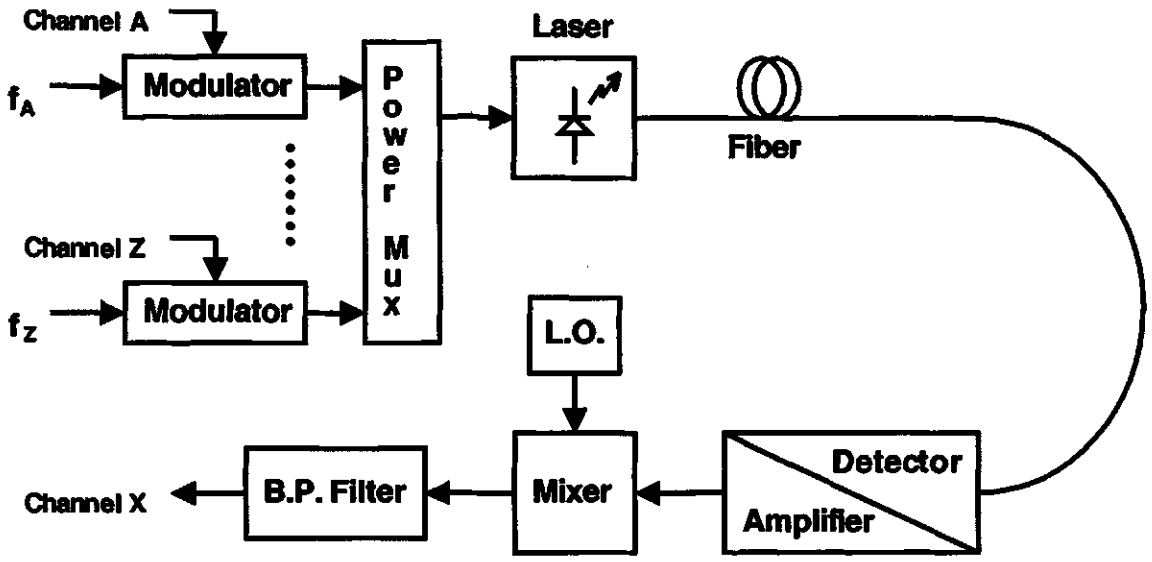

Figure 1.2: Example of a Sub-carrier Multiplexed Transmission System

sub-carriers, combined using FDM, the result is a broadband, complex, time–varying waveform. The LD non-linearity, which has a frequency dependent element, unfortunately contributes significant signal distortion when the complex waveform has 'high–frequency' contents. In addition to the frequency factor that causes optical signal distortion, an increase in the number of channels carried by the system increases the peak–to–rms ratio of the modulating signal. This means that the number of channels will also affect the distortion from the LD.

Because the distortion effects from one channel may fall inside the bandwidth of several other channels, the greater the number of channels carried by the optical SCM system, the greater the problem with inter–channel interference. The greater the non-linearity of the LD modulation characteristic, the more prominent the interference, and the lower the signal–to–noise ratio (SNR) for each multiplexed channel. This problem can be avoided by either using modulation systems that are nearly linear over a broader bandwidth or by limiting the channel count. The degree of linearity required will depend on the number of channels (or sub-carrier frequencies) provided by the system, as well as the tolerance of each channel to noise and interference.

In an effort to improve the spectral efficiency of an optical transmission system beyond that of an analogue SCM scheme, hybrid systems have drawn some exploratory attention. For the sake of spectral efficiency, a hybrid system may have its modulating signal configured as shown in Figure 1.3. The placement of a high frequency digital channel above an already maximized SCM frequency plan can figuratively appear to provide the most information throughput. However, this goal to exploit optical bandwidth is not an easy one to achieve. Published work dealing with hybrid optical systems highlight that a number of trade–offs must be carefully considered [2],[3]; the system designer must trade the quality of the analogue channels for the quality of the digital channel [3].

In order to minimize the occurrence of clipped information within the SCM component of the hybrid system, the modulation index of each channel must decrease if the number of channels is increased. Since resource use improves when more sub-carriers are added, each modulation index is reduced to permit greater spectral efficiency — often to the point where a broadband analogue channel risks falling below its required SNR. An SCM scheme alone will tolerate, and be designed to permit, some occasional clipping when channel signals peak during the same instant, provided that the frequency of this occurrence does not produce excessive noise for any one chan-

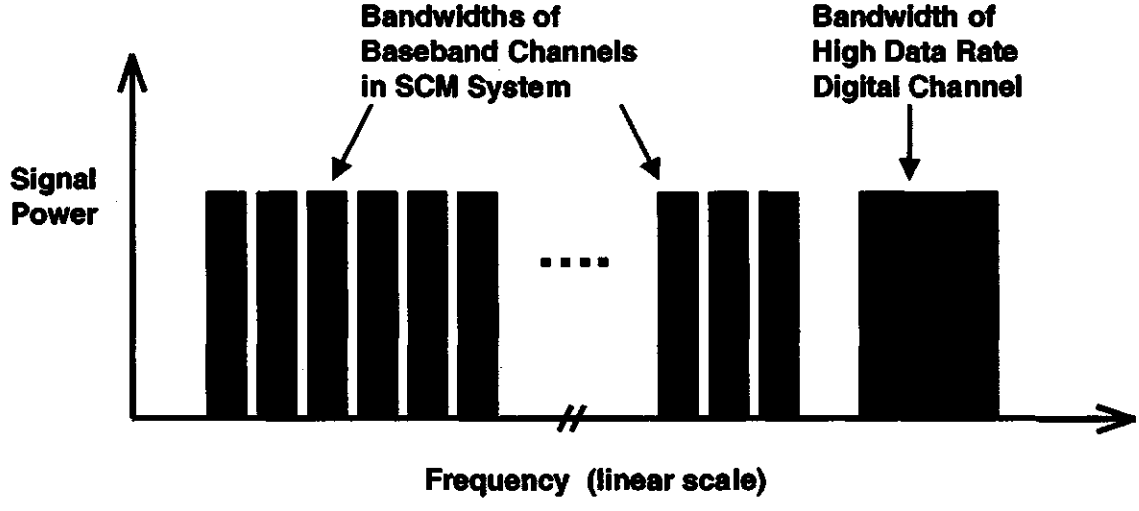

Figure 1.3: Frequency Plan for a Digital/SCM Hybrid Modulation Signal

nel. In a hybrid arrangement, the occurrence of any clipping of the composite signal causes bursts of errors in the digital channel, presenting a limit to the digital channel capacity.

A digital channel depends on its symbols being detectable above the noise level. The lower its modulation index, the greater the impact of noise and the higher the BER. If the high data rate digital channel were to compensate for the noise by having a slower symbol rate, the analogue channels would become cramped in frequency and fewer in number. A slower symbol rate reduces the efficiency of the hybrid system because the SCM channel scheme prefers the more linear lower frequencies. In addition, more distortion products from a slower digital channel could contribute to greater interference among the analogue channels. This added interference and distortion would suggest an increase in the common modulation index to maintain the required analogue channel SNRs, but consequently would lead to more clipping, error bursts and a further decrease in digital channel capacity.

Aside from data formats and modulation plans, an optimally designed optical transmission system will also require the thorough consideration of dispersion. Dispersion is a bandwidth limiting distortion effect that occurs inside the optical waveguide [4, pp.88-95]. It may be reduced by decreasing the length of travel within the fiber, by using expensive narrow line–width lasers, or by using spectral wavelengths near or at the zero–dispersion transmission wavelength.

Due to the nature of most distribution networks, the main trunk segments that are long enough to face dispersion limitations can afford the high costs of hand–picked, 'high–end' light sources. Because the transmission service provided by such a trunk segment is shared among very many downstream clients, its high cost may also be distributed and justifiable. Among network segments where distances are often relatively short, dispersion effects are far less significant. This realm of application permits LD line–width requirements to be less restrictive and less costly.

1.3 Application Dependent Requirements and Constraints

Future fiber optic systems may permit as much as 30 Terahertz (30,000 GHz) of information bandwidth per fiber. This means that many data applications would share the same transmission/distribution system. When combined with the facts that data volumes and network sizes are rapidly increasing, it is no surprise that system requirements are becoming more complex. The data may experience several re-ordering, re-formatting, re-directing and/or translation operations. Therefore, considerable work has been done by system planners, who have often identified that the lack of linearity in small, affordable light sources is a major obstacle restricting the general commercialization of high value broadband services [5, pp.3–8],[6].

Compared with other optical transmission system technologies, the direct intensity modulation of a LD using a CATV signal is conceptually simple and not difficult to construct. It is for this reason that the deployment and study of directly modulated SCM systems has been attractive to a variety of service providers, not only those handling television (TV) images. However, there are some known difficulties. Study has shown that a high channel–count optical CATV system is among the most demanding applications when it comes to achieving the overall system signal requirements [6].

The CATV industry has accepted the analysis of Darcie and Bodeep [1] and requires the optical system performance levels shown in Table 1.1. Their work considered the standard amplitude modulated vestigial sideband (AM-VSB) format used for TV. The performance levels they determined were found to be necessary in order to substitute a directly modulated optical system for one based on a coaxial cable design. These optical performance requirements should avoid degrading the signal fidelity that CATV viewers experience and expect.

Table 1.1: System Requirements for Optical CATV Signals, According to [1]

Transmission Segment	No. of Channels	CNR (dB)	CSO (dBc)	CTB (dBc)
Trunk	40 – 80	$\geq$ 55	$\leq$ -55	$\leq$ -65
Subscriber Loop (FTTC)	20 – 40	$\geq$ 48	$\leq$ -50	$\leq$ -55

North American CATV requirements, and other similar SCM systems, specify a signal–to–noise measure in terms of the carrier power for each channel, and refer to it as the carrier–to–noise ratio (CNR) [1],[7]. Carrier–to–noise ratio measurement practices, straightforward and easy to perform during service calls, address quantitatively the signal resolution and strength. It is an accepted system performance measure because the relationship between the SNR and the CNR has been determined from the knowledge of system regulatory requirements. The CSO and CTB measures respectively address practical second- and third-order distortion concerns [7, pp.157–162], and will be described in a later chapter.

In optical systems where interference from noise and distortion present a major challenge for signal recovery, an analogue frequency modulated (FM) format could also be applied. An SCM channel having an FM format is much less sensitive to system non-linearities and noise than an analogue amplitude modulated channel, but it would use approximately 30 MHz per video channel — five times more bandwidth than the standard television (TV) allocation. If the AM-VSB/FM conversion equipment and additional transmission bandwidth can be afforded, FM video signals could significantly relax the CNR requirements for a CATV system to as little as 16.5 dB [8].

In a similar way, an SCM system may also contain baseband channels having digitally modulated information. However, a frequency– or phase–shift keyed (FSK or PSK) digital video channel requires a bandwidth allocation capable of 100 Mb/s (432 Mb/s for high definition TV) [5, p.23]. These bit rates, even when reduced by compression techniques, demand much more bandwidth than a comparable channel using AM-VSB. It is for this reason, plus the added costs of conversion to an analogue signal prior to the viewers' TV, that presently make an AM-VSB SCM scheme most attractive for the optical delivery of video services.

Because competitive systems require low-cost, long-life technologies, it is also possible that the versatility of a broadband optical SCM system provides an advantage in the preparation for change. If, and when, a sub-carrier of a different format is desired, additions to, or replacement of, TV channels in a standard CATV system could be accomplished without the alteration to any optical infrastructure. In this way, future

network services will not have their costs constrained by possibly expensive hardware up-grades.

The primary key to efficiently and affordably distributing large amounts of information in an optical network is the linear performance of the operating components. Given this performance, system operators could deliver present service needs while also having the flexibility for growth and change. Commercial light source modules that use a highly linear LD and contain distortion compensating drive circuitry have allowed the distribution of as many as 110 analogue video channels, but have cost $1500 per module. Although costly, linear light source performance is evidently available, a solution that linearizes an inexpensive, less linear laser may result in a more attractive component cost. This could then facilitate a more rapid implementation of high bandwidth systems and services.

Prior work on the general topic of improving optical system linearity has extended in many directions. This is partly due to changing system service requirements as well as changing material, device and system technologies. Several of the prior approaches have been concisely summarized by Sieben [9, pp.22–36] and others [5, pp.11–13] so that an emphasis in new directions can be made.

Over the last twenty years there has been much research into the performance, modulation and structures of optical devices. Some work has involved real components, while much of the recent work has involved models. Having developed the tools and knowledge that allow accurate model studies, optical specialists now have a good understanding of different devices and material behaviors, and are less constrained when exploring new and more complex light source possibilities. Application research need not, therefore, be as costly in both time and money as it once was.

1.4 Thesis Objectives

The object of this work was to linearize a laser. The work has involved the simulation of a modeled LD and a matched distortion compensation circuit. The method of distortion compensation considered was a continuation of work by Sieben [9], who previously derived an electrical pre-distortion circuit using Volterra analysis. The

coefficients for the pre-distorter that will minimize second- and third-order distortion in SCM systems having bandwidths up to 1 GHz have been determined and reported in this thesis. A further objective of this work was to develop an adaptive structure for the pre-distortion circuit so that it will be capable of addressing LD aging and temperature effects.

There were practical limitations faced by Sieben in realizing a working pre-distortion system using hardware. This research, therefore, has employed a user–friendly SPICE–based tool to better explore the potentials concerning the construction and application of an electrically enhanced optical transmitter. This simulation approach has provided an easy and cost-effective means for determining the operating functions and performance desired for the electrically adaptive pre-distorter. In this way, the initial development of a transmitter module containing both a LD and a Volterra–structured pre-distortion circuit may be thoroughly considered prior to tackling any hardware issues in a lab.

1.5 Organization of this Thesis

Following this introductory chapter, a fundamental explanation of the operation of a laser diode is given in Chapter 2. This provides a foundation for understanding the equations used to model the device, as well as the inherent non-linear behavior that becomes more noticeable with high modulation frequency, temperature change or aging. Chapter 3 contains an introduction to a novel LD 'circuit' model and the signal distortion mechanisms related to the device. The Volterra structure for a compensative distortion system is also included in this chapter. In Chapter 4, the benefits offered by applying adaptive feedback to a distortion compensation system are discussed. These benefits are highlighted in that chapter using a generic trial–of–concept circuit study. Then, in Chapter 5, the models used to simulate the pre-distorted LD, with and without adaptive feedback, are presented in detail. The adaptive strategy and its performance results are also found in this chapter. Summary comments and conclusions follow in Chapter 6.

Chapter 2

The Laser Diode

2.1 Overview

The laser diode is a complex micro-structure made of semiconducting materials. When careful attention is given to the material selection and placement, the fabrication processes and the device operation within its application environment, the diode may function as a laser.

Diodes conduct electrical current only while the voltage applied across the device has the proper polarity and sufficient magnitude. This operation is dependent on the quantum–electronic properties of two adjoined semiconductor materials. A LD, however, is a special type of diode that is explained using a combination of both semiconductor junction theory and laser physics.

The LD is unique among optical semiconductor devices in that, when the device operates above its threshold, it emits packets of optical energy, called photons, at discrete wavelengths. With the special material combinations and geometries used for LDs, this means that essentially all the photons have the same wavelength and are in-phase, producing what is called coherent light. Coherent light cannot be generated from a light emitting diode (LED) because its micro-structures do not permit the needed wavelength selections and restrictions.

The acronym 'laser' came from the phrase: 'light amplification from stimulated emission of radiation'. A semiconductor device must, therefore, attain a level of stimulated emission that results in a net optical gain before significant light output can be produced. The late 1950's and early 1960's saw the launch of functioning lasers

and the application of laser concepts to the semiconducting diode [10, pp.28–33]. This then led to the development of a room temperature, continuous beam device in 1970, and more powerful commercial LDs in 1975.

2.2 Fundamentals of Photonic Emission

Semiconductor lasers are junction devices that have developed from many of the concepts that explain the operation of LEDs. Simply stated, conduction band electrons from an n–type semiconductor recombine with valence band holes from a p–type semiconductor in the junction region to produce light under forward bias conditions.

An externally supplied forward voltage provides the energy required for both types of electrical carriers to overcome the potential barrier formed by the material discontinuity at the junction. The forward bias condition causes the majority carriers in each of the materials to diffuse away from their respective sources as they become injected into the junction, or more appropriately called the active region. The recombination of the electrons and holes results in the release of potential energy. Laser diodes and LEDs are designed to emit this energy as photons, or light, and therefore exhibit the phenomena known as 'injection electroluminescence'.

A recombination event is dependent on the meeting of these excited, oppositely charged carriers at a common atomic site during the same instant. It is not until after injection into the active region that a sufficient number of oppositely charged carriers are encountered, enabling recombination. High rates of recombination are achieved by increasing carrier mobilities and shortening diffusion lengths. An improved ease of recombination permits the device to be more responsive to its electrical input signal, and allows the distance across the active region to be reduced so that its optical output is easier to collect and use.

The emission intensity from the device can be further increased by injecting more of both carrier types into the active region. Since under equilibrium conditions of constant temperature, external light and external voltage, an equal amount of energy is absorbed in generating electron—hole pairs (EHPs) as is lost in eliminating them (see Figures 2.1(a) and 2.1(b)). A net increase in photon intensity implies an in-

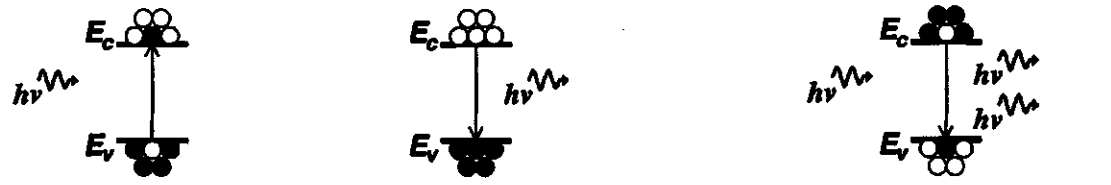

Figure 2.1: Energy State Transfers Involving Photons and EHPs
Energy may be transferred during electron energy state transitions from (a) optical to electrical forms, (b) electrical to optical forms, spontaneously, or (c) electrical to optical forms, stimulatively, meaning one photon triggers the generation of an additional in-phase, same wavelength photon, where EHPs are plentiful and a population inversion exists.

crease in device power consumption. This power is usually provided by an externally controlled electrical source.

An increased forward voltage, $V(t)$, changes the carrier concentrations throughout the device, increasing the current density, $J(t)$. This behavior is quantified using the familiar diode equation, [11, pp.41–47]

$$J(t) = J_{sat} e^{\frac{qV(t)}{nkT}} , \tag{2.1}$$

and results in a greater probability per–unit–time that an electron—hole pair (EHP) recombination will produce a photon in the active region. In Equation (2.1), J_{sat} represents the device–specific reverse saturation current density, q is the electron charge (1.602E-19 coulombs), n is the ideality factor ($1 < n < 2$), k is Boltzmann's constant (1.381E-23 joules/kelvin), and T is the device temperature in kelvin.

Electron—hole pair recombination can occur through direct and indirect means. Both release energy. Since direct recombination involves only the presence of an electron and a hole, nothing remains, except that a photon is released. An indirect recombination occurs as the result of interaction with at least one more entity (i.e. a trapping site or a particle collision). This indirect recombination produces a phonon. A phonon is a kinetic vibration in the atomic bonding or lattice structure, and is

not light. Because the purpose of a LD is to emit light energy, materials with direct bandgap characteristics are required in the active region.

Materials having direct bandgap characteristics, however, can be inefficient photon producers. They may also respond poorly to current variations if impurities and crystal defects at the atomic level are not minimized. This is why both material selection and device fabrication technologies are very important. Table 2.1 lists emission characteristics for some semiconductors used in opto-electronic devices that are well suited for telecommunications applications.

Table 2.1: Optical Properties of Some Light Emitting Semiconductors

Semiconducting Material	Direct Bandgap Energy, E_g (eV)	Approximate Wavelength Emitted, λ (μm)
GaAs	1.42	0.87
InP	1.34	0.92
$In_{.74}Ga_{.26}As_{.56}P_{.44}$	0.94	1.31
$In_{.63}Ga_{.37}As_{.80}P_{.20}$	0.80	1.55

Generally, conduction band electrons have a distribution of energies that average a fraction of an electron–volt above the conduction band energy level, E_c, and valence band holes reside in a similar, but mirrored, distribution below the bandgap and valence band energy level, E_v. If the bandgap represents an energy difference of E_g, where $E_g = E_c - E_v$, then an electron at the bottom of the conduction band recombining with a hole at the top of the valence band releases the wavelength, λ_{max}, defined as

$$\lambda_{max} = \frac{hc}{E_g} = \frac{c}{\nu_{min}} \quad , \tag{2.2}$$

where h is Planck's constant (6.626E-34 joule–seconds), c is the speed of light (2.998E8 metres/second) and ν_{min} is the material–specific minimum frequency for a photon.

If other EHPs having energies greater than E_g recombine, various wavelengths of light less than λ_{max} result. The distribution of energy states in a semiconductor, therefore, explains the generation of broad–spectrum light produced by LEDs,

and under powered LDs operating below their lasing threshold. An electron in any conduction band state can independently recombine with a hole in any valence band state at any time (see Figure 2.1(b)). This independent release of photon energy is known as a spontaneous emission, and produces non-coherent light. Non-coherent light is comprised of out of phase photons that have wavelengths distributed across a broad spectrum. It is characteristic of LEDs and incandescent bulbs.

2.3 Stimulated Emission

A stimulated emission occurs where one photon triggers an EHP recombination without causing absorption, loss or change. This means a second and additional photon, with the same phase, can be produced by this recombination event (see Figure 2.1(c)). It has been shown in other works [12, pp.330–335],[13, pp.177–183, 214–218] that stimulated emission will occur if more electrons occupy conduction band states than upper valence band states, and more holes exist in the valence band than in the lower conduction band. This required and un-natural condition is known as a population inversion.

Normally, and according to Fermi–Dirac statistics [14, pp.70–81],[13, pp.86–92], the majority of electrons in a semiconductor occupy energy states in the valence band and are thereby eligible to absorb any photon that has an energy which exceeds the bandgap energy. Similarly, most holes normally occupy conduction band states.

To facilitate stimulated emission, a laser diode must confine both the injected EHPs and emitted photons to the same 'active' region. This is essential for efficient laser operation. Confinement within the transversal bounds of the region — between the cathode and anode materials — is almost always done using a double–heterojunction (DH) device structure. Lateral and longitudinal confinement are also important, but are achieved through a greater variety of techniques, often dictated by the intended application of the device. Because the population inversion is not a naturally occurring energy state for any material, all stimulated EHP recombination events are bound geometrically.

Without EHP and photon confinement techniques, stimulated emissions may

travel in any direction, and possibly depart from the active region. Outside the active region, and away from the population inversion, a photon has no chance of generating an additional emission and will eventually be absorbed, or otherwise have its energy dissipated. For the purposes of characterizing LD design structures and accounting for the usefulness a photon has in repeating the stimulated emission process, device analysts have created a quantifiable measure: the confinement factor. The confinement factor simply represents the probability that each photon will stimulate the emission of another, identical photon.

2.4 Heterojunction Structures

Research in the late 1960's and early 1970's suggested the use of a heterojunction structure as a means of defining an active region and helping the creation of a population inversion. This important device structure refers to a junction created by joining two dissimilar semiconductors. They need not have different majority carrier types, but because of the uniqueness of bandgap energy characteristics, they are quite identifiably different materials. When referring to a heterojunction, the material having the greater bandgap energy is designated with a capital, resulting in a P–n or a p–N junction designation. The designation is also used when referring to isotype junctions as P–p or N–n.

The heterojunction structure, in all its variations, is, and has been, the standard for commercial semiconductor lasers since 1975. Its introduction as a pulse–mode laser by Kasonocky, Cornely and Hegyi in 1968 was quickly followed by a continuous beam, room temperature structure in 1970 [10, p.28]. Significantly lower threshold currents and longer device lifetimes gained it the favor now demanded from the optics industries. Many device designs make use of two heterojunctions — one on either side of a smaller bandgap material. When such a device is forward biased, the center material becomes the active region, receiving large concentrations of carriers from both its anode and cathode materials. Depending on the characteristics of the three key semiconductors used for a DH laser, representations for its structure could be P–p–N or P–n–N.

In DH lasers, the outer two materials are heavily doped (but need not be degenerate, or over-doped) so that their Fermi–energy levels, E_f, are close to their appropriate bandgap limits. The center layer material, having a bandgap smaller than those beside it, is lightly doped so that its Fermi level is near the center of its bandgap. The band diagram for no applied voltage (see Figure 2.2(a)) has noticeably stepped valence and conduction levels, and the Fermi level, straight across both junctions, being higher than the highest valence band 'step' and lower than the lowest conduction band 'step'. Potential barriers at both junctions confine the carrier populations within each material.

In a P–p–N device, the forward bias condition (see Figure 2.2(b)) adds the energy required for holes to flood into the center–layer material, overcoming the P–p valence

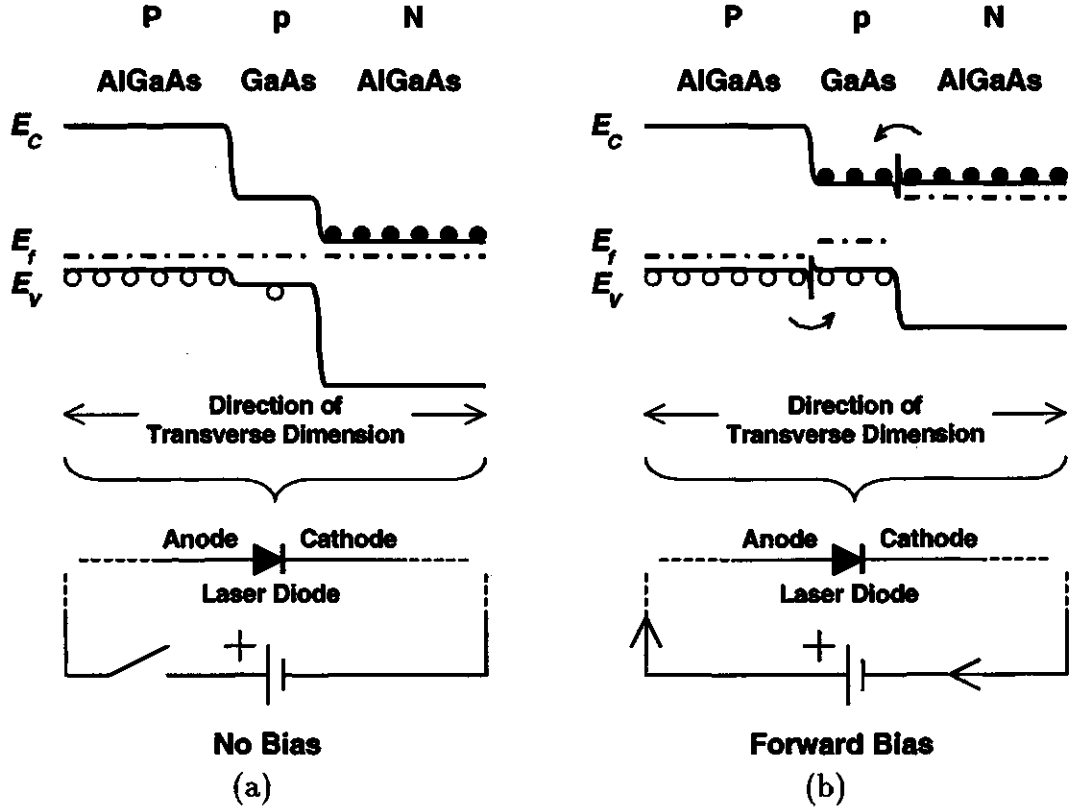

Figure 2.2: Energy Levels for a P–p–N Double Heterojunction Structure
(a) represents the energy levels when no voltage is applied to the device, while (b) represents the energy levels when a forward voltage is applied to the device.

band barrier, while electrons overcome the p–N conduction band barrier. The smaller bandgap material naturally offers good transverse carrier confinement since the injected holes find a significant potential barrier at the p–N isotype junction, as do electrons at the P–p junction. A population inversion is now easily achieved without the need for significant levels of applied energy.

The forward–voltage that produces the threshold current density in a DH device is much less than that for a homojunction device having the same active material. In a DH device as shown in Figure 2.2(b), transverse carrier confinement is very good, and the needed injection rates are easier to sustain because lower operating current densities are possible. This reduces internal heating, helping to stabilize device performance and reduce aging effects and reliability issues.

Laser diodes using a DH design also benefit by having a well defined active region that has a slightly higher refractive index than the adjoining N– and P–type materials. The higher refractive index helps to confine photons within the transversely limited active volume. It is important to understand that better EHP and photon confinement leads to a greater device efficiency, lower power consumption, lower threshold current, greater device linearity and greater modulation bandwidth. Confinement with respect to the lateral and longitudinal dimensions is a design concern currently addressed by a variety of complex fabrication processes and material structures. Longitudinal confinement will be discussed in the following section. The technical details of lateral confinement, however, are not relevant within the scope of this thesis, so they have not been included.

While carriers diffuse through the active region, and away from their point of injection before releasing energy as a photon, their concentrations diminish. Some may even travel through the entire active region. This is, however, not preferred, as those carriers become much less likely to be part of recombinations that will involve stimulated emissions. Short carrier lifetimes and diffusion lengths are thereby important design considerations that lead to low–power devices. The devices may then be highly efficient in the conversion of electrical to optical energy. The two factors are similarly important to enabling the device to respond linearly to rapid variations in

current density, or its modulating signal.

2.5 Amplification

Once initiated, stimulated emissions continue as long as the population inversion exists and photons are present to trigger other emissions. This is one of the reasons that a minimum or threshold current density is defined for LDs. Above this point, an increase in the carrier injection rate leads to an increase in stimulated emissions. Below it, a population inversion does not occur, and only spontaneous emissions can take place.

In 1962, Robert Hall at General Electric departed from conventional thinking [10, pp.177–189] and arranged simple mirrored surfaces perpendicular to the material layers. These mirrored surfaces reflected photons back into the material from which they originated, effectively lengthening the path for other EHP recombinations and additional stimulated emissions. The reflecting surfaces improved the device efficiency by creating a resonant volume that selects and amplifies certain optical wavelengths produced by the EHPs and stimulated emissions. Today, a variety of additional reflective techniques, including the change of refractive indexes present in DH structures, may be used to optically confine and help amplify the emitted wavelength(s).

The resonant cavity can be created using different reflective mechanisms. In one type of device, the semiconducting material layers are cleaved and coated so that optical reflection occurs abruptly at both ends of the cavity. This is called a Fabry–Perot (FP) laser. Another type of device uses a distributive grating mechanism causing Bragg scattering [11, pp.180–184]. If the Bragg corrugated structures are produced as extensions to each end of the cavity, the device is referred to as a distributed Bragg reflector (DBR) laser. If, instead, the corrugations are distributed along the length of the cavity, a distributed feedback (DFB) laser is produced. DFB lasers exhibit superior temperature stability, lower operating thresholds and very narrow spectral linewidths [15, pp.235–249]. They also are difficult to fabricate due to the fact that the period of corrugation may be as small as 0.2 μm.

Cavity dimensions play a significant role in defining the resonant mode(s) of os-

cillation. For transverse and lateral fundamental mode operation, at wavelengths of approximately 1 μm, active regions must be no thicker or wider than 10–15 μm. Due to lateral carrier diffusion and the current leakage [11, pp.165–166], this is an impractical lateral confinement requirement for simple planar stripe lasers. For illustration, the stripe laser shown in Figure 2.3 has the lateral dimension of the cavity defined by the least resistive current path, from the substrate, through the active material layer, to the metal stripe. (To allow simplification of the illustration, the commonly present contact layers have not been shown.)

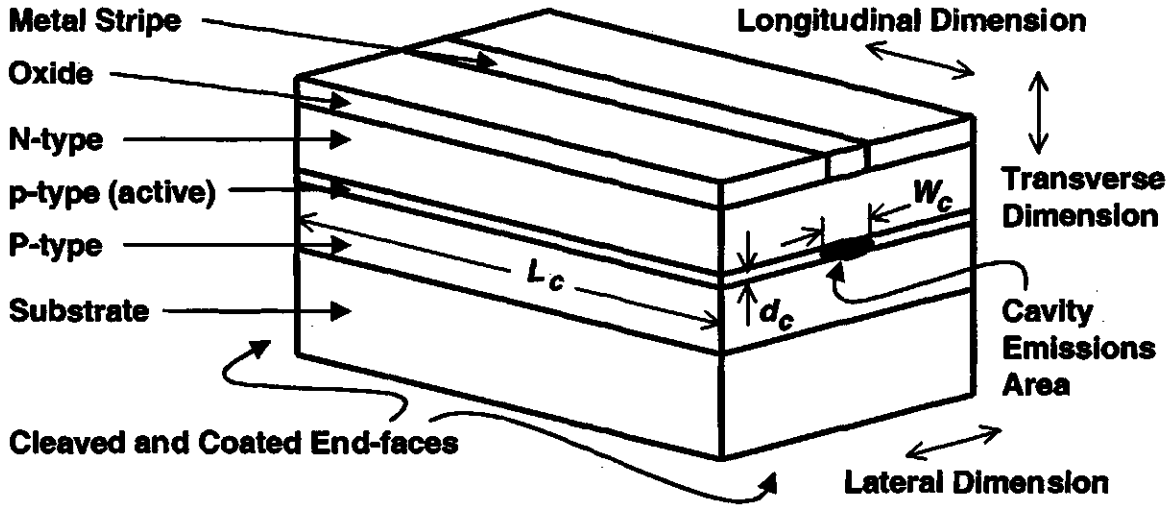

Figure 2.3: A Simple DH Stripe Laser

Single mode LDs are commonly designed so that the active region is 'buried' between non-conducting, low refractive index material layers [11, pp.173–176]. Complex fabrication processes also enable the necessary transverse confinement, and can create active material layers as thin as 40 Å, or 4.0 nm, for graded index separate confinement heterostructure multiquantum well (GRINSCH–MQW) lasers [11, pp.195–200].

In order to produce a coherent output beam having discrete emission wavelengths, the per–unit–length optical gain or generation at the threshold, g_{th}, must equal the losses for each oscillatory path, or mode. This is shown as [11, pp.134–136]

$$g_{th} = \frac{1}{\Gamma}\left[\alpha + \frac{\ln(\frac{1}{R_1}\frac{1}{R_2})}{2L_c}\right] , \tag{2.3}$$

where Γ is the optical confinement factor, α is the cavity absorption loss per–unit–length, R_1 and R_2 are the reflectivities of the 'end-faces' and L_c is the cavity length. The second term in the equation effectively distributes the 'end-face' transmissions, $\frac{1}{R_1}$ and $\frac{1}{R_2}$, on a per–unit–length basis.

Electron–hole pair recombinative emissions may produce various wavelengths, based on the statistical distributions of electrons and holes among energy levels within the cavity. However, in the defined energy states for the active material, the stimulated emissions will be the stronger wavelengths that can resonate within the device. Those wavelengths will be the ones supported by stimulated emissions that can survive absorption and confinement losses along the cavity. The emission wavelengths must also remain in-phase after completing a roundtrip travel in the cavity, as explained by standing wave theory. For those wavelengths to which Equation (2.3) applies, an increase in device current leads to a nearly proportional increase in stimulated emissions and optical output power.

Figure 2.4 illustrates a representative LD light versus current (L-I) characteristic, along with example input/output waveforms that could be found in direct intensity modulated (IM) analogue applications. This is an accurate representation for static and 'low–frequency' operating behavior. Below the threshold current, I_{th}, spontaneous emissions do not significantly exceed absorption rates. At this point, emission levels are too low for optical gain and resonance to exist in the cavity; the device will operate in a manner similar to that of a LED that is barely conducting. Above the LD threshold, stimulated emissions become dominant. Ideally, it is the reflective losses from the resonant cavity, or the end-face transmissions, that then become the useful, external beam of light.

2.6 Optical Power and Intensity Relationships

Having covered the principles for achieving lasing behavior in a semiconductor device, it is now useful to consider the common expression describing a LD threshold

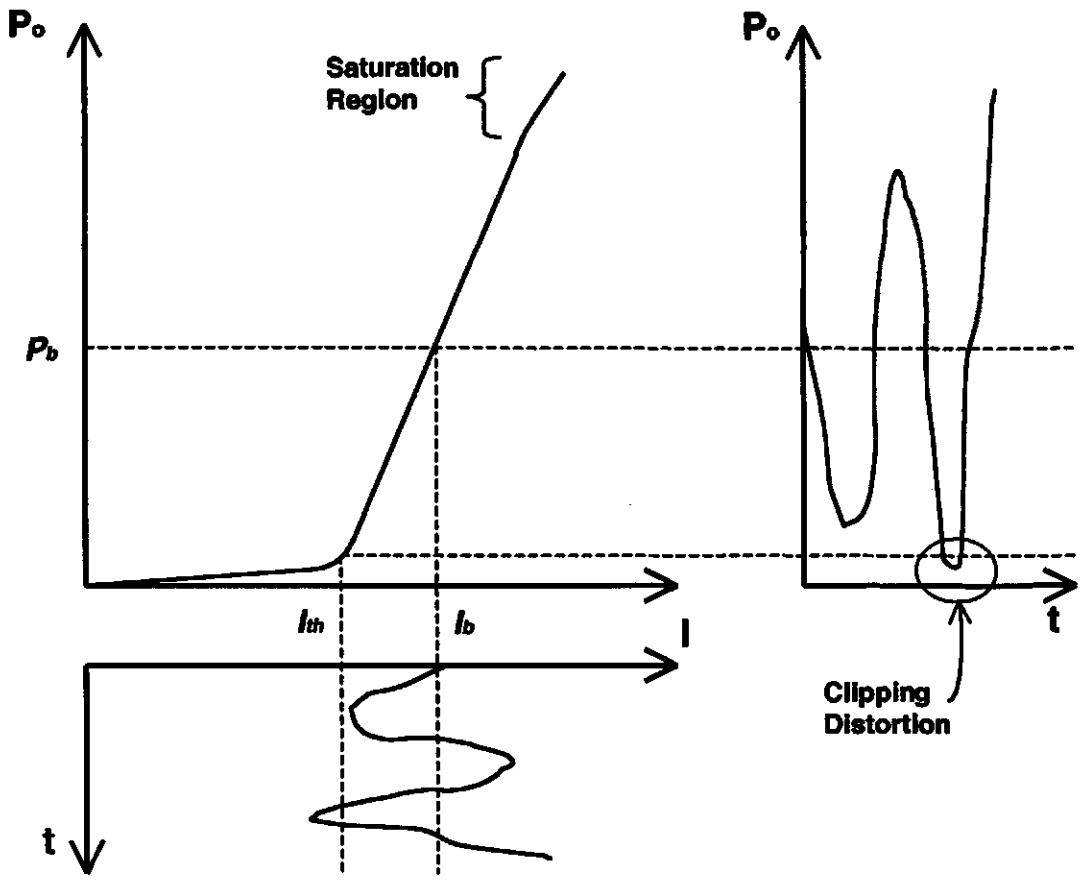

Figure 2.4: Laser Diode Output Power/Light vs. Current Characteristic
This generic L-I characteristic illustrates the use of a forward bias current, I_b, and the distortion effect created during intensity modulation when the LD threshold current, I_{th}, is not maintained.

current density, J_{th}. It may be written as [11, pp.134–135]

$$J_{th} = \frac{J_o d_c}{\eta_i}\left[1 + \frac{g_{th}}{g_o}\right] , \tag{2.4}$$

where d_c is the transverse dimension of the cavity, or active region depth, and η_i is the internal quantum efficiency, or ratio of photon emitting recombinations to *all* EHP recombinations. The normalized, unsaturated 'static' device gain and current density, respectively represented by g_o and J_o, are constants applicable to the 'linear' region just above threshold. Whether above or below threshold conditions, the current

density is related to the device drive current, $I(t)$, by the expression

$$I(t) = L_c W_c J(t) \ , \tag{2.5}$$

where L_c and W_c, respectively, are the length and width of the LD cavity.

The optical output power from a device can be shown for 'low–frequency' signals as [11, pp.138–140]

$$\begin{aligned} P_o(t) &= \frac{hc}{\lambda}\left[\frac{I(t)-I_{th}}{q}\right]\eta_{ext} \\ &= \frac{hc}{\lambda}\left[L_c W_c \frac{J(t)-J_{th}}{q}\right]\eta_{ext} \ , \end{aligned} \tag{2.6}$$

when operating above threshold, and where η_{ext} is defined below. Under this circumstance, this equation justifiably overlooks the normally trivial contribution from spontaneously emitted photons. It also uses the external differential efficiency for the device, η_{ext}, that can be expressed in terms of the stimulated emission efficiency, η_{st}, as

$$\begin{aligned} \eta_{ext} &= \frac{\text{total optical output power transmitted}}{\text{total power consumed}} \\ &\approx \eta_{st}\left[\frac{\frac{\ln\left(\frac{1}{R_1}\frac{1}{R_2}\right)}{2L_c}}{\alpha+\frac{\ln\left(\frac{1}{R_1}\frac{1}{R_2}\right)}{2L_c}}\right] \\ &\approx \eta_{st}\left[\frac{2L_c\alpha}{\ln\left(\frac{1}{R_1}\frac{1}{R_2}\right)}+1\right]^{-1} \ . \end{aligned} \tag{2.7}$$

When Equation (2.7) is substituted into Equation (2.6), the resulting expression contains no variables that relate to spontaneous emissions. From a functional and external perspective, the efficiency of the device cavity highly depends on η_{st}, being

the ratio of stimulated recombinations to all photon emitting recombinations. It is also important to note that it is a reduction of the stimulated emission efficiency that creates the non-linear 'saturation region' in the L-I characteristic when above normal current levels are applied to the device.

Laser diode output power is also the product of the area of the emitted optical beam and the beam intensity. Because, by definition, intensity is the rate of net energy flow per–unit–area, this can be shown by representing the laser output intensity in terms of its photon density, $S(t)$, as

$$P_o(t) = W_c d_c \left[\frac{hc/\lambda}{\tau_p}\right] \left[\frac{S(t) L_c \eta_{ext}}{\Gamma}\right] , \tag{2.8}$$

where $P_o(t)$ includes both 'end-face' losses and τ_p is the lifetime of a photon. Since the cavity dimensions and the material properties of the device are essentially fixed, the optical output power, photon density and current all vary nearly proportionally. If the signal frequency does not remain 'low', these 'linearly' related variables begin to vary in a dynamically non-linear manner.

2.7 Temperature and Aging Issues

Temperature can have a significant effect on the performance characteristic for a laser, as illustrated in Figure 2.5. Higher temperatures raise intrinsic carrier populations and equilibrium generation and recombination rates. This means that more carriers occupy states of higher energy, making a population inversion more difficult to attain. It also means that the LD quantum efficiencies decrease. Thermal variations also affect the device operating power and linearity, not to mention other performance measures for the transmission system.

As in other electronic devices, there will be natural operational heating due to a non-ideal lattice makeup and carrier/lattice scattering. This is unavoidable when the device is in use. However, for semiconductor lasers, an important operational benefit can be gained in this regard if manufacturing processes, device designs and system designs can minimize and stabilize thermal variations and/or improve stimulated and

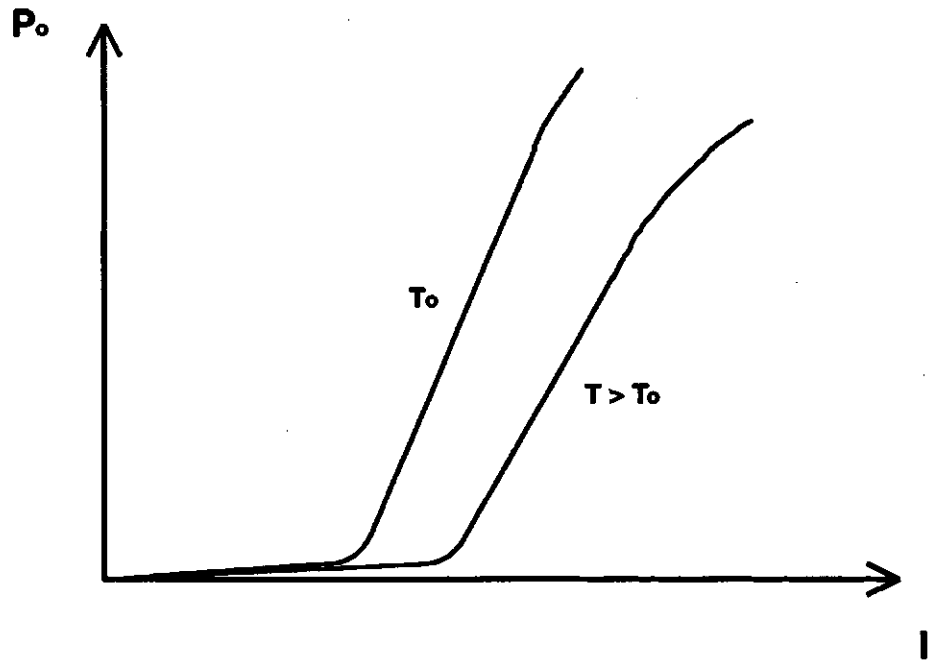

Figure 2.5: Effect of Temperature on LD Performance

external efficiencies.

Over the years, fabrication processes have done this by producing semiconductor lattices that have fewer atomic dislocations, impurities and trapping sites. This decreases the absorption loss in the cavity and the resistive losses from the materials. It also allows for the increased confinement of carriers and photons. Additionally, device designs may now include integrated Peltier–effect cooling structures to help control operating temperatures. These improvements all come with a cost that, of course, reflects their lack of simplicity and manufacturing convenience.

Thermal variations may also be reduced by minimizing the signal current variations from the bias current level. This should be done by the application engineers involved with system designs, and MQW devices in particular [6]. As such, explanation and exploration of expanded and new optical system designs is bringing to light the need for growing consideration of problems and approaches that address temperature and aging variations. Device and system technologies have matured, and now rely on application–specific refinements.

From work with MQW devices, Pan *et al.* [16] reported that external quantum efficiencies were degraded primarily due to the temperature dependence of the stimulated recombinations. In considering the possible operating temperatures for FTTH systems, device efficiencies can also be expected to suffer from carrier confinement changes.

Work by Wang *et al.* [17] measured a 5 dB change in second harmonic distortion (HD_2) over a 50 °C temperature range for a DBF laser. The work also showed that if leakage current around the cavity is minimized through good device design and manufacturing processes, signal distortion is mainly generated by gain saturation and other non-linearities in the optical medium. It was also shown that HD_2 increases with the device temperature.

Through the lifetime of a semiconductor device, a history of use accumulates that both permits and encourages permanent changes at the atomic level. Like temperature, device aging is another means of varying and degrading LD performance characteristics. Because many telecommunication system components have been expected to have operating life–spans measuring in decades, the gradual parametric changes that occur in LDs over time may sometimes determine their suitability for use in demanding applications. Often, the aging effect resembles the undesirable device behavior produced during a temperature increase. However, unlike temperature changes, aging is not temporary.

Wood [11, pp.222–224] discusses both temperature and aging effects, along with some simple compensative drive circuits. He mentions that the lasing threshold may change by about +1%/°C, and that digital systems can be very sensitive to any change in threshold levels and transmitted power.

Recently, vertical-cavity surface-emitting lasers (VCSELs) have attracted a growing number of research studies. Much of the work has focused on the high thermal sensitivity of this small, complex–structured device, even though the basic performance is similar to other lasers.

Dutta *et al.* [18] presented results that show the decrease in optical output, caused by a small increase in cavity temperature, is due to the series resistance within the

device. In a VCSEL, and other LDs, increased temperatures and operating currents lead to reduced emission efficiencies because of decreases in the cavity confinement abilities. From this, a change in temperature of only a few degrees can cause a very significant increase in device non-linearity and reduce the power output.

Mena *et al.* [19] reported that the complicated interactions within a VCSEL cavity have created difficulty for models used in design work; the prominent thermal effects have not been easy to mathematically express in a practical way. However, they found that, in recognizing the effect temperature has on the VCSEL gain constant, modeled performance has improved. By considering the sometimes small, but probable, device temperature variations, it was shown that tool and application research can make valuable advances.

2.8 Chapter Summary

The LD has been introduced, and the technical explanations for the critical and unique operating concepts have been presented. General expressions and relationships have also been reviewed that should help describe LD performance in common applications. Although not mathematically developed in this chapter, the complexity of the interaction between electrical and optical energy forms within the device cavity was described. This was done so that the parameters and variables normally used to model the LD dynamic system have a framework for reference and understanding. This chapter has also included a summary look at LD temperature change and aging effects, so that an awareness has been created in regard to the conditional properties that some device parameters can include.

Chapter 3

Modeling Lasers and Signal Distortion

3.1 Expressions for Inherent Device Behavior

As the principles of operation for a LD are well known, device structures can be accurately simulated in order to adapt and optimize design variations and operational performances. A book by Wood [11], like many other sources [6],[4],[20],[21],[22], contains the development and discussion of the time–varying relationship between electrical carriers and photon emissions. Because device dynamics depend on the interaction of electrical and photonic systems, there are two rate equations that are commonly used to describe the operational behavior for a device above its threshold:

$$\frac{dN}{dt} = \frac{I}{qV_c} - \frac{N}{\tau_s} - g(N - N_o)S \quad \text{and} \tag{3.1}$$

$$\frac{dS}{dt} = \Gamma g(N - N_o)S - \frac{S}{\tau_p} + \Gamma\beta\frac{N}{\tau_s} \quad . \tag{3.2}$$

The equations express the density of conduction band electrons, N, and density of photons, S, within an active cavity volume, in terms of the device drive current, I. The device dependent parameters are: V_c, the volume of the active region; τ_s, the average electron or carrier lifetime before spontaneous emission; g, the optical power gain from the generation of stimulated emissions; N_o, the electron density at the lasing threshold; Γ, a measure of the useful photon–involvement called the optical confinement factor; τ_p, the average photon lifetime before absorption; and β, the

fraction of spontaneously emitted photons that are in-phase with the lasing emissions.

In Equation (3.1), the first term on the right–hand side represents the rate of charge carriers, or EHPs, that are injected into the active region on a per-volume basis. The second term equates to the rate of decrease in the electrical carrier density due to spontaneous recombinations. The final term represents the rate of decrease in the electrical carrier density due to the photon stimulated recombinations, and is only existent above the lasing threshold, when $N > N_o$. dN/dt has units of EHPs m^{-3} s^{-1}.

The first term on the right–hand side of Equation (3.2) represents the rate that useful, confined photons are stimulated on a per-volume basis in the cavity. The second term equates to the rate of decrease in the stimulated photon density due to absorption. The final term represents the rate of increase in stimulated photon density due to the contribution of some spontaneous emissions that remain confined to the cavity and happen to be in phase with the stimulated, or lasing, emissions. dS/dt has units of photons m^{-3} s^{-1}.

High–speed, single mode lasers are more accurately represented when Equations (3.1) and (3.2) are modified to include an expression containing ε, the power gain compression factor [23]. It is a parameter that helps to account for the non-linear relationships between carriers and photons during stimulated recombinations. Some of the factors it accounts for are discussed in [24], each one contributing to a damping effect on the gain coefficient. Use of the expression in Kuo's work [21], and also that of Neusy and McGee [25], proved it useful in more accurately quantifying the operating performance of some LDs. Due to this previous use of the power gain compression factor with the single mode LD modeled in this thesis, the following modified rate equations will be appropriate for use, henceforth, in this document:

$$\frac{dN}{dt} = \frac{I}{qV_c} - \frac{N}{\tau_s} - g(N - N_o)(1 - \varepsilon S)S \quad \text{and} \tag{3.3}$$

$$\frac{dS}{dt} = \Gamma g(N - N_o)(1 - \varepsilon S)S - \frac{S}{\tau_p} + \Gamma\beta\frac{N}{\tau_s} \quad . \tag{3.4}$$

The terms in Equations (3.3) and (3.4) continue to represent the rates to which they

correspond in Equations (3.1) and (3.2).

Each of the two equations can be represented with their respective equivalent–system circuit concepts as shown in Figure 3.1(a) and (b). The two system concepts

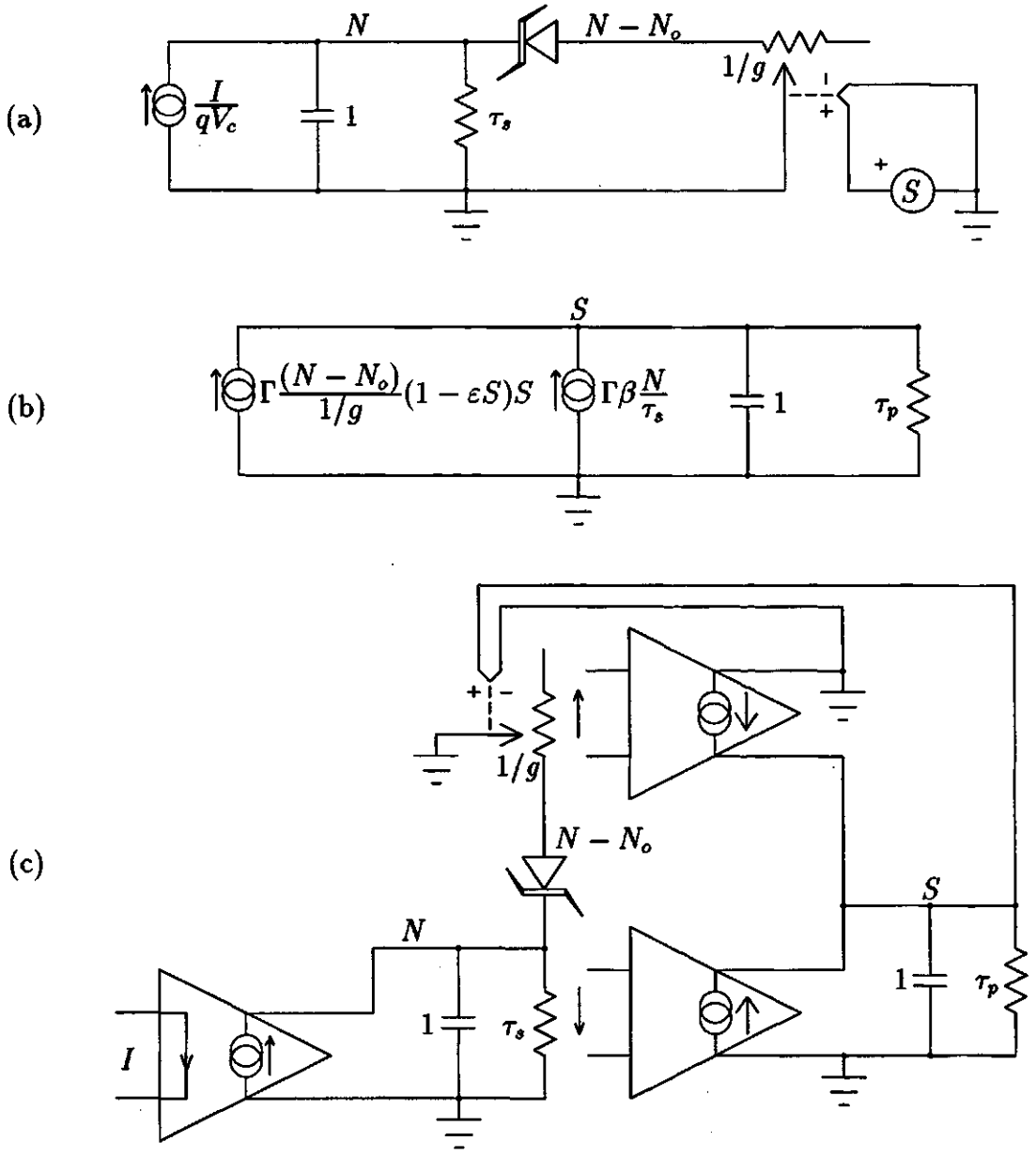

Figure 3.1: Schematic Models for Laser Diode Rate Equations
(a) and (b) represent Equations (3.3) and (3.4), respectively, while (c) represents the entire electro–optic system, illustrating the interaction between electrical carriers and photonic densities in the cavity.

may also be combined as the more complex, single system shown in Figure 3.1(c). Together as a single system the optical output of a LD may be computed from the knowledge of the device drive current.

The single mode rate equations have been used to model steady–state and large– and small–signal dynamic device behaviors using circuit–equivalent systems. Tucker [23] and Way [22] have demonstrated that typical packaging and chip parasitics do not significantly affect the accuracy of the model for high–speed devices. Mena, Kang and DeTemple [26] have provided further adaptations of the rate equations so that the unique carrier – photon interactions throughout a MQW structured device are accurately modeled, capturing behavioral effects just outside the active QW–layers in the confinement material. Gorfinkel and Luryi [6] have also explored a MQW device with the common equations, but added a third energy expression that helped them predict the effects of electrical carrier heating from optical losses and the modulated power–flux entering the MQW cavity. Through an electrical schematic form similar to Figure 3.1(c), Equations (3.3) and (3.4) have also provided the starting point for the transmitter system studies in this thesis.

3.2 Modeled Performance of a Laser Diode

Table 3.1 lists the characteristic parameters for a single mode DFB LD studied by Kuo [21] and by Sieben [9]. The parameters have been applied to the simulation of the schematic–equivalent model shown as a circuit in Figure 3.2. Another set of parameters, representing a less–efficient high–speed single mode laser, was used by Way [22], Neusy and McGee [25] and Sieben [9] when simulations were performed using the same modeling method. However, because of its greater suitability for use in modern communication systems, only the parameter set for the LD used in Kuo's work will be applied in this thesis. For identification purposes, the device will be referred to as Laser 'A' in this work.

Intusoft's SPICE–based simulation program, ICAP/4 [27], has been used to generate the results presented in this thesis. Tucker [23], Dodds and Sieben [28], Mena *et al.* [26] and others used similar tools and techniques to model LDs in their work,

Table 3.1: Device Parameters used for Modeling Laser 'A'

Parameter	Definition	Quantity	Units
Γ	Optical Confinement Factor	0.34	...
τ_s	Spontaneous Electron Lifetime	3E-9	s
τ_p	Photon Lifetime	2E-12	s
N_o	Transparent Carrier Density	1E24	m^{-3}
g	Optical Power Gain	3E-12	$m^3\ s^{-1}$
ε	Power Gain Compression Parameter	3E-23	m^3
β	Probability of Spontaneous Emission caused by a Photon from Stimulated Emission	1E-3	...
qV_c	Product of Volume of Active Region and Electronic Charge	5.76E-37	C m^3
I_{th}	Threshold Current	280	μA

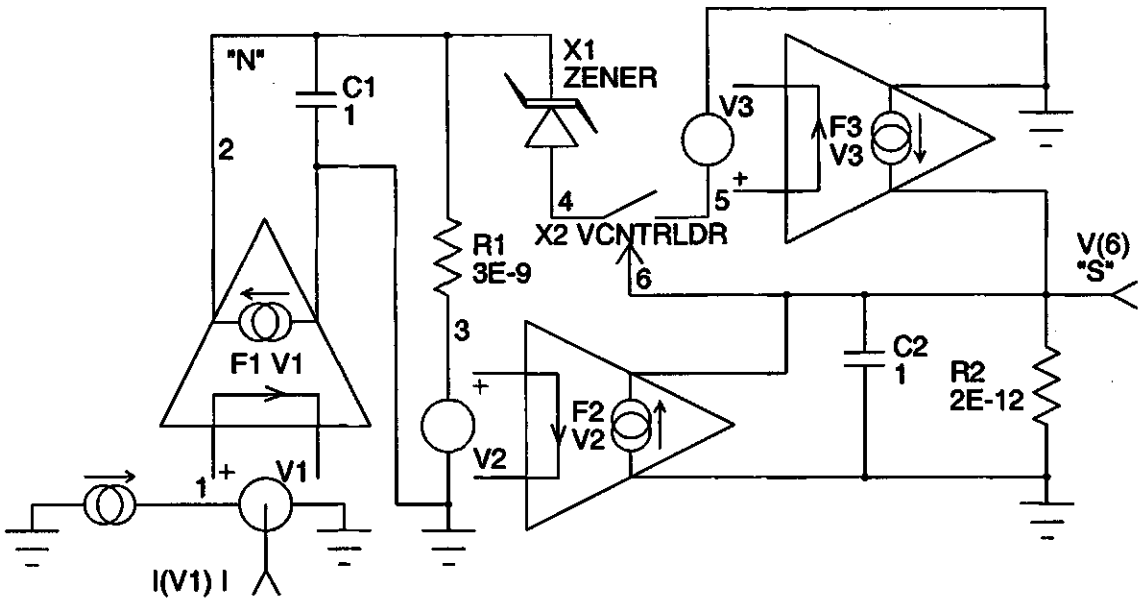

Figure 3.2: Circuit Schematic for Simulation of Laser 'A' in ICAP/4
The SPICE netlist, containing component connections, definitions and values, can be found in Appendix D.1.

all producing results that have very good agreement and accuracy. Simulated results can therefore be substituted for measurements acquired from costly, real system experiments.

The distortion in output waveforms was observed to vary with input frequency and bias settings. Figures 3.3 and 3.4 respectively illustrate the behavior typical of LDs when excited with a step input current and a 'high–frequency' modulation signal. Compared to the device input signal, the optical output differs in both wave shape and time delay. This is attributable to the inherent non-linear characteristic of the device. These figures illustrate that this behavior can be modeled by the two rate equations.

Observation of this behavior is not new to the optical research community, but it deserves emphasis before proceeding. The behavior is accurate, and not attributable

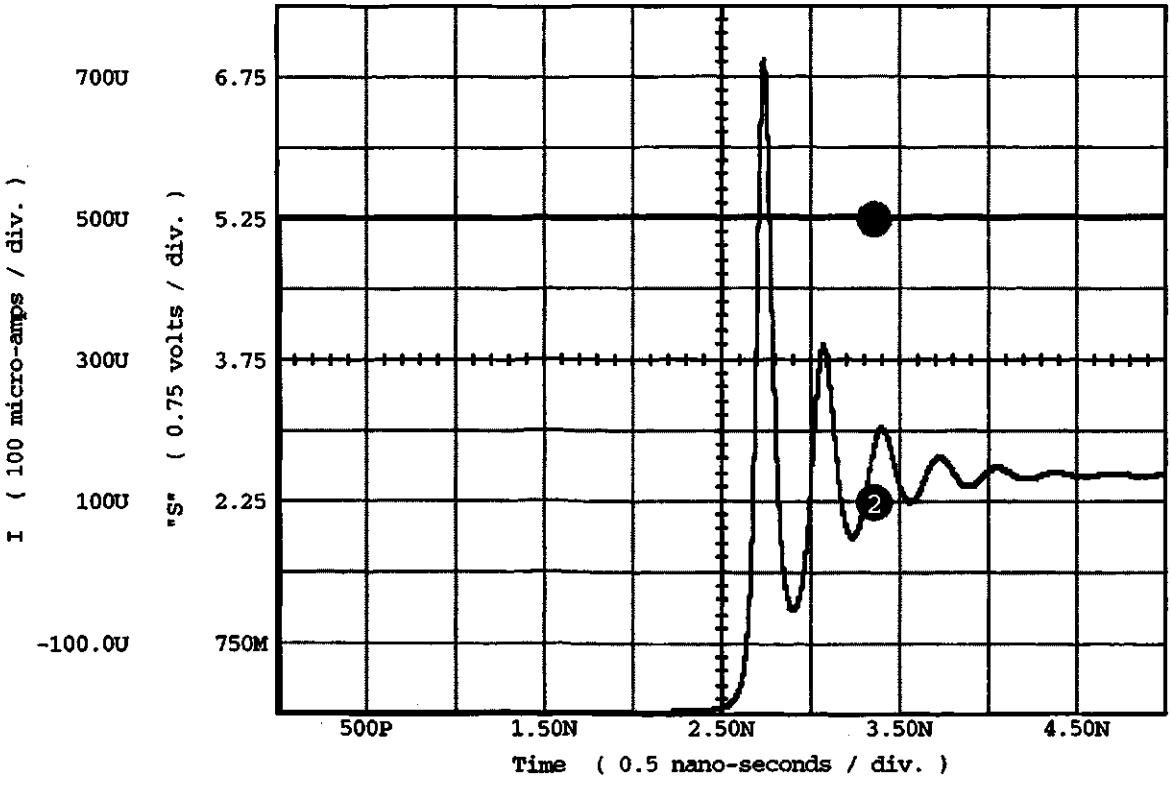

Figure 3.3: Simulated Step Input Response for Laser 'A'
Waveform 1 shows the LD input drive current, I. Waveform 2 shows the LD output photon density, S, represented by ICAP/4 as a voltage where 1 volt = 1E20 photons/m^3.

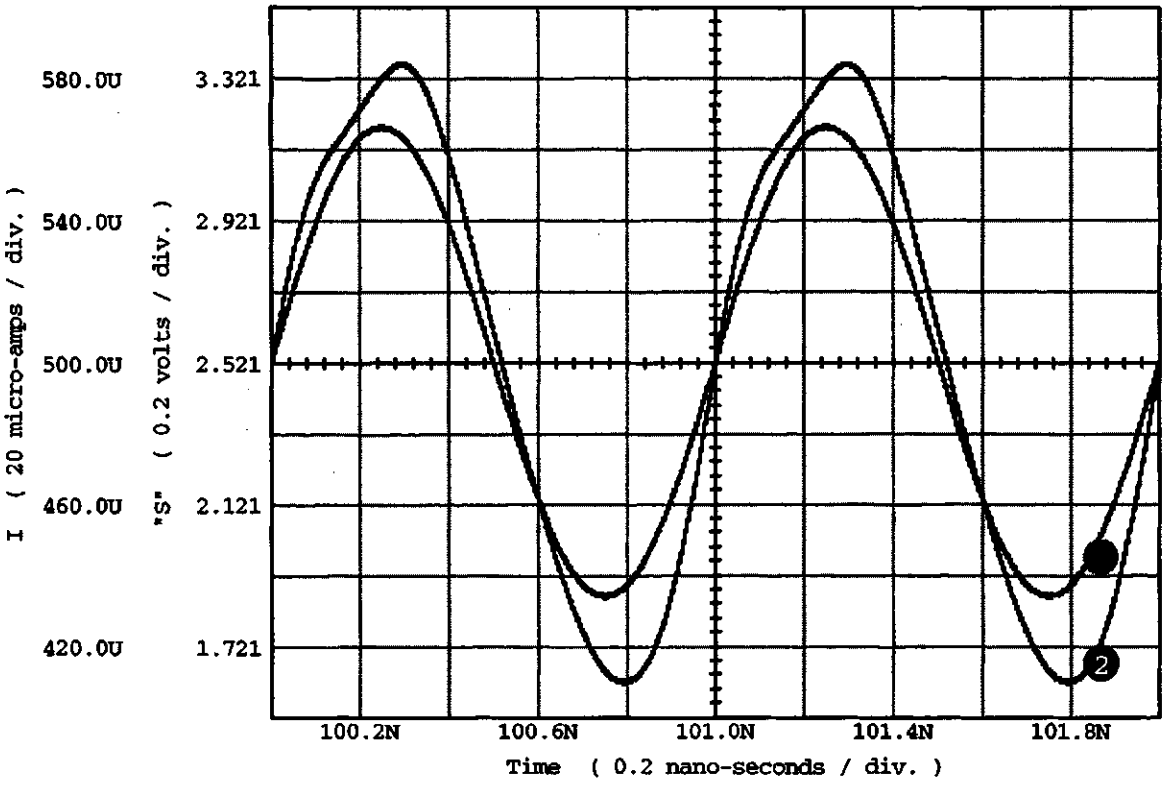

Figure 3.4: Simulated 1 GHz Sinusoidal Response for Laser 'A'
Waveform 1 shows the LD input drive current, I. Waveform 2 shows the LD output photon density, S, represented by ICAP/4 as a voltage where 1 volt = 1E20 photons/m^3.

to any problem with the modeling method. Figure 3.5 shows that signal distortion significantly worsens when LD intensity is modulated with an even greater 'high-frequency', now in the microwave range at 2 GHz. Device dynamics that affect signal fidelity clearly exist, and they become more noticeable from the magnitude and phase inconsistencies as the modulation frequency increases.

3.3 Laser Diode System Planning and Performance Issues

The optical signal from a LD can become distorted due to several factors. Some factors may be compensated for using one of the several methods considered by Sieben [9] (opto–electronic feedback, phase–shifted signal combination, electro-optic

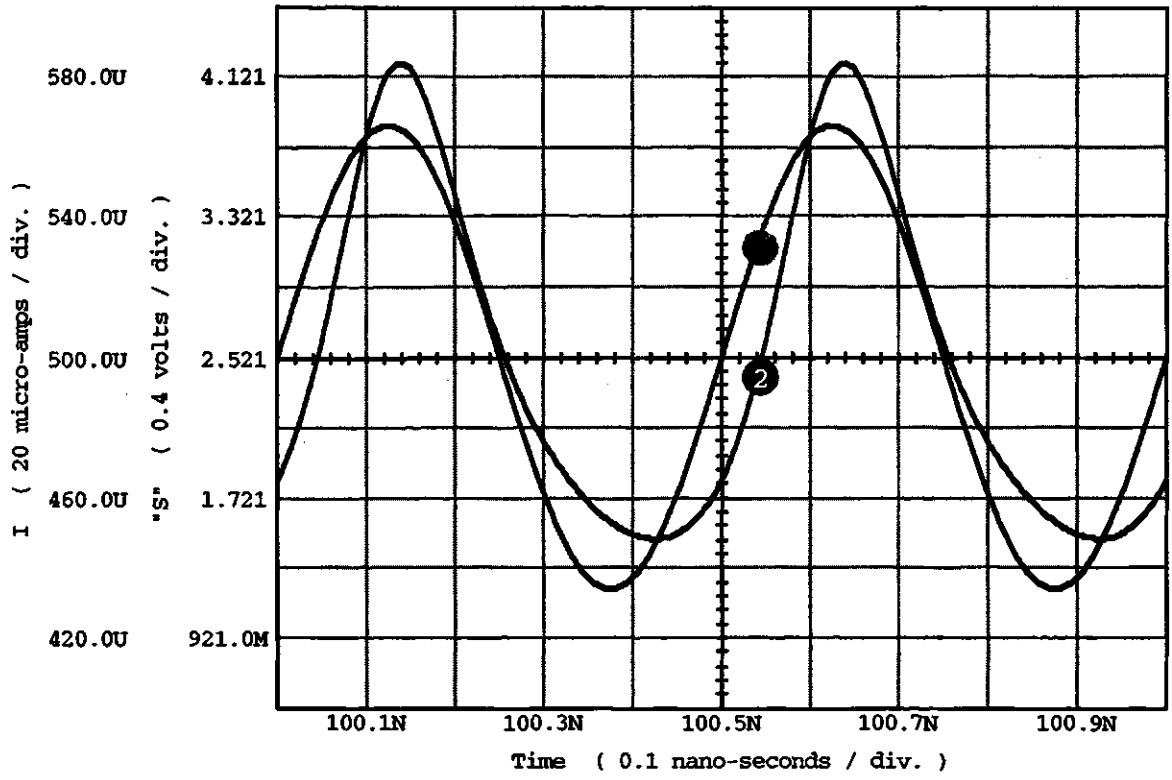

Figure 3.5: Simulated 2 GHz Sinusoidal Response for Laser 'A'
Waveform 1 shows the LD input drive current, I. Waveform 2 shows the LD output photon density, S, represented by ICAP/4 as a voltage where 1 volt = 1E20 photons/m^3.

quasi–feedforward, optical feedforward, electrical and optical post-distortion, electrical pre-distortion and adaptive electrical pre-distortion), while others may only be addressed by carefully considering the application requirements and configuring the transmitter to operate appropriately.

For many applications that aim to exploit the relative simplicity offered by intensity modulated (IM) light sources, a LD output signal, $P_o(t)$, can be expressed as

$$P_o(t) = P_b\big[1 + M_s i(t)\big] \ , \tag{3.5}$$

where M_s is the modulation sensitivity and is related to the slope of the L-I charac-

teristic near the operating point, $i(t)$ is a time-varying signal current and P_b is the optical bias power, being dependent on the device bias current. For simple, non-SCM, analogue systems, at the peak signal current, $M_s i(t)$ equals the optical modulation index (OMI), σ. This OMI element in Equation (3.5) is more clearly shown as

$$\sigma \;=\; M_s \,\mathrm{MAX}[i(t)] \;=\; \frac{\mathrm{MAX}[I(t)] - I_b}{I_b - I_{th}} \quad . \tag{3.6}$$

Equation (3.5) explains the use of the device in the most simple, linear form. It does not include the origins of signal distortion or noise.

When an information signal is available for optical transmission, two important device bias limits must be determined before operation a LD in a direct IM configuration. The maximum bias is limited by either the relative intensity noise (RIN) from the LD, or the saturation region on the L-I characteristic. The minimum bias depends on the lasing threshold and the OMI required by the signal and system. These maximum and minimum limits define the useable 'linear' range of the L-I characteristic.

In the 'linear' operating region, a laser produces the modulated output signal and also a noise component, due to modal instabilities and spontaneous emissions. The instabilities and other emissions have un-ordered, random tendencies that cause small intensity fluctuations, or signal noise. As a group, they are expressed as the ratio of the mean square of the fluctuations to the square of the mean intensity. This ratio is the RIN value for the device, and is unique to each model of LD.

Since the RIN impact on direct–detection receivers increases with the square of bias power, P_b, it is desirable to operate a LD below a system determined power level. This may ensure a system meets SNR and CNR requirements. Because for analogue transmission systems, where detected optical power levels are usually higher than those for digital systems, RIN often becomes the limiting factor [5, pp.34–36]. However, for non-SCM analogue systems P_b commonly has a maximum that is limited by the impact of the saturation region on signal distortion, rather than RIN.

In regard to the minimum bias level, it is fundamental to note that serious signal distortions can result if operation above the LD threshold is not maintained. In applications using direct intensity modulation, the designer must ensure that the

bias current and modulation index are selected so that clipping-induced distortion is minimized. The OMI is generally chosen so that $M_s i(t) > -1$, or $I_b + i(t) > I_{th}$. Because an SCM system has a composite input signal in which some or all individual channels may peak simultaneously, the simple OMI definition mentioned earlier is replaced with an *rms* OMI [29],[30]. For CATV systems the OMI is expressed as

$$\sigma = \sqrt{\frac{m_{ch}^2 N_{ch}}{2}} \quad , \tag{3.7}$$

where m_{ch} is the OMI from the perspective of having a single channel system, and N_{ch} is the number of channels frequency–division multiplexed within a multi-channel composite signal, $i(t)$.

Transmission systems having a small OMI and very low bias power may experience difficulty in keeping the detected optical signal above the noise level of the receiver circuitry. In SCM systems of this nature, the composite-signal clipping distortion is computed as a contributory noise component for each channel in the system [29],[30],[31], potentially lowering SNRs. Gorfinkel and Luryi [6] studied this using a MQW laser and showed that in an 80-channel CATV system m_{ch} must be below 0.045. However, sensitive, low-noise optical detectors/receivers are readily available, and m_{ch} can be very small the before SNR requirements for a channel are jeopardized by the use of a direct IM transmission system.

3.4 The Problem with Non-linearity

Equation (3.5) represents the ideal linear performance relationship for the device. However, no real system or device is in any way purely linear. This reality is the cause of signal degradation in optical sources.

Most LDs appear to have a linear L-I characteristic for signals below 600 MHz, and are suitable for direct intensity modulation in analogue signal applications having 'low' bandwidth requirements. However, direct modulation using higher frequencies causes the inherent dynamic non-linearity to become much more significant and even visually recognizable (see Figure 3.4). This distortion limits broadband system capac-

ity and cannot be eliminated by adjusting the static bias point for the LD. Figure 3.6 confirms that a 66 μA sinusoid biased at 500 μA — like those shown in Figures 3.4 and 3.5 — would not suffer any significant distortion due to saturation or clipping effects. Often in systems, non-linear distortion from LDs is related to only the frequency of the modulating signal and the resulting dynamic activity within each device.

Distortion caused by the dynamic non-linearity in LDs, primarily due to the cavity resonance and carrier—photon interactions, peaks at what is known as the relaxation–oscillation (R-O) frequency. This frequency is dependent on, among other things, the LD bias point, and is expressed as [1],[23],[22]

$$f_r = \frac{1}{2\pi}\left[\frac{N_o\Gamma g\tau_p + 1}{\tau_s\tau_p}\right]^{\frac{1}{2}}\left[\frac{J}{J_{th}} - 1\right]^{\frac{1}{2}} = \frac{1}{2\pi}\left[\frac{gS_b}{\tau_p}\right]^{\frac{1}{2}} \quad . \tag{3.8}$$

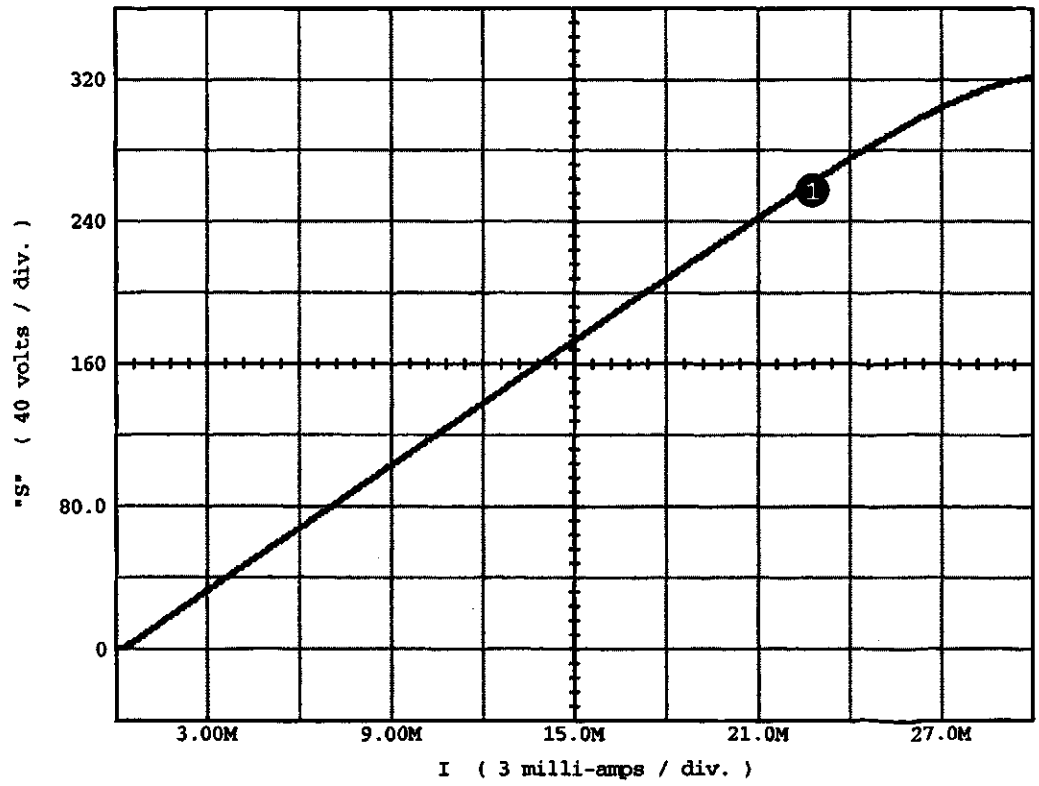

Figure 3.6: Simulated Static Light vs. Current Characteristic for Laser 'A'
Optical power is proportional to the LD photon density, S, represented by ICAP/4 as a voltage where 1 volt = 1E20 photons/m^3.

Darcie and Bodeep [32] show that LDs having an f_r of approximately 7 GHz should be capable of meeting the stringent distortion requirements for 60- to 75-channel CATV systems.

Realistically, and unlike Equation (3.5), a LD operating above its threshold may be considered to have a non-linear characteristic. That can be expressed by the Taylor expansion

$$y = c_0 + c_1 x + c_2 x^2 + c_3 x^3 + c_4 x^4 + c_5 x^5 + \cdots , \tag{3.9}$$

where x and y are the input and output signals, respectively, and c_0, c_1, c_2, etc. represent Maclaurin series coefficients.

If the input signal is time-varying with only one frequency, say $x(t) = A \sin \omega_1 t$, then the output will have terms with frequencies at $2f_1$, $3f_1$, etc. These higher order terms contribute to harmonic distortion (HD), a performance measure computed by comparing the power or amplitude of a certain spectral term to that of the fundamental signal. Because Equation (3.9) could be expanded up to the fifth term to become

$$y(t) = c_0 + \frac{c_2 A^2}{2} + \frac{3c_4 A^4}{8} + \left(c_1 A + \frac{3c_3 A^3}{4} \right) \sin \omega_1 t - \left(\frac{c_2 A^2}{2} + \frac{c_4 A^4}{2} \right) \cos 2\omega_1 t$$

$$- \frac{c_3 A^3}{4} \sin 3\omega_1 t + \frac{c_4 A^4}{8} \cos 4\omega_1 t + c_5 \left[x(t) \right]^5 + \cdots , \tag{3.10}$$

it is possible to show that the second-order harmonic distortion, HD_2, takes the form expressed as

$$\mathrm{HD}_2 \ (\mathrm{dB}) = 20 \log \left[\frac{\left| -\frac{1}{2} c_2 A^2 - \frac{1}{2} c_4 A^4 + \cdots \right|}{\left| c_1 A + \frac{3}{4} c_3 A^3 + \cdots \right|} \right] . \tag{3.11}$$

When considering broadband SCM systems like that of CATV over fiber, there can be very many carrier frequencies modulating the LD. As such, some of the HD components often contribute to the noise experienced by other channels. Although

HD components usually do not individually cause major system problems, they are related to other distortion effects and are simple, apparent indicators of non-linearity within a system.

If the input signal contains the two frequencies, f_1 and f_2, equal in amplitude, the output will contain the additional mixed products at $f_1 + f_2$, $f_1 - f_2$, $2f_1 + f_2$, etc. [33, pp.224–227]. Then mathematically from Equation (3.9), after substituting the sinusoidal input $x(t) = A\sin\omega_1 t + A\sin\omega_2 t$, expanding and simplifying the terms with c_1, c_2 and c_3, the LD output becomes

$$\begin{aligned} y(t) \;=\; & c_o + c_2A^2 + \left(c_1A + \frac{9}{4}c_3A^3\right)(\sin\omega_1 t + \sin\omega_2 t) - \frac{c_2A^2}{2}(\cos 2\omega_1 t + \cos 2\omega_2 t) \\ & - c_2A^2\Big[\cos(\omega_1+\omega_2)t - \cos(\omega_1-\omega_2)t\Big] - \frac{c_3A^3}{4}(\sin 3\omega_1 t + \sin 3\omega_2 t) \\ & - \frac{3c_3A^3}{4}\Big[\sin(2\omega_1+\omega_2)t - \sin(2\omega_1-\omega_2)t + \sin(\omega_1+2\omega_2)t \\ & + \sin(\omega_1-2\omega_2)t\Big] + c_4\Big[x(t)\Big]^4 + c_5\Big[x(t)\Big]^5 + \cdots \quad . \end{aligned} \tag{3.12}$$

The mixed product terms (where more than one frequency is required to evaluate the term) are called intermodulation products (IMPs). These terms, such as

$$-\frac{3c_3A^3}{4}\Big[\sin(2\omega_1+\omega_2)t\Big] \quad ,$$

are caused by the different input signals (and their harmonics) interacting with each other. Each IMP is not part of the input signal, and contributes to what is collectively called intermodulation distortion (IMD).

For a LD and other systems or devices that are very nearly linear, the magnitudes of the coefficients in the appropriate equations similar to Equations (3.9) and (3.12) quickly decrease as the series expressions progress beyond the square-law terms. Chiddix *et al.* [1] have shown that, because signal distortion typically becomes insignificant

to system engineers beyond the third-order IMPs, the key optical analogue system performance measures for distortion are composite second-order (CSO) and composite triple beat (CTB). These measures are usually applied to each channel within a CATV or SCM system.

The CSO measure is computed by collecting all of the in-band second-order IMPs, or ones containing the sum or difference of two input carrier frequencies, and comparing that to the signal component for the channel of interest. This is done on a power basis and can be calculated for SCM systems using the equation

$$\text{CSO (dB)} = 10\log\left(\frac{\text{sum of power from in-band second-order IMPs}}{\text{carrier power for the channel}}\right) . \quad (3.13)$$

Similarly, CTB is the power comparison of all the in-band third-order IMPs, such as $2f_1 + f_2$, $2f_1 - f_2$ or $f_1 - f_2 + f_3$, to the carrier for the channel of interest. Again, for SCM systems where the information signal for each channel varies with time, the carrier strength of the channel is used, giving

$$\text{CTB (dB)} = 10\log\left(\frac{\text{sum of power from in-band third-order IMPs}}{\text{carrier power for the channel}}\right) . \quad (3.14)$$

The impact of LD non-linearity on SCM system measures, CSO and CTB, can vary with the carrier frequency offsets chosen. In order for CATV systems to manage CSO, CTB and other issues, regulations for that industry permit a choice from among three slightly different carrier–frequency allocation schemes [7, p.94,p.174]: Standard; harmonically related carriers (HRC); and incremental coherent carriers/incremental related carriers (ICC/IRC). In the Standard scheme, the second-order IMPs do not all share the same offset from the channel carrier. In HRC systems, all second- and third-order IMPs fall in-band, exactly on the carrier. But the ICC/IRC scheme creates the least perceivable CSO and CTB problems, mainly because it places more of the second- and third-order IMPs outside (on the edge) of the channel bandwidths than the other two options. Therefore, it is possible to slightly reduce the non-linearity problem in SCM systems if the designer has some channel placement flexibility.

3.5 Optical Distortion due to LD Dynamic Non-linearity

Table 3.2 shows a fast–Fourier transform (FFT) analysis of the photon density from the simulated model of Laser 'A'. The laser was driven by a 1 GHz sinusoid having a 66 μA amplitude and a 500 μA bias. The photon density produced has a bias level of approximately 2.521E20 photons/m^3 and a fundamental or carrier amplitude of approximately 0.866E20 photons/m^3. The HD_2 and HD_3 in the optical output are both shown as -24.0 dBc and -24.1 dBc, respectively.

Table 3.2: Harmonic Distortion from Laser 'A' Operating at 1 GHz

Frequency in GHz	Signal Amplitude in 1E20 photons/m^3	Signal Amplitude in dBc	Phase wrt sine-referenced Input in Degrees
0	2.52118	...	...
1	0.865786	0.0	-6.1004
2	0.0547101	-23.9869	44.1201
3	0.0537584	-24.1393	56.9984
4	0.0222401	-31.8055	1.50449
5	0.00389746	-46.9326	-47.473
6	0.000453131	-65.6237	-26.338

Figure 3.7 illustrates the signal strength of the second, third and fourth harmonic distortions across a range of input frequencies up to 1 GHz. As the input signal frequency increases toward the R-O frequency for this device, it can be observed that distortion levels become progressively worse.

Analogue video applications are very sensitive to any signal distortion. This challenge is stated by the requirements in Table 1.1. Sub-carrier multiplexing systems face an even greater challenge when they attempt to concentrate and transmit an increased number of channels. Because CSO and CTB calculations use the sums of IMP powers, channel–count works against performance quality. As SCM networks grow in channel capacity, or channel–count, so do the number of IMPs [6],[7],[5, pp.182–183]. Considering that IMPs originate from unique combinations of carrier frequencies present within the SCM signal, this IMP increase due to channel–count

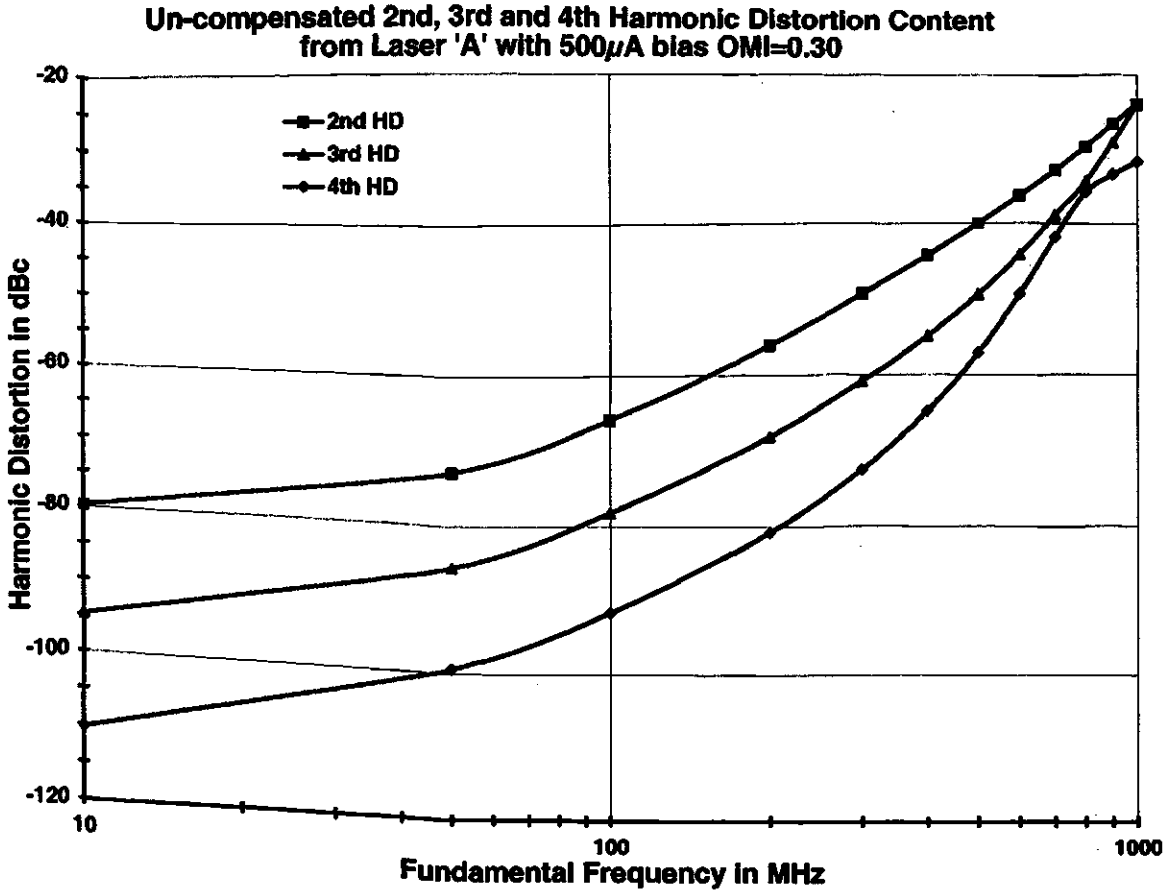

Figure 3.7: Harmonic Distortion Content vs. Frequency for Simulated Laser 'A' using Direct Intensity Modulation and a Sinusoidal Signal

can be illustrated by Figure 3.8. However, if N_{ch} increases, the per–channel modulation index, m_{ch}, is often decreased to avoid signal clipping, meaning the carrier power for each multiplexed channel decreases, too. This, then, forces the CSO and CTB distortion measures up, closer to performance failure limits.

3.6 Methods to Improve Light Source Linearity

Because the linearity of an optical transmitter can be closely related to the transmission capacity for a system, work by Angenent [34], by Chung and Jacobs [31] and by Gorfinkel and Luryi [6] has focused on defining device and system relationships. These relationships help designers select optimal performance arrangements,

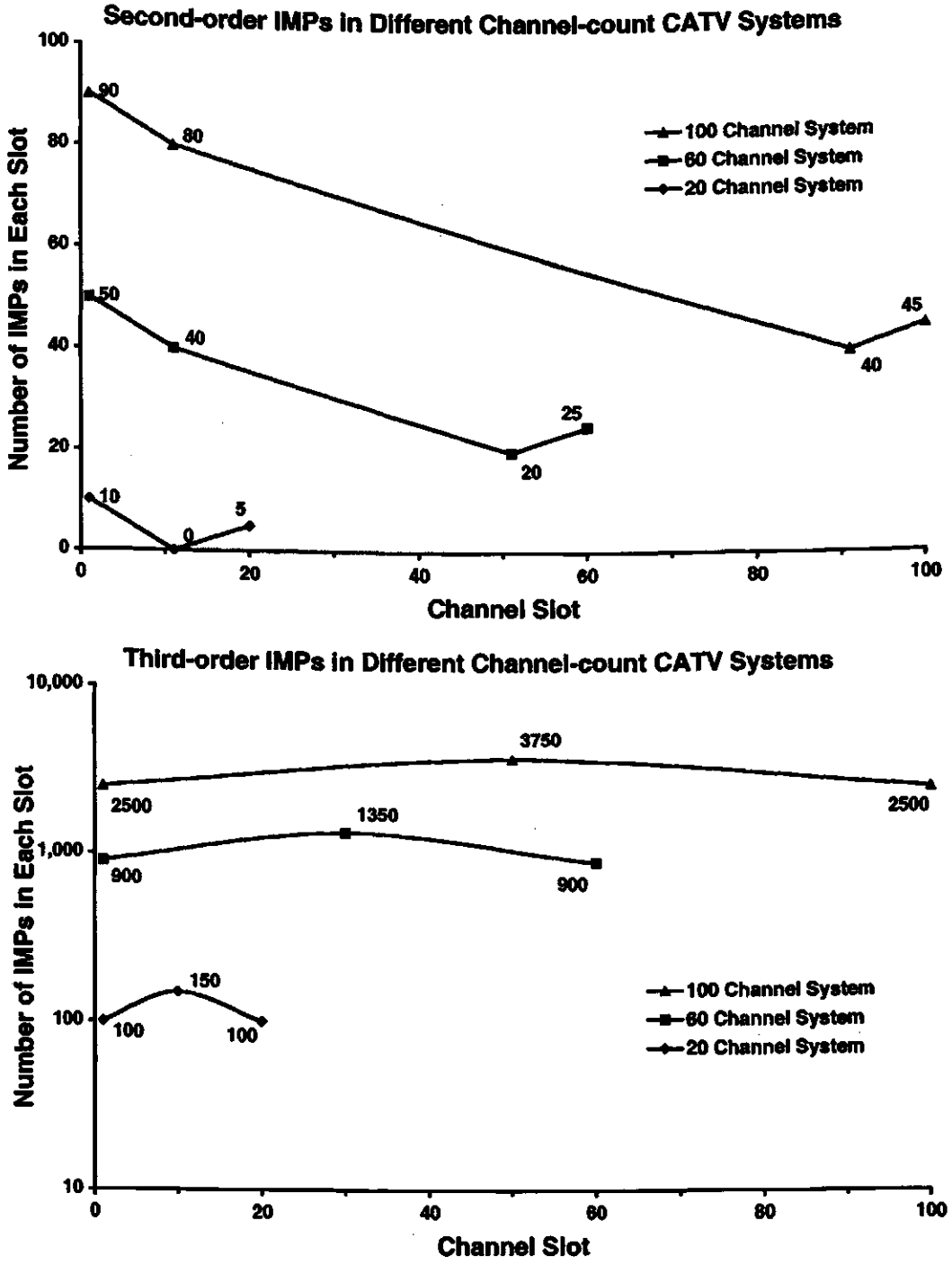

Figure 3.8: Occurrence of Second- and Third-order Intermodulation Products contributing to Distortion in CATV Systems
Illustrations were adapted from [6], [7, p.163] and [5, p.183], and use values calculated from only the fundamental, or channel carrier, frequencies.

and identify if necessary requirements are even achievable. The obstacle that the dynamic non-linearity in LDs poses for 'high–frequency', direct IM links has led to the studying of alternatives and variations for the transmitter modules.

One alternative could be to use a highly linear external modulator immediately after a non-modulated, continuous wave (CW) laser. External modulators such as Mach–Zehnder (MZ) devices exist, but they do not provide perfectly linear modulation and can significantly add to the optical loss of a system. Consequently for high channel–count SCM systems, the non-linear output from a MZ device remains a problem; work by Sabella [3] and by Darcie and Bodeep [32],[35] indicates that, when compensation is used, lower levels of distortion may be achievable from a direct IM source in comparison to a CW LD with an external modulator.

Several distortion compensation methods that address LD non-linearity have been discussed by Sieben [9]. For ease of implementation, a pre-distortion approach is often the preferred method of compensation. Sieben's reasoning and choice do not stand in isolation, since Lucent Technologies [36] and others [37] have chosen a simplified form of this method for recently available optical CATV transmitter modules.

Although Sieben's research did not allow him to successfully demonstrate a working pre-distortion circuit, his use of Volterra analysis to achieve a simulated solution proved to be a capable approach and encouraged further study. He was able to simulate a combined electrical distortion circuit and LD model, demonstrating the potential of a pre-distortion solution. His derivations and analysis followed those published earlier by Biswas and McGee [20], and have been highlighted in Appendixes A and B as a basis for the extended work presented in this thesis.

3.7 Volterra Analysis of LD Non-linear Distortion

A pre-distortion approach is much like a post-distortion approach, except that the compensation is applied to the signal before modulation distortion occurs. Because the input current for a LD can be expressed in terms of its photon density more easily than the reverse, Biswas and McGee [20] and Sieben [9] applied a post-distortion approach. They manipulated Equations (3.3) and (3.4) so that the current could be

determined from the photon density, and a post-distortion system was in hand.

The expression derived for a post-distortion system capable of addressing LD distortion up to the third-order is

$$\begin{aligned} i &= a + bs + cs' + ds'' + es^2 + fss' + gss'' + hs's' \\ &\quad + ks^3 + ls^2s' + ms^2s'' + nss's' \quad , \end{aligned} \tag{3.15}$$

where $i = i(t) = I(t) - I_b$, $s = s(t) = S(t) - S_b$ and a, b, c, etc. are constants determined from device parameters and bias levels, as explained in Appendix A. Equation (3.15) can be considered to represent a non-linear time–invariant system, if temperature and other variables are neglected. The system has no memory, and its performance is frequency sensitive. This is due to the facts that there are no time offset terms, and that there are derivatives of s with respect to time. Such a system can be re-defined by using Volterra analysis, as has been shown by Narayanan's work with transistors [38],[39] and Biswas and McGee's work with LDs [20].

In order to reduce the non-linear distortion that occurs in LDs with 'high–frequency' signals, the idea of first highlighting and then maybe eliminating the frequency sensitivity of the device was seen as a possible solution. By following this approach, Volterra analysis promised much help. When applied to the LD post-distortion expression, Equation (3.15), Volterra analysis could then identify the systems and functions required to compensate for the frequency sensitivity in light source modules.

The Volterra approach permits Equation (3.15) to be thought of in a form similar to Equation (B.2), expressed as $i(t) - a = \boldsymbol{D_1}[s(t)] + \boldsymbol{D_2}[s(t)] + \boldsymbol{D_3}[s(t)]$. If the constant a is ignored, the new form of the expression can be represented by the block diagram of the distortion system shown in Figure 3.9, where $\boldsymbol{D_1}[\cdot]$, $\boldsymbol{D_2}[\cdot]$ and $\boldsymbol{D_3}[\cdot]$ are the respective first-, second- and third-order Volterra operators. In parallel, these operators form a complementary opposite distortion system, specific to LDs.

The distortion system operators each have a representative transfer function, and

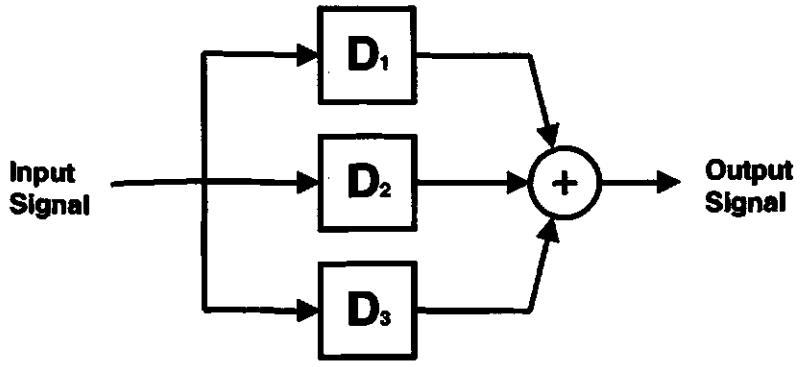

Figure 3.9: Block Diagram of Third-order Volterra Distortion System

have been identified through the derivations in Appendix B.1. The derivation method follows the particular system excitation and analysis approach used by others in previous work [5, pp185–187],[20],[9]. The method uses the premise that different aspects of the distortion system can be revealed if a specific excitation or 'probing' is provided.

To define the first-order function, $D_1(j\omega_1)$, the post-distortion expression in Equation (3.15) was 'probed' by setting $s = s_{pk}e^{j\omega_1 t}$ and used s_{pk} to represent a time–invariant peak magnitude. The result was arranged to take the form $D_1(j\omega_1)e^{j\omega_1 t}$, so that $D_1(j\omega_1)$ could be identified. Then $D_2(j\omega_1, j\omega_2)$ was similarly found by 'probing' with $s = s_{pk}\left(e^{j\omega_1 t} + e^{j\omega_2 t}\right)$ and noting the coefficients of the terms containing $e^{j(\omega_1+\omega_2)t}$. And finally, $s = s_{pk}\left(e^{j\omega_1 t} + e^{j\omega_2 t} + e^{j\omega_3 t}\right)$ was used in Equation (3.15) so that $D_3(j\omega_1, j\omega_2, j\omega_3)$ could be equated to coefficients of terms containing $e^{j(\omega_1+\omega_2+\omega_3)t}$.

The Volterra transfer functions for the third-order LD post-distortion system have been identified as

$$D_1(j\omega_1) = s_{pk}\left(b + j c\omega_1 - d\omega_1^2\right) \quad , \tag{3.16}$$

$$D_2(j\omega_1, j\omega_2) = s_{pk}^2\left(2e + jf(\omega_1+\omega_2) - h(\omega_1+\omega_2)^2\right) \quad \text{and} \tag{3.17}$$

$$D_3(j\omega_1, j\omega_2, j\omega_3) = s_{pk}^3\left(6k + j2l(\omega_1+\omega_2+\omega_3) - 2m(\omega_1+\omega_2+\omega_3)^2\right) \quad . \tag{3.18}$$

It has been shown in Appendix B.2 that these three Volterra transfer functions create the block system with time-domain functions, as illustrated in Figure 3.10. Since this system definition may affect signal compensation for a LD, either before or after the electro-optic device, it can be applied before the LD, normalized for the different, but appropriate, input and output values and used as a pre-distortion system instead.

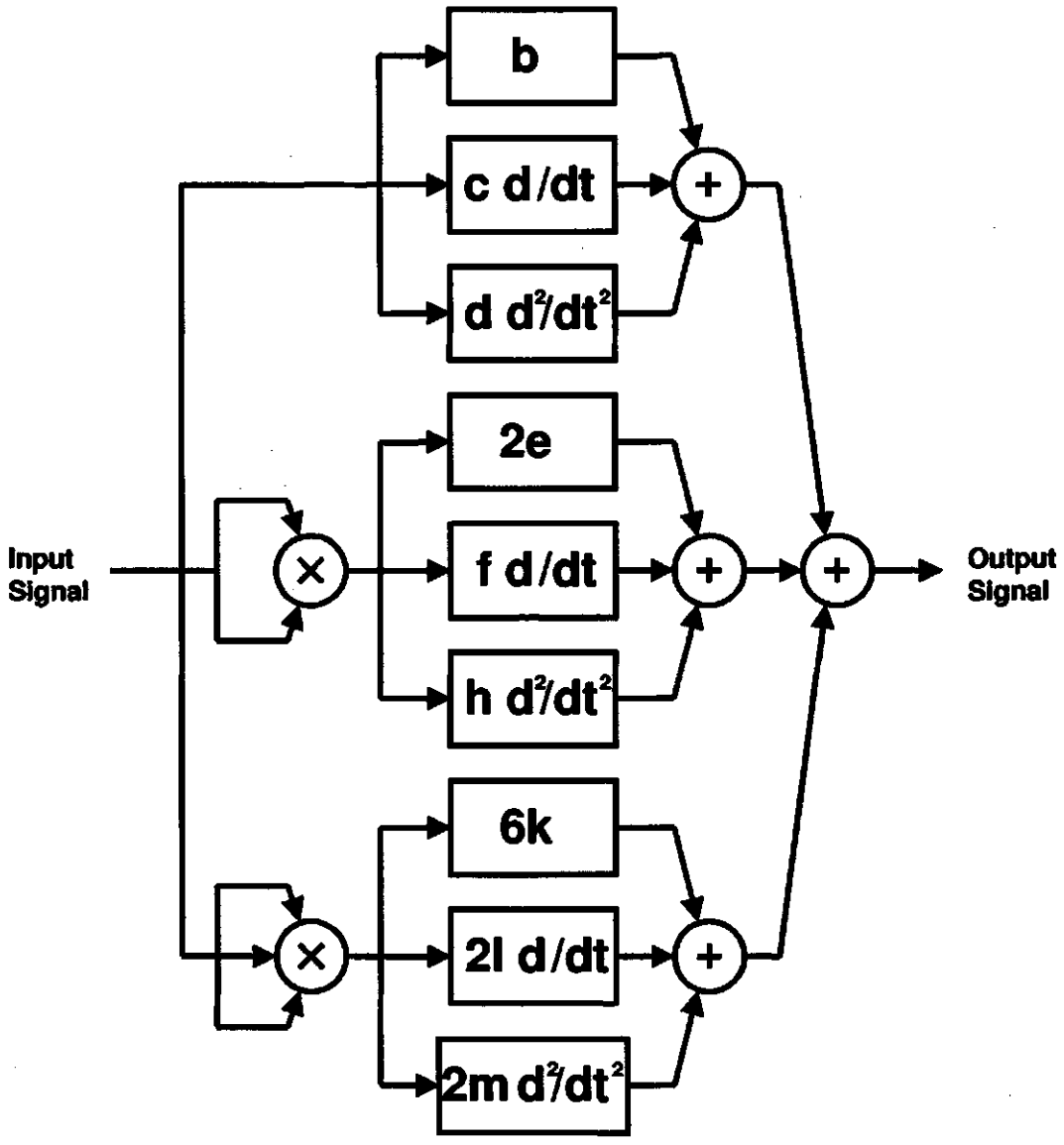

Figure 3.10: Distortion System Structure that Compensates for Dynamic Non-linearity in a LD

On observation of the third-order Volterra distortion system, it should be noted that a common structure (see Figure B.2) presents itself three times. On each occasion of appearance in Figure 3.10, the structure operates on a different variation of the input signal — the fundamental, squared and cubed versions of the input waveform. Although each of the three structures has uniquely different coefficient values, each produce a frequency–dependent signal modification that can be similarly explained by the phasor diagram in Figure 3.11.

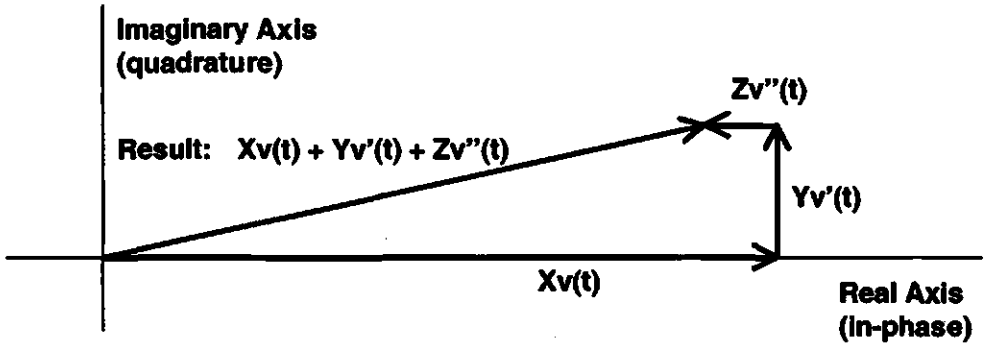

Figure 3.11: Phasor Diagram of the Common Structure Sub-system in the Volterra–developed Distortion System

From Figure 3.11, whether $v(t)$ represents the fundamental, squared or cubed version of the real input signal, it can be seen that each of the common structure sub-systems affect a change to the magnitude and phase of its input phasor, $v(t)$. For the fundamental branch of Figure 3.10, the constant coefficients b, c and d could respectively replace the arbitrary fixed-value coefficients X, Y, and Z in Figure 3.11. The squared-law and cubed-law branches could be similarly considered.

Because the distorter coefficients depend on the characteristics and bias conditions of the LD, b, c, d, etc. can be considered constants during normal operation. This means that each of the resulting phasors from the common structures have a magnitude and phase that varies directly with the frequency of the respective $v(t)$. By looking at the signs ($\pm$) of the distorter coefficients (calculated in Appendix C), it appears that as the frequency of the input signal grows, the fundamental branch produces a resulting phasor of decreasing magnitude and advancing phase. Similarly,

both the squared-law branch and cubed-law branch produce phasors of decreasing magnitude and advancing phase. The sum of the three branches becomes the signal output from the Volterra–developed distortion system.

3.8 Chapter Summary

The content in this chapter built on the understanding gained in Chapter 2. Here two rate equations, expressing both the electrical carrier and photon densities within a LD, have been introduced. Within this chapter, it has been shown how these two equations can be transformed into an equivalent 'circuit' model, and then used to simulate real LD performance. While doing this, a quantitative characterization of the LD transient behavior has been presented. The non-linear distortion produced during device operation across a broad band of modulation frequencies has also been determined and recorded, to provide a foundation for later results.

The chapter contained an overview of the present application environment most challenging to LD performance: direct intensity modulation using a broadband SCM signal. System performance measures dealing with signal distortion, such as HD, CSO and CTB, have been reviewed, and the relations to LD operation discussed. This chapter was then concluded with an explanation of a favored approach to LD distortion compensation. That approach used Volterra analysis, and has defined a complementary opposite pre-distortion system structure that will be developed further in a later chapter.

Chapter 4

Adaptive Pre-distortion for Non-linear Components

4.1 Conceptual Approach

If the distortion from a non-linear device is to be minimized using a pre-distorter, certain amplitude and phase characteristics that are the exact inverse match (or complementary opposite) of the device must be produced by the pre-distorter. The optimal characteristics of a pre-distortion circuit can be determined during its design. However, in circumstances where it is useful to maintain a good inverse match in times of system variability, the pre-distorter characteristics may be actively controlled and adapted during ongoing operation.

Work by Ghaderi on adaptive linearization of power amplifiers for RF applications [40] provides a basis for the employment of a similar concept using laser diodes. His thesis examined methods for the dynamic adjustment of pre-distortion circuit coefficients. He showed that gradual changes occurring in the non-linear device can be tolerated by a pre-distorter, and near optimal system performance maintained.

Ghaderi applied signal processing to a tapped portion of the modulated power amplifier output. He then adjusted the necessary distortion system coefficients using the error (or difference) between the pre-distorter and the signal processing circuit at the system output.

Because the signal processing applied to the tapped portion of the amplifier output was very similar to the pre-distorter, it may be thought of as a *post*-distortion

system. This post-distorter should not, however, directly contribute to the output signal improvements. It was used to evaluate the ongoing complementary opposite match condition of the signal pre-distorter to the non-linear amplifier. If the match condition differed from the designed setting, coefficients in both the distorters would be actively adjusted to maintain optimal performance.

Application of the adaptive pre-distortion concept within the design of an optical transmitter would allow the module to compensate for temperature and aging affects, or any other long–term variations relative to the modulating signal frequency. The signal flow and the block processes necessary for implementation of such an optical transmitter are shown in Figure 4.1.

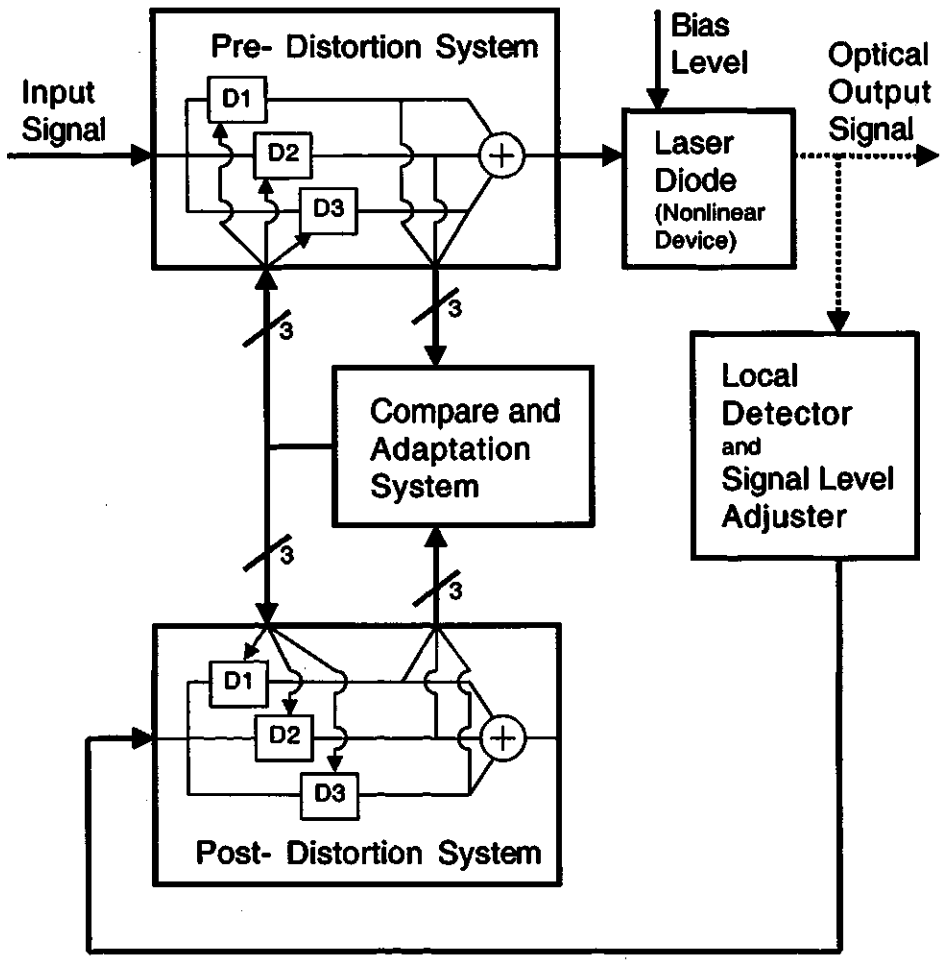

Figure 4.1: Concept of a Pre-distorted LD with Adaptive Feedback

Figure 4.1 shows that the signal path in this feedback system is not directly closed, and that it is not completely electrical. Combining these observations, and the fact that any stable closed-loop control system must have a time constant shorter than the event period it is intended to address, helps in recognizing that this system does not employ a traditional electrical feedback approach. Although the adaptive nature of this system concept involves a feedback loop, it is important to note that its design is not intended to provide any real-time adjustments that compensate for the instantaneous signal distortion caused by the dynamic non-linearity of a laser diode. The signal frequencies for which dynamic distortion compensation is needed are simply too high to avoid the system instabilities that would result if the complementary opposite distortion was controlled directly and instantaneously by an electrical feedback loop.

In the non-traditional feedback approach considered here, the pre-distortion from the Volterra–based system provides the needed frequency dependent signal distortion, while the distortion system feedback signals contribute only indirectly to system performance. This feedback is used to adapt the pre-distorter coefficients to the significant but small and slow changes that occur within the modulated 'device'. Similar to Ghaderi's work, control of the adaptable distortion coefficients is provided by using the comparative analysis of the pre- and post-distortion systems.

4.2 Trial of Concept

The system shown in Figure 4.2 can be used to simulate and explore the concept of adaptive pre-distortion. Because it has been previously noted in other publications that pre-distortion solutions for an optical system can be extremely sensitive to distortion system design implementations [5, pp.11–13],[32], it was felt that any adaptive version of the pre-distorter would require a similarly sensitive control definition. The trial–of–concept (TOC) will use third-order distortion compensation systems and highly precise comparison operations. The simplistic system in Figure 4.2 contains only some elements of a conceptual pre-distorted LD module, but will permit a better focus on the adaptive functions.

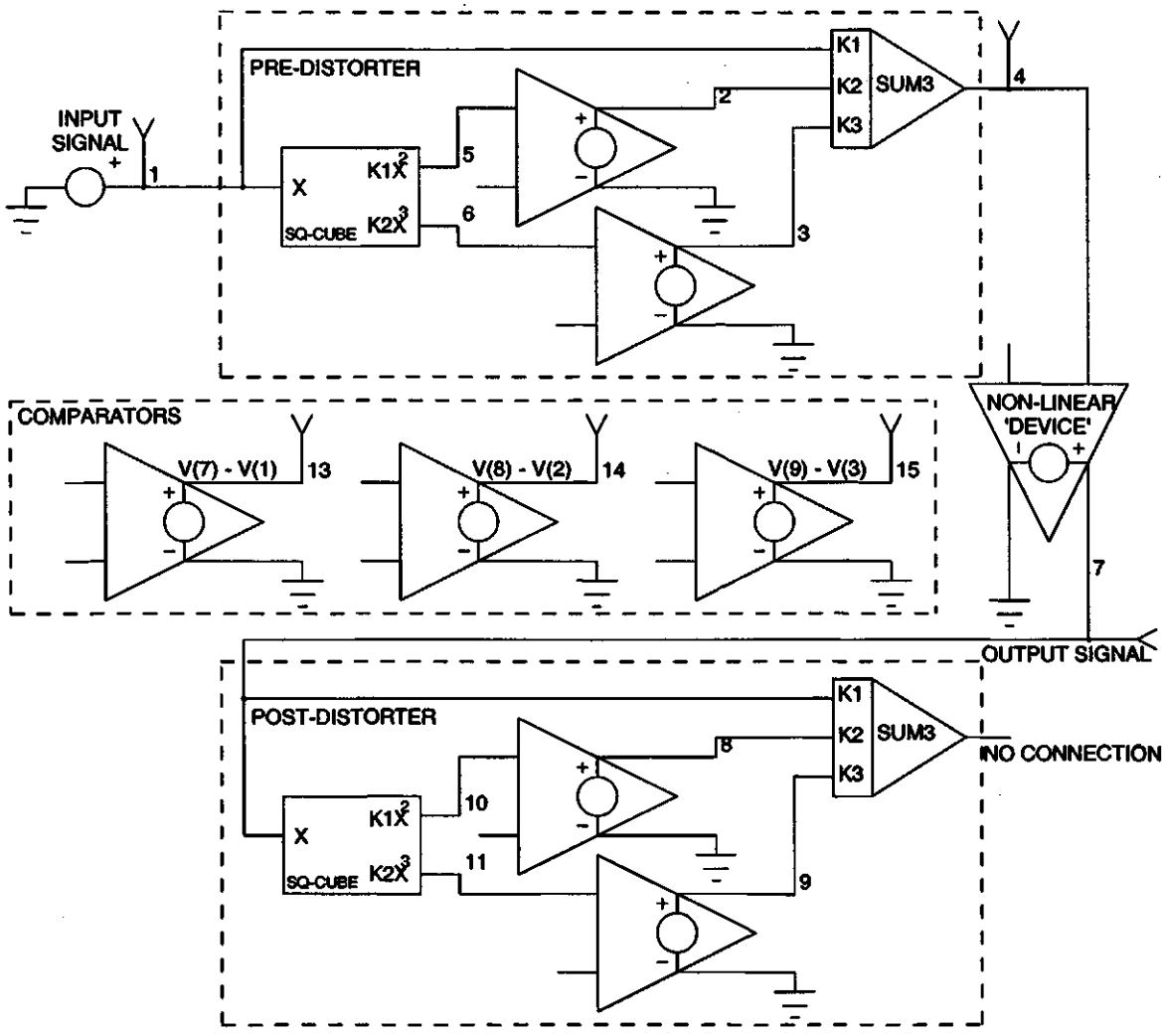

Figure 4.2: Simulated System for Exploring an Adaptive Pre-distortion Concept in ICAP/4
The netlist can be found in Appendix D.2.

The ICAP/4 system schematic shown contains a non-linear 'device' that loosely corresponds to a LD. Exact operations will be explained later. The third-order distortion systems are attached immediately before and after the non-linear 'device'. Both distortion systems are theoretically identical, and are constructed to allow their corresponding coefficients to be equally altered according to the signal difference between corresponding system nodes. Even though the coefficients within both distortion systems can be optimized, and set for operation with a specific non-linear 'device', the

adaptation rule(s) may need to overlook some slight signal differences between the two systems. The differences will be caused by the fact that both distortion system inputs cannot be truly identical.

If the optimal pre-distortion characteristics could produce an exact inverse match to the non-linear 'device' distortion, the post-distorter input, node 7, would be identical to the overall system input. But because a pre-distortion system is only a finite-order approximation of the complementary opposite to the non-linear 'device', some distortion will always be present in the overall system output signal. By using the post-distorter to help characterize the amount of distortion present in the output signal under optimal pre-distortion conditions, any deviation from these reference levels can help indicate a need for re-optimizing the inverse match conditions.

This simulated TOC will use linear relationships to affect the adaptive control on the distortion system coefficients. Voltages at nodes 2, 3, 8 and 9 will reflect the distortion system signal changes that are computed relative to the preset optimal coefficient values. For adaptive purposes their control will be based on the differences between the pre- and post-distorters, as determined by the comparators. All the function blocks used within the two distortion systems and the three comparison operations will be ideal. Therefore, any distortion system signal differences detected by the comparators will be due to the distortion present in the overall system output signal at node 7. In theory, this will only happen when the inverse match of the pre-distorter to the non-linear 'device' has not been maintained.

Before investigating the adaptive abilities of the simulated circuit, an initial set of distortion system coefficients must be identified and the compensative performance noted. A change to the non-linear 'device' will then be made to simulate aging, or a departure from the original optimal match condition. After applying the 'device' change, a new match must then be determined by altering the distortion system and restoring its complementary opposite performance. Through the consideration of the necessary manual coefficient alterations that will take place, expressions or rules can be defined that complete the development of a self-adaptive concept for this TOC system.

4.3 Discussion of Results

Because the purpose of this trial was to investigate the development of an adaptive algorithm that allows the pre-distortion system to address LD aging and temperature changes, and that the pre-distortion system was presumed to already address any necessary frequency dependent distortion issues, frequency was considered a constant within the scope of this TOC investigation. As such, the non-linear 'device' in this chapter was not given a frequency dependent characteristic and could be expressed using the simple series equation

$$y_{V7}(t) = c_0 + c_1 x_{V4}(t) + c_2 x_{V4}^2(t) + c_3 x_{V4}^3(t) \quad , \tag{4.1}$$

where $c_0 = 0$, $c_1 = 1$, $c_2 = 0.1$ and $c_3 = 0$. The time–varying signal at system node 4 in Figure 4.2 was represented as $x_{V4}(t)$, and the output voltage at node 7 as $y_{V7}(t)$.

The two identical distortion systems (pre- and post-) were expressed as

$$y_d(t) = c_{d1} x_d(t) + c_{d2} x_d^2(t) + c_{d3} x_d^3(t) \quad , \tag{4.2}$$

where $x_d(t)$ can represent the input signals at nodes 1 and 7, and $y_d(t)$, the output signals at respective nodes 4 and 12.

The distortion systems expressed in Equation (4.2) were initially given the manually optimized coefficient settings of $c_{d1} = 1$, $c_{d2} = -0.105521$ and $c_{d3} = 0.021804$. This was because their preset values were chosen expecting Equation (4.1) to hold true, representing a stable non-linear device. In this way, baseline results were determined, allowing the later development of an adaptive system.

For visual reference, Figure 4.3 shows the input and output waveforms collected during the simulation of the Figure 4.2 system. Initially, no adaptive operations were applied. The voltage waveforms displayed were acquired using the 'transient analysis' simulation mode of ICAP/4 and are labeled with the corresponding node number in parentheses. The harmonic distortion in the TOC output was determined using a 1 GHz sinusoidal signal, and are shown in Table 4.1. These numeric results were

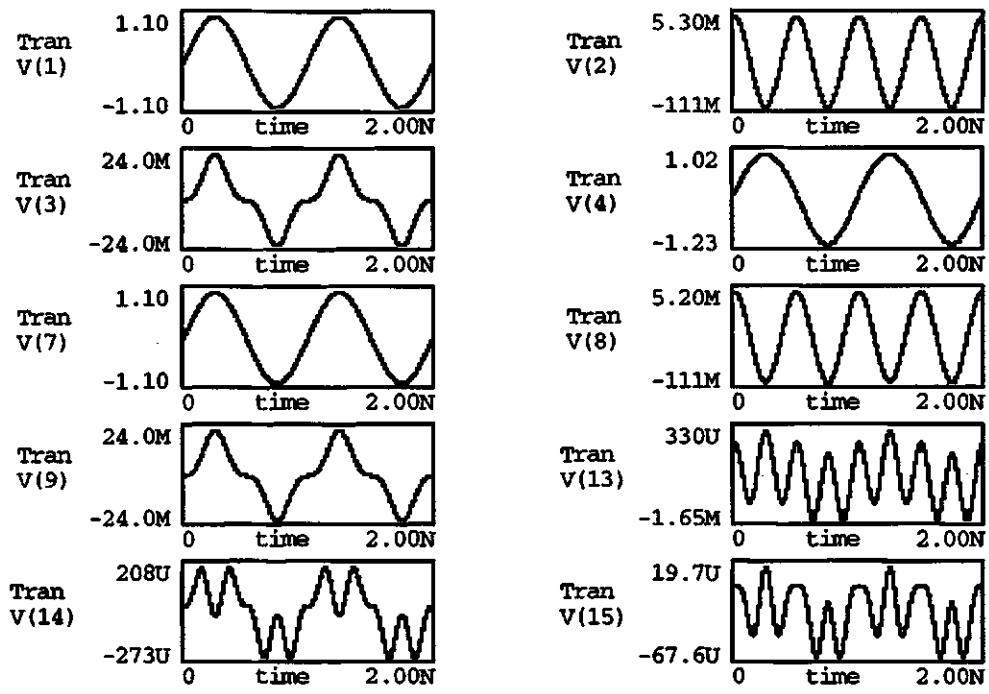

Figure 4.3: Waveforms from Trial of Concept System using Baseline Settings

Table 4.1: Harmonic Distortion from Trial of Concept System using Baseline Settings

Frequency in GHz	Signal Amplitude in volts	Signal Amplitude in dBc	Phase wrt sine-referenced Input in Degrees
0	-0.00069279	...	...
1	1.00024	0.0	1.17842E-10
2	0.00000108198	-119.318	90
3	0.0000311513	-90.4448	180
4	0.000693199	-63.1849	90
5	0.0000287598	-90.8264	180
6	0.00000148568	-116.564	-90

identified by using FFT analysis tools.

Next, the value of c_2 in Equation (4.1) was changed to 0.102. This was done to simulate an aging effect within the non-linear laser–like component in Figure 4.2. Waveforms collected during this simulation are shown in Figure 4.4, also using the same input sinusoid at 1 GHz. The output signal FFT results are shown in Table 4.2.

These new waveforms may be compared to the un-'aged' ones in Figure 4.3. Although the 'aged' and un-'aged' waveforms at node 7 look very similar, comparison of the waveforms at nodes 13, 14 and 15 indicate that an 'aging' effect has degraded performance.

Nodes 13, 14 and 15 represent the comparative signal differences between corresponding nodes in the pre- and post-distortion systems. The representative operations have been expressed as

$$y_{V13}(t) = x_{V7}(t) - x_{V1}(t) \ , \tag{4.3}$$

$$y_{V14}(t) = x_{V8}(t) - x_{V2}(t) \ \text{and} \tag{4.4}$$

$$y_{V15}(t) = x_{V9}(t) - x_{V3}(t) \ , \tag{4.5}$$

where $x(t)$ and $y(t)$ respectively are input and output voltages for the difference comparisons, and the subscript designators refer to the voltage node numbers found in Figure 4.2. These difference signals will be used to calculate the relative change needed for adapting the distortion system coefficients during simulated system aging conditions.

When the peak-to-peak range of the difference signals at nodes 14 and 15 change from the values produced during un-'aged', optimal operation, it can be visually recognized that the second and third harmonic distortion components produced by the non-linear 'device' in the post-distortion system become significantly different from those of the pre-distorter. Because of this, the magnitude of the comparison operations can be used to adjust the pre- and post-distorter coefficients, allowing the

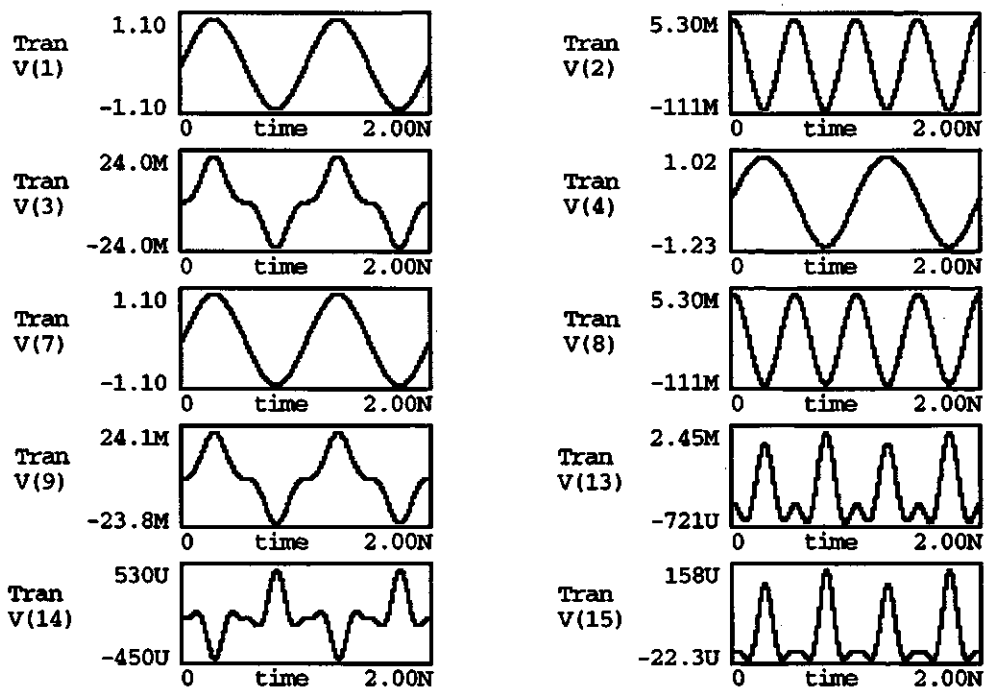

Figure 4.4: Waveforms from 'Aged' Trial of Concept System with Fixed Pre-distortion

Table 4.2: Harmonic Distortion from 'Aged' Trial of Concept System with Fixed Pre-distortion

Frequency in GHz	Signal Amplitude in volts	Signal Amplitude in dBc	Phase wrt sine-referenced Input in Degrees
0	0.00034856	...	...
1	0.999915	0.0	1.179E-10
2	0.00105411	-59.5415	-90
3	0.0000772457	-82.2418	9.4839E-07
4	0.000707063	-63.0101	90
5	0.0000293350	-90.6515	180
6	0.00000151539	-116.389	-90

TOC system itself to compensate for the changes in the non-linear 'device'.

In order to confirm that adjustment of the pre-distorter coefficients could be controlled by the comparison operations, coefficients settings of $c_{d1} = 1$, $c_{d2} = -0.10785$ and $c_{d3} = 0.02262$ were applied, while the non-linear 'device' coefficient, c_2 in Equation (4.1), remained 'aged' at 0.102.

Because very small coefficient changes were required to address the 'aging' effect studied, and any other approach would only unnecessarily complicate the adaptive operation of the overall system, it can be understood that a linear scheme will be suitable for controlling the coefficient adjustments. The adaptive coefficient expressions were then constructed using minimum and maximum peak values from signals y_{V14} and y_{V15}. The two identical distortion systems remain as expressed in Equation (4.2), but now use coefficient values defined by the expressions

$$c_{d1} = 1 \ , \tag{4.6}$$

$$c_{d2} = -0.105521 - 0.002329 \left(\frac{(\text{MAX}[y_{V14}] - \text{MIN}[y_{V14}]) - 438\text{E-}6}{34\text{E-}6} \right) \quad \text{and} \tag{4.7}$$

$$c_{d3} = 0.021804 + 0.000836 \left(\frac{79.4\text{E-}6 - (\text{MAX}[y_{V15}] - \text{MIN}[y_{V15}])}{4.6\text{E-}6} \right) \ . \tag{4.8}$$

Since c_{d1}, c_{d2} and c_{d3} have only been defined to be effective for the range of performance from where the non-linear 'device' was not 'aged' to where it was (to the extent described in this simulated scenario), the TOC system should be explored further if operation beyond these expressed circumstances is desired. It may be necessary to employ a non-linear scheme to the adaptive coefficient expressions if 'aging' variations increase and more precise controls are required.

The waveforms at nodes 13, 14 and 15, collected while applying the adaptively determined pre-distortion coefficients, are shown in Figure 4.5 and are very similar to Figure 4.3. These new waveforms indicate that any difference between the two distortion systems was mainly due to that of the fourth harmonic of the input frequency.

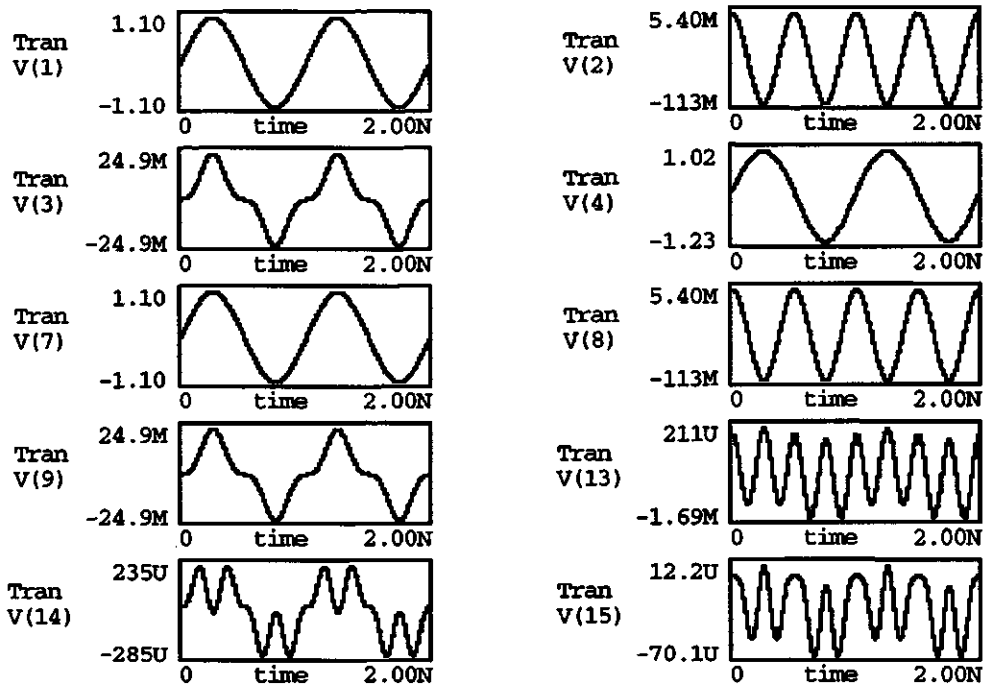

Figure 4.5: Waveforms from 'Aged' Trial of Concept System with Adapted Pre-distortion

The simple, linearly adaptive relationships in Equation (4.7) and (4.8) make it possible to maintain the low levels of harmonic distortion shown in Table 4.3. These levels are nearly the same as those shown in Table 4.1. Any observed difference will be due to the effort expended in manually determining the optimal coefficient values.

4.4 Chapter Summary

An approach to linearization was introduced in this chapter that can provide a method and understanding toward the development of an adaptive pre-distortion system for LDs. The approach was based on an adaptive linearization concept used by Ghaderi [40], but has been arranged in this chapter for the exploration of its operation with a Volterra–structured pre-distortion system. A simple, general system configuration was analyzed. The configuration used a post-distorter after the modulated 'device' to help determine the optimal coefficient values for the pre-distorter. This demonstrated how the pre-distorter coefficients can be used to adapt the compensative

Table 4.3: Harmonic Distortion from 'Aged' Trial of Concept System with Adapted Pre-distortion

Frequency in GHz	Signal Amplitude in volts	Signal Amplitude in dBc	Phase wrt sine-referenced Input in Degrees
0	-0.00073335	...	...
1	1.00015	0.0	1.26491E-10
2	0.0000000844628	-141.468	89.9998
3	0.000000872336	-121.188	9.25787E-05
4	0.0007349	-62.6767	90
5	0.0000311046	-90.1448	180
6	0.00000163094	-115.753	-90

distortion to changes within the 'device'. The intended focus for the chapter has been the means for computing the adaptive control signals and the linkages between the pre- and post-distorters. From the arrangement presented, a non-traditional control loop and some basic mathematical operations have been shown to be functionally effective in providing those linkages and signals.

Chapter 5

Compensation for Laser Diode Distortion

5.1 Pre-Distortion for Laser Diodes

Previous researchers have demonstrated compensation for the signal distortion created in laser diodes using simulated device and circuit models [41],[9]. Because computational hardware and software tools have greatly improved with time, it is now easier to attain more precise simulated results in little time. Before considering an adaptive pre-distorted LD system it is important to first understand the capability and limitation of a non-adaptive system. For later reference within the context of the adaptive model studied, performance results for a non-adaptive pre-distorted LD system will therefore first be developed.

To reduce the computational difficulties encountered when performing the double-derivative operations for a third-order Volterra pre-distortion system, the block diagram of Figure 3.10 can be modified to become that shown in Figure 5.1. This change uses the results of related and already necessary derivative operations within the distortion system. Corresponding to this modification, certain gain values have also been changed. All of theses changes are visually apparent from the two diagrams.

It is important to note that, because all function blocks and operations used in the modeled pre-distortion system are essentially ideal, all proceeding simulation results do not contain effects from non-ideal propagation delays, nor other realistic issues that would be found in a hardware implementation. Details of this type may be added to the basic system if future work were to require it.

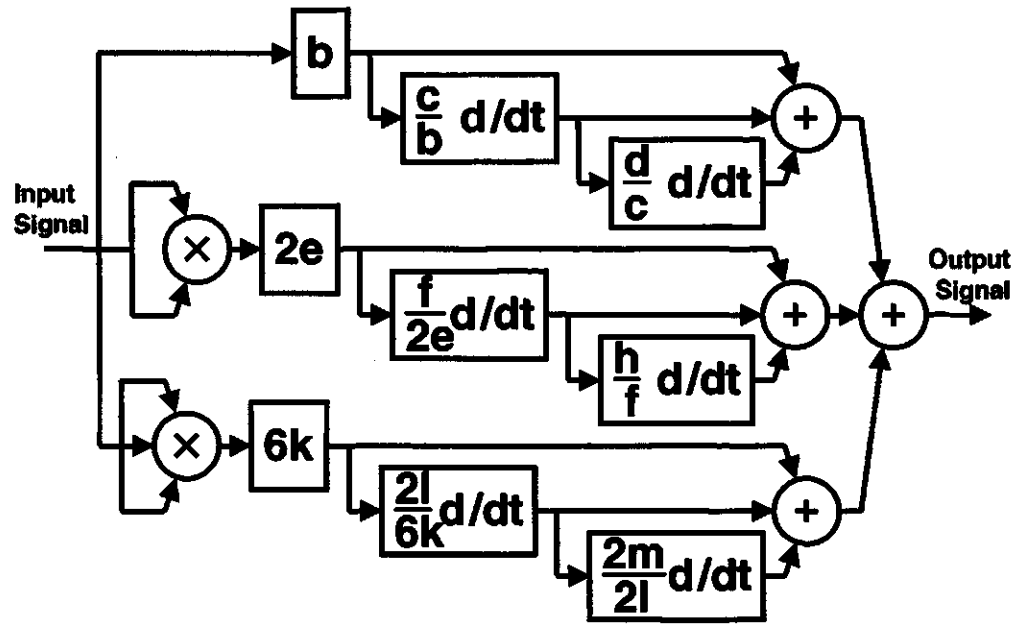

Figure 5.1: Computationally Simplified Block Diagram of LD Distortion Circuit

The ICAP/4 [27] representation of the simulated Volterra distortion system is shown in Figure 5.2. Due to the frequencies and signal levels involved, the differentiators used for the simulations were not those defined in the ICAP/4 library. The

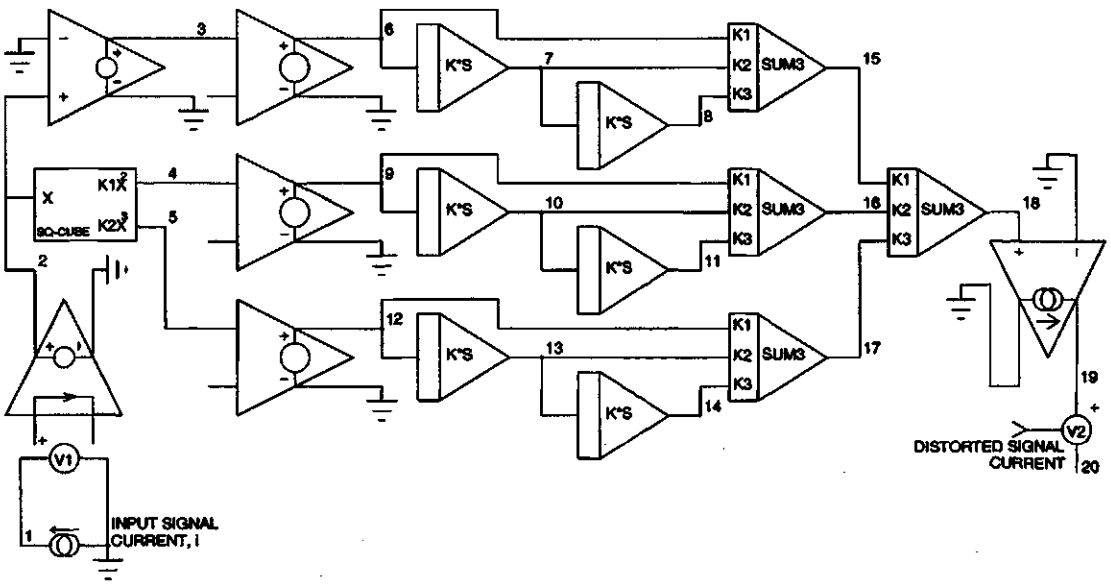

Figure 5.2: Schematic Construct of Third-order Distortion System in ICAP/4

derivative operations, labeled as 'K*S' in the figure, required the newly defined underlying sub-circuit constructs found in Appendix D.3.

Also of special note, the input to the pre-distortion system does not involve any bias current. Although the distortion system is designed with knowledge of the LD bias setting, it only compensates for the time–varying current, i. The bias current for the LD will be added to the distorted signal elsewhere, together resulting in the drive current for the laser.

Because the distortion system will be using an appropriate magnitude for its conventional input signal current, the gain coefficients must be normalized in order to produce the appropriate current magnitude required by the LD model. This normalization is required since the concept for the distortion system as described by Equations (3.16), (3.17) and (3.18) is expressed as a post-distorter. Rather than using a conventional input signal current, the post-distorter was derived to accept an input signal having units of photon density. If the compensation system is to be electrically implemented as a signal pre-distorter, then both the system input and output levels must deal in quantities of current, and not photon density. Appendix C contains the necessary coefficient calculations and normalization work in reference to this matter.

Figure 5.3 illustrates the combined system, showing both the pre-distorter and LD model. Here, the distorted current from the pre-distorter is added to the LD bias current prior to driving the laser. This schematic shows that the system input current is connected at node 1, the bias current is connected at node 20 and the modeled LD output, represented as a voltage, is available from node 25.

The node numbering provided in the ICAP/4 schematic corresponds to the visualizations displayed during simulation. For example, during the transient analysis of the pre-distorted LD system, node–voltage 4 (after the pre-distorter squaring operation) is illustrated in Figure 5.4 as 'Tran V(4)'.

Shown as 'Tran I(V1)' (current through 'monitor' voltmeter 'V1'), the input signal is a 10 μA peak input sinusoid at 1 GHz. It has no offset and is plotted by ICAP/4 using a vertical scale having limits of ± 11.0 μA. Pre-distortion operations up to and

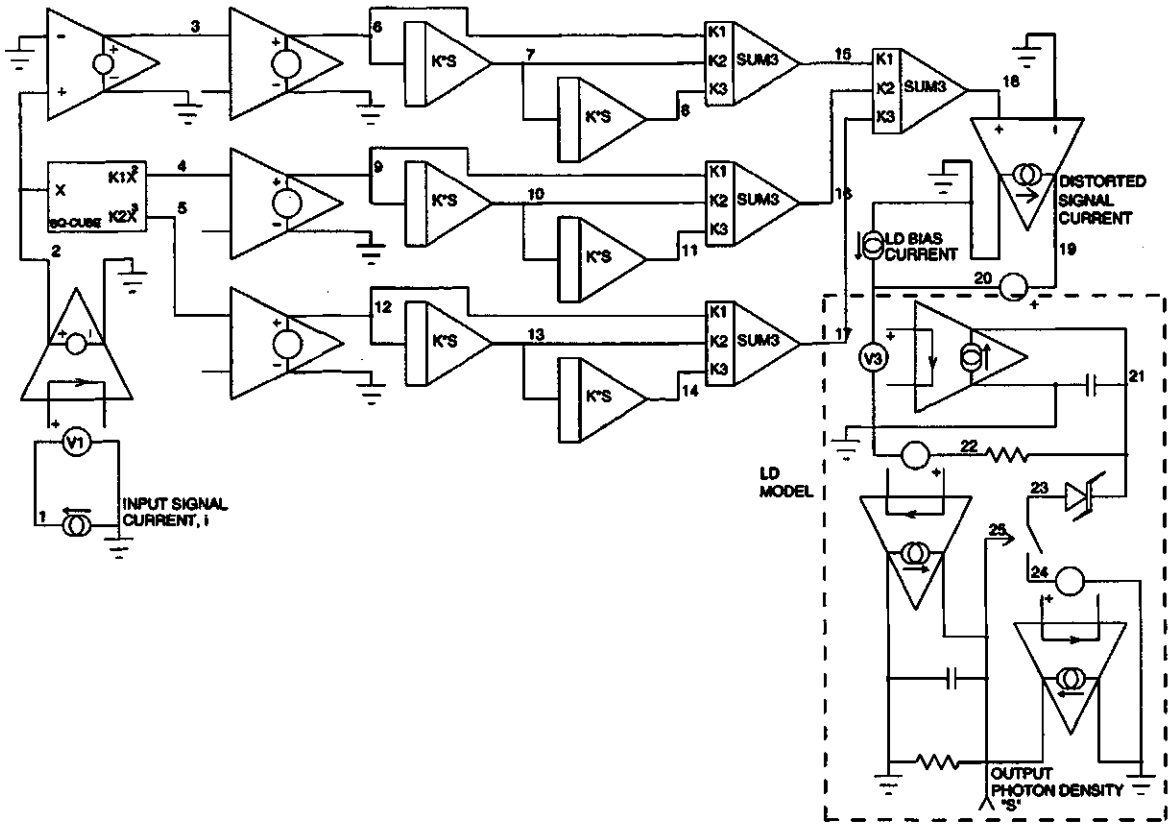

Figure 5.3: Schematic Construct of Pre-distorted Laser 'A' in ICAP/4
ICAP/4 uses labels on some of its generic operator icons. Although the labeling may suggest that operator parameters like 'K1' are equal throughout the system schematic, each operator included in the system is uniquely defined. A system netlist may be found in Appendix D.3

including coefficients b, $2e$ and $6k$ (as displayed in Figure 5.1) are applied to the input signal and shown as 'Tran V(3)', 'Tran V(4)' and 'Tran V(5)', respectively.

Numerically exact observations are not possible from the illustrations in Figure 5.4, but it is possible to see some general frequency, phase and magnitude relationships. For instance, because coefficient e has a negative value, 'Tran V(4)' shows an offset second harmonic waveform with a negative value, the result of $2e[i(t)]^2$.

For present purposes, the function blocks between nodes 3 and 6, nodes 4 and 9 and nodes 5 and 12 in Figure 5.3 can be considered unity operations. This means that if Figure 5.4 had included a view labeled 'Tran V(6)', it would appear identical to the view that is included and labeled 'Tran V(3)'. Also, waveforms 'Tran V(9)'

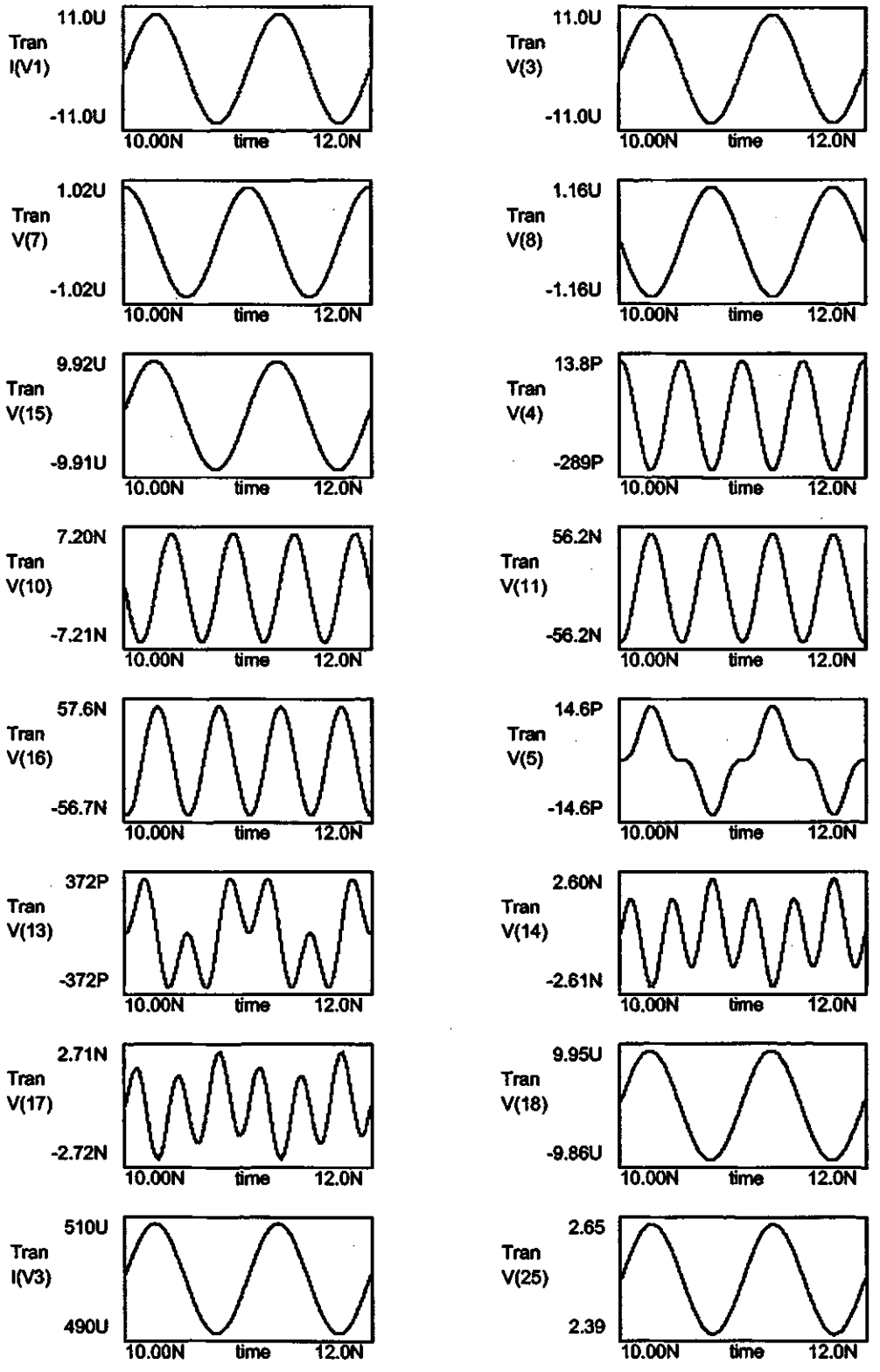

Figure 5.4: Waveforms Corresponding to the Schematic of Pre-distorted Laser 'A'

and 'Tran V(12)' equate to 'Tran V(4)' and 'Tran V(5)', respectively.

When the waveforms of 'Tran V(6)', 'Tran V(7)' and 'Tran V(8)' are added together, they produce the fundamental branch output, 'Tran V(15)'. If this is compared to 'Tran I(V1)', 'Tran V(15)' can be observed to be slightly advanced in phase, and slightly attenuated. This will be one of the three main signal components produced by the Volterra-based system as compensation for the LD distortion that will follow. Other key signal relationships throughout the system can be recognized from similar observations of other waveform combinations.

After performing the operations along each of the fundamental, squared-law and cubed-law branches, the pre-distorted signal components are rejoined at node 18. This is the complete third-order pre-distorted signal, represented as a voltage. From the vertical scale limits that ICAP/4 has used to plot 'Tran V(18)', it is apparent that the waveform is not a simple sinusoid since positive and negative waveform peaks are not equal. This agrees with expectations since, for the most part, this will be the complementary opposite of the LD distortion shown in Figure 3.4. Further along the signal path, 'Tran V(18)' is converted to a current, added to the LD bias current and fed into the LD model, already discussed in Section 3.2.

For the sake of comparison to previously published work, quantified performance results using an OMI of 30 % have been collected from this entire system. The 30 % optical modulation index means that a peak input amplitude of 66 μA is used when a 500 μA laser bias is applied (refer to Equation (3.6) and the threshold value for Laser 'A' in Table 3.1). The harmonic content from the LD using pre-distortion with a 1 GHz input signal is shown in Table 5.1, and the second and third harmonics when other inputs below 1 GHz have been applied are shown in Figure 5.5. These results are similar to those shown in others' work [9],[21].

The results with pre-distortion in Table 5.1 and Figure 5.5 may also be compared to those without pre-distortion (see Table 3.2 and Figure 3.7). With pre-distortion, the HD_2 strengths in the laser output reach only -68.4 dBc. Across the 10–1000 MHz frequency range, the second harmonic of the carrier was reduced by 25 to 44 dB. Also, the HD_3 strengths remain below -62.5 dBc. Across the same range of frequencies, the

Table 5.1: Harmonic Distortion from Pre-distorted Laser 'A' Operating at 1 GHz

Frequency in GHz	Signal Amplitude in 1E20 photons/m^3	Signal Amplitude in dBc	Phase wrt sine-referenced Input in Degrees
0	2.52108	...	...
1	0.777406	0.0	-0.0087928
2	0.000295562	-68.4000	-16.699
3	0.000571812	-62.6679	1.78029
4	0.00140601	-54.8532	110.377
5	0.000234373	-70.4148	46.4333
6	0.0000190610	-92.2100	-1.4526

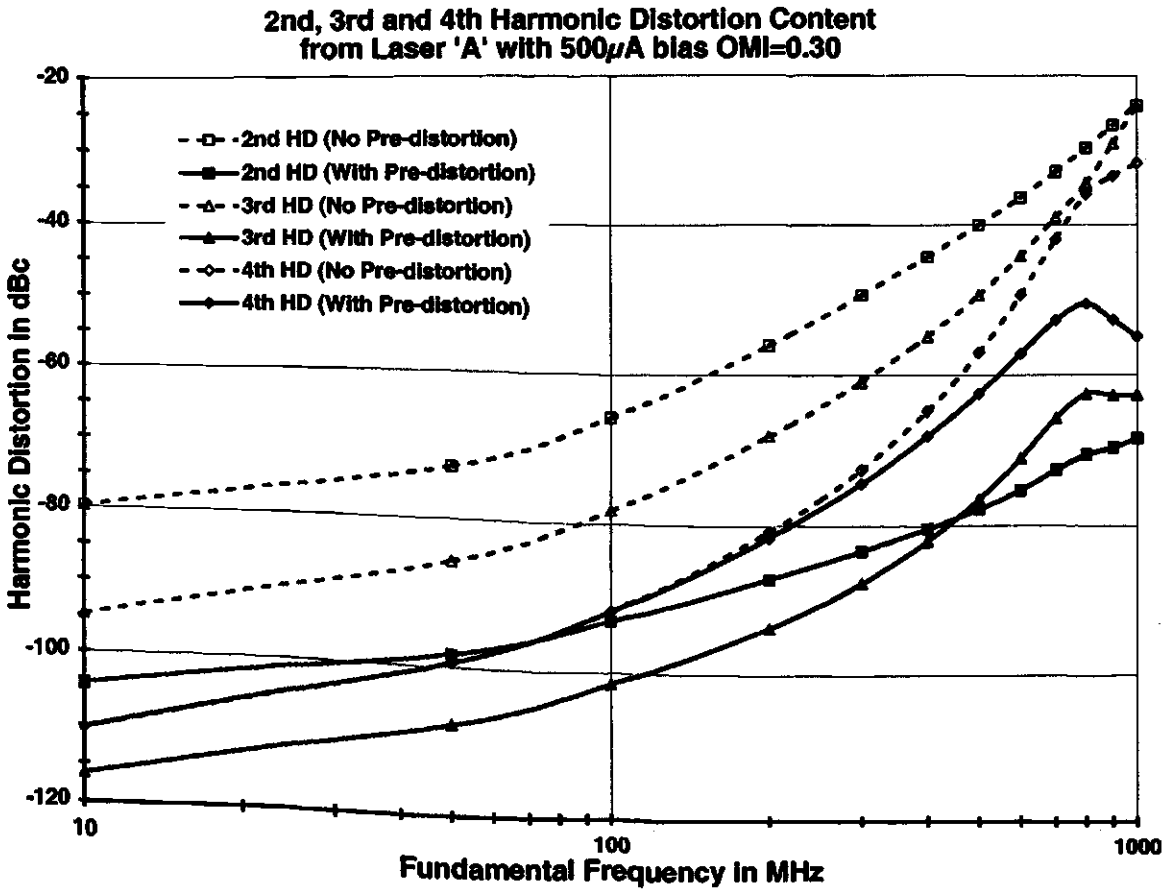

Figure 5.5: Harmonic Distortion vs. Frequency for Simulated Laser 'A' with Fixed Pre-distortion (OMI = 30 %)

third harmonic was reduced by 22 to 39 dB. In both cases, the greatest reductions were at the higher frequencies. This can be especially beneficial, because the unwanted HD content is most noticeable at these higher frequencies.

The waveforms for the input signal current and LD output after using a pre-distorter are shown in Figure 5.6. The improvement in the optical signal quality from Figure 3.4 can be easily observed when the input sinusoid is used as a reference.

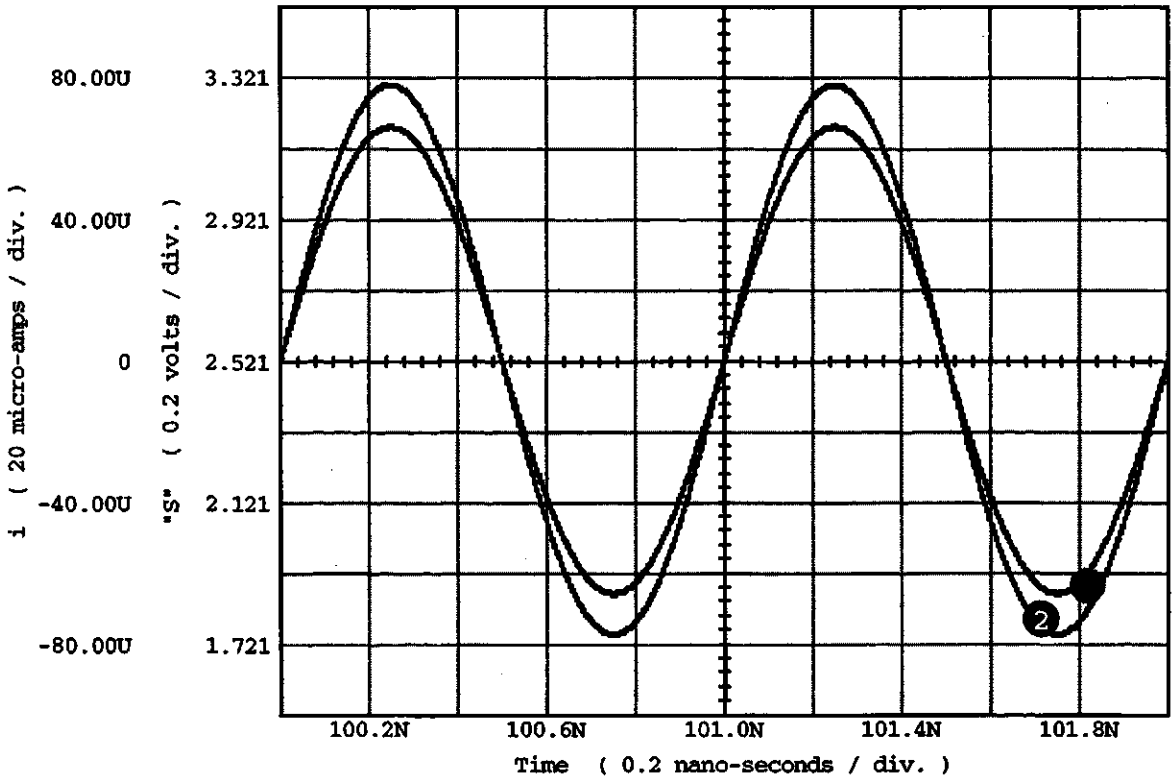

Figure 5.6: Simulated 1 GHz Sinusoidal Response for Pre-distorted Laser 'A' Waveform 1 shows the input signal current, i. Waveform 2 shows the LD photon density, S, represented by ICAP/4 as a voltage where 1 volt = 1E20 photons/m^3.

For the same range of carrier frequencies, the strength of the fourth harmonic distortion components have also been reduced from the levels shown in Figure 3.7. Although the pre-distorter helped to reduce HD_4 in the LD output shown in Figure 5.5, HD_2 and HD_3 have dropped below it at the higher frequencies. Unlike HD_2 and HD_3, none of the referenced work shows concern for this component of signal

distortion in practical system configurations.

For a CATV application having more than 80-channels, the system constraints of Table 1.1, and other factors, dictate a per-channel modulation index to be approximately 4 %. (An 80-channel SCM system would have σ = 25.2 %, as per Equation (3.7).) Multiple sub-carriers, each having a 4 % OMI, require the peak current amplitude for every one of the channel signals to be 8.8 μA. Because simulation of an 80-channel system is difficult, one carrier having the typical characteristics for this system can be alternately considered. To aid any comparison to other results, previously published or presented here, a LD bias current of 500 μA should be maintained for the superficial analysis of this possible, but hypothetical, SCM system. Results from using the 8.8 μA input current should help in understanding system performance from a growing and practical application perspective.

Simulation shows that a single channel within the 4 % OMI system would generate harmonic distortion at levels found in Figure 5.7. With pre-distortion, those second and third harmonic components drop significantly. Table 5.2 shows the detailed output harmonic content when only one 1 GHz sinusoidal input signal is present. Appropriately, a channel with a 4 % OMI can expect lower levels of optical distortion, compared to a single channel signal having a 30 % OMI. This is due to the 8.8 μA input using a smaller portion of the LD L-I characteristic, and similarly experiencing less of the non-linear cavity dynamics excited by other larger signals.

5.2 Aging Degradation

If temperature or aging effects are applied to the model of Laser 'A', values for the parameters τ_s, Γ and τ_p should be changed. For the simplicity in presenting an 'aged' scenario, it will be assumed that all three parameters have decreased by two percent. With all other parameters remaining unchanged, τ_s now becomes 2.94E-9 seconds, Γ, 0.333, and τ_p, 1.96E-12 seconds. The 'aged' parameter values will result in a change to the LD threshold current. It will increase from 280 μA, now becoming 290 μA.

Aging and temperature effects will afflict all other electrical circuits and devices having a similar situation and exposure. Because the implementation and the relative

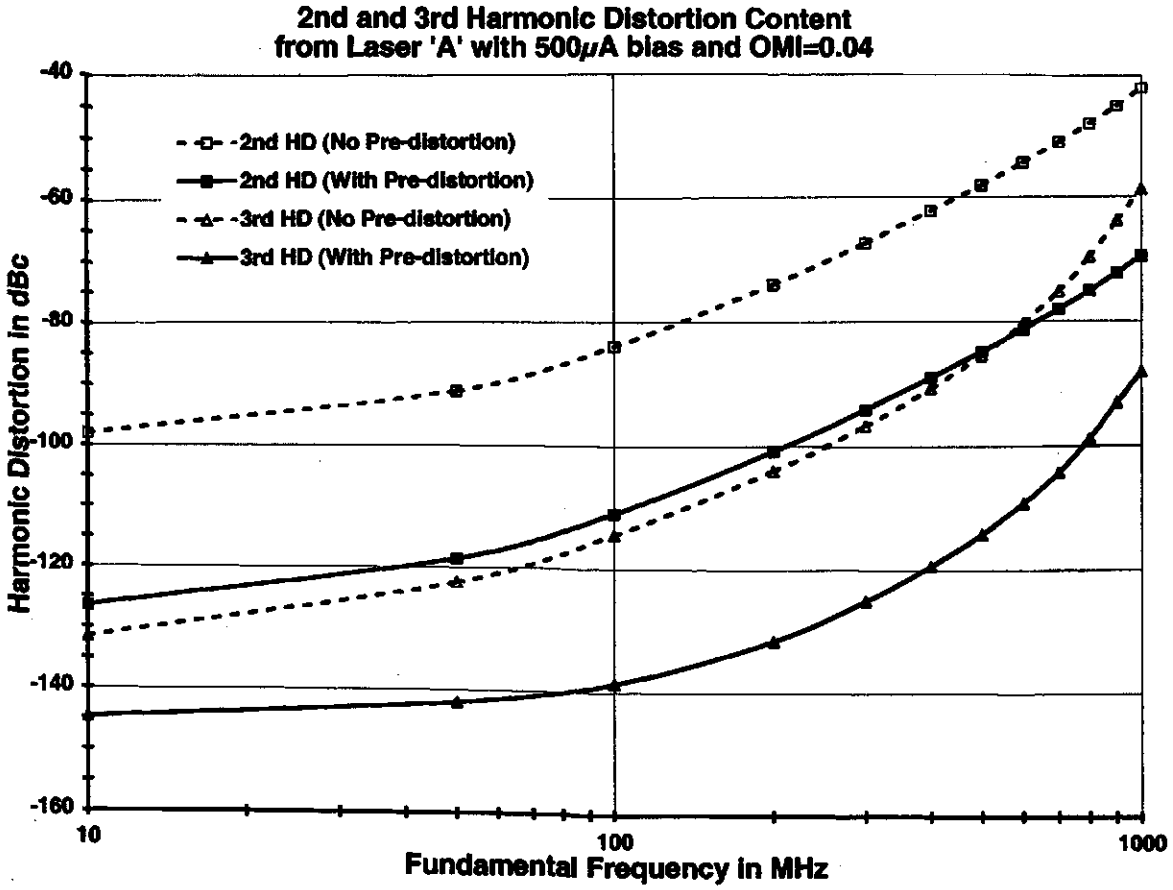

Figure 5.7: Harmonic Distortion vs. Frequency for Simulated Laser 'A' with Fixed Pre-distortion (OMI = 4 %)

Table 5.2: Harmonic Distortion from Pre-distorted Laser 'A' Operating at 1 GHz with a Single Channel OMI of 4 %

Frequency in GHz	Signal Amplitude in 1E20 photons/m^3	Signal Amplitude in dBc	Phase wrt sine-referenced Input in Degrees
0	2.52108	...	...
1	0.103652	0.0	-0.0055675
2	0.0000343317	-69.5976	-114.27
3	0.00000403230	-88.2005	-97.318
4	0.000000504303	-106.258	134.248
5	0.00000000613907	-144.550	38.7857
6	0.00000000616330	-144.515	-78.046

sensitivity of the pre-distortion system is not known at this time, it was assumed to have a constant performance ability during simulated aging of the LD. The 'aged' results shown in this work will therefore highlight only some of the performance degradation for the system when the optimal complimentary opposite match between the pre-distorter and LD is not maintained.

Because the pre-distortion system was designed and optimized for use with an un-'aged' LD, the harmonic content from a single channel OMI of 30 % indicates that the performance of the pre-distorted LD system has indeed been degraded by the 'aging' effect (see Figure 5.8 and Table 5.3). Similar degradation occurred for the 4 % single channel OMI results shown in Figure 5.9 and Table 5.4.

In consideration of a real system, it was assumed that the LD optical bias would be maintained by a small change to its bias current. This is possible since transmitter modules may be fabricated with 'built-in' optical signal monitoring circuitry that enables feedback for adjusting the device bias current [11, pp.222–224]. The 'aged' LD now required a bias current of 518.82 μA in order to produce the initial optical bias power. It was further assumed that the distorted signal current would have to be amplified slightly so that the OMI could be maintained while 'aging' changes occur. Both of these alterations are necessary to maintain consistency in the optical domain of a transmission system, when there is even a small change in the LD L-I characteristic.

5.3 Adaptive Pre-Distortion for Lasers Diodes

As shown in Chapter 4, the degradation caused by 'aging' may be reduced if some method of adapting the complimentary pre-distorter was applied. Because precise alteration of all nine parameters in the pre-distorter would be difficult to implement in hardware, a simpler goal involving three control points was simulated. In this way, the very critical phase relationships [9, pp.80–93] within the already optimized pre-distorter could remain intact, while needed variations to signal amplitudes that minimize HD_2 and HD_3 would be made.

Adaptation of the pre-distorter will closely follow the concept illustrated in Fig-

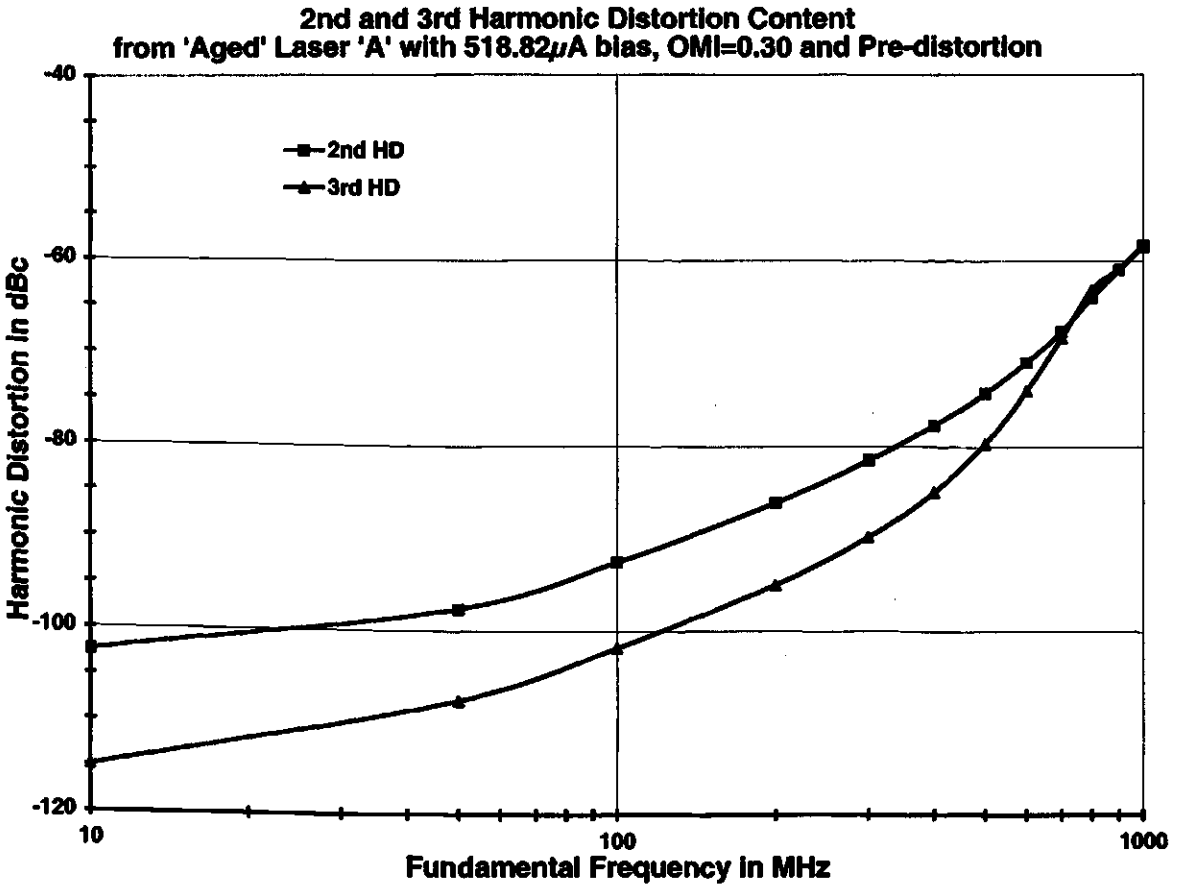

Figure 5.8: Harmonic Distortion vs. Frequency for Simulated Laser 'A' After 'Aging' with Fixed Pre-distortion (OMI = 30 %)

Table 5.3: Harmonic Distortion from Pre-distorted Laser 'A' Operating at 1 GHz After 'Aging' with a Single Channel OMI of 30 %

Frequency in GHz	Signal Amplitude in 1E20 photons/m^3	Signal Amplitude in dBc	Phase wrt sine-referenced Input in Degrees
0	2.52101	...	...
1	0.777227	0.0	0.0286617
2	0.000947404	-58.2803	-102.35
3	0.000927052	-58.4689	-60.826
4	0.00143729	-54.6601	123.976
5	0.000239484	-70.2254	59.3937
6	0.0000205870	-91.5391	10.324

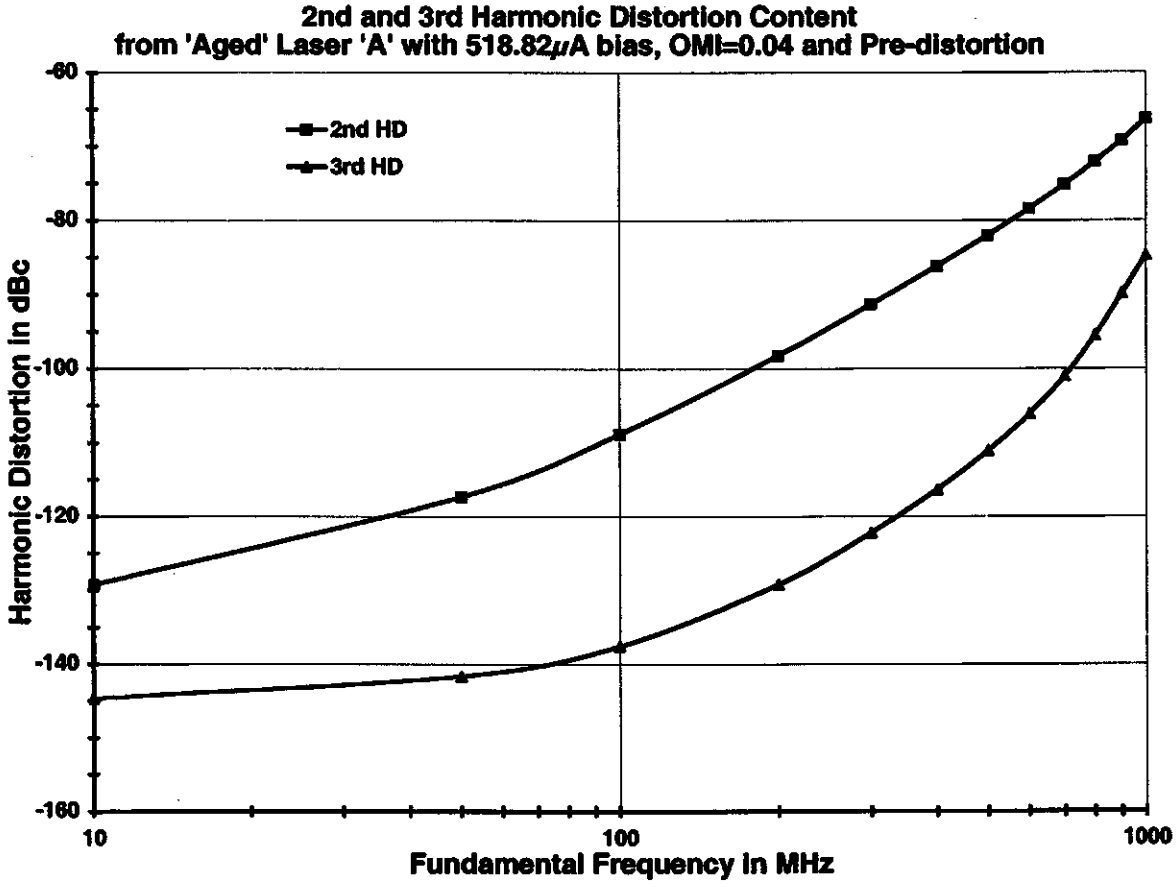

Figure 5.9: Harmonic Distortion vs. Frequency for Simulated Laser 'A' After 'Aging' with Fixed Pre-distortion (OMI = 4 %)

Table 5.4: Harmonic Distortion from Pre-distorted Laser 'A' Operating at 1 GHz After 'Aging' with a Single Channel OMI of 4 %

Frequency in GHz	Signal Amplitude in 1E20 photons/m^3	Signal Amplitude in dBc	Phase wrt sine-referenced Input in Degrees
0	2.52100	...	...
1	0.103636	0.0	0.0296308
2	0.0000500825	-66.3165	-113.78
3	0.00000601236	-84.7293	-92.963
4	0.000000534106	-105.758	146.095
5	0.00000000572398	-145.156	61.5227
6	0.00000000617929	-144.491	-77.993

ure 4.1, and will simply alter the weighting of the fundamental, squared-law and cubed-law branches of the distortion systems. In other words, the Volterra transfer functions for the adaptive distortion system will become

$$D_{A1}(j\omega_1) = \Psi_1 s_{pk}\left(b + j\alpha\omega_1 - d\omega_1^2\right) \quad , \tag{5.1}$$

$$D_{A2}(j\omega_1, j\omega_2) = \Psi_2 s_{pk}^2\left(2e + jf(\omega_1+\omega_2) - h(\omega_1+\omega_2)^2\right) \quad \text{and} \tag{5.2}$$

$$D_{A3}(j\omega_1, j\omega_2, j\omega_3) = \Psi_3 s_{pk}^3\left(6k + j2l(\omega_1+\omega_2+\omega_3) - 2m(\omega_1+\omega_2+\omega_3)^2\right), \tag{5.3}$$

where Ψ_1, Ψ_2 and Ψ_3 are the newly introduced first, second and third branch weighting factors, respectively.

During initial configuration of the system, all three branch weighting factors would have unity values so that the optimal pre-distorter coefficients could be determined as before. This would then allow identical performance to that of Equations (3.16), (3.17) and (3.18). Through the lifetime of an optical transmitter these branch weighting factors, in a fully adaptive pre-distorter, can be easily altered in accordance with LD changes. Although the finite complexity of this method of pre-distortion and adaptation does not permit a perfectly optimized complementary opposite match to the LD, it can be reasonably effective for relatively small changes to the LD characteristic parameters.

For the same LD 'aging' effect discussed in Section 5.2, Ψ_1, Ψ_2 and Ψ_3 were respectively found to be 1, 0.979 and 0.993 using a manual 'trial and error' re-optimization method. Applying these three values to the adaptive system with an OMI of 30 % will produce the harmonic content shown in Figure 5.10 and Table 5.5. Figure 5.11 and Table 5.6 show results for a system using a single channel OMI of 4 %. The HD_2 and HD_3 results from the 'aged' LD having an adaptive pre-distorter compare closely with the un-'aged' results graphed earlier in Figure 5.5 (OMI of 30 %) and Figure 5.7 (OMI of 4 %).

Adjustment of the branch weighting factors can be automatically determined in

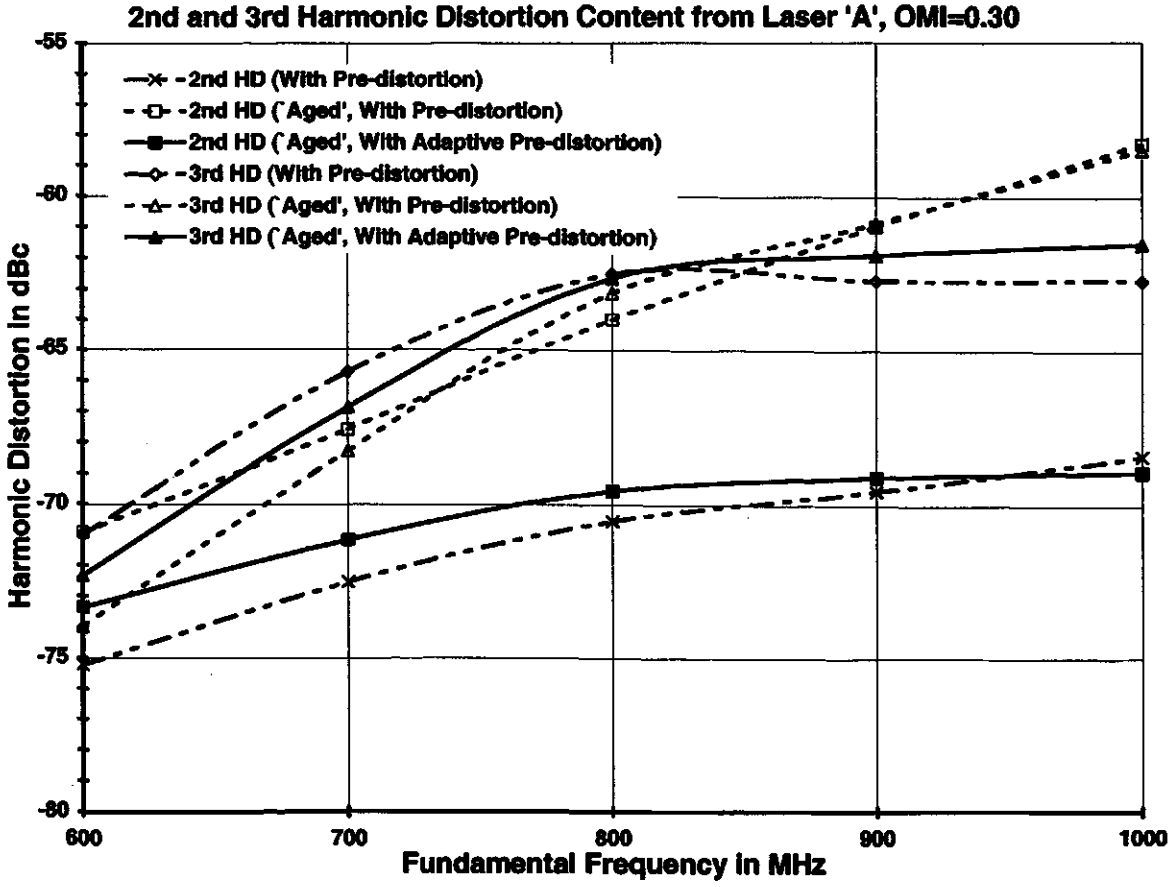

Figure 5.10: Harmonic Distortion vs. Frequency for Simulated Laser 'A' After 'Aging' with Adapted Pre-distortion (OMI = 30 %)

Table 5.5: Harmonic Distortion from Adaptively Pre-distorted Laser 'A' Operating at 1 GHz After 'Aging' with a Single Channel OMI of 30 %

Frequency in GHz	Signal Amplitude in 1E20 photons/m^3	Signal Amplitude in dBc	Phase wrt sine-referenced Input in Degrees
0	2.52101	...	...
1	0.777252	0.0	0.0270265
2	0.000278620	-68.9110	-28.822
3	0.000654158	-61.4976	-25.118
4	0.00141759	-54.7802	115.718
5	0.000240413	-70.1921	51.8038
6	0.0000203238	-91.6511	3.59463

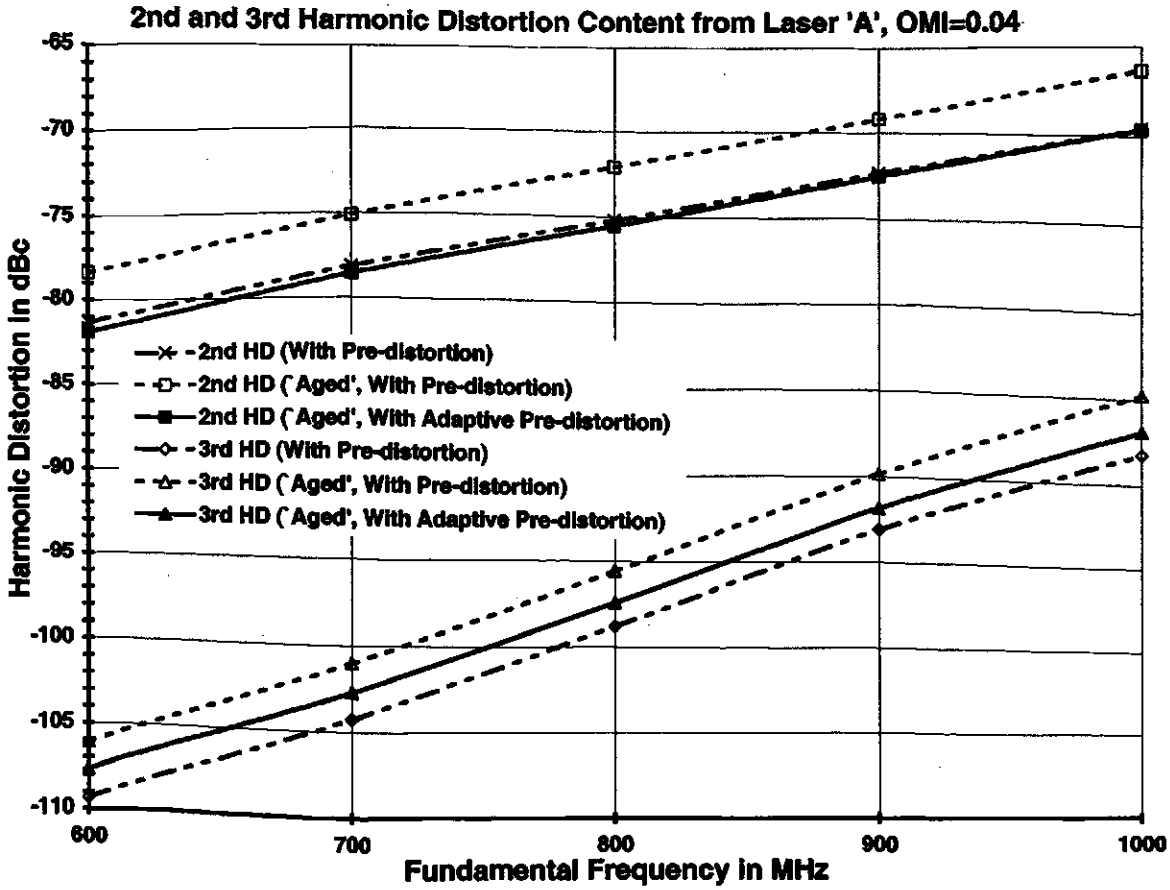

Figure 5.11: Harmonic Distortion vs. Frequency for Simulated Laser 'A' After 'Aging' with Adapted Pre-distortion (OMI = 4 %)

Table 5.6: Harmonic Distortion from Adaptively Pre-distorted Laser 'A' Operating at 1 GHz After 'Aging' with a Single Channel OMI of 4 %

Frequency in GHz	Signal Amplitude in 1E20 photons/m^3	Signal Amplitude in dBc	Phase wrt sine-referenced Input in Degrees
0	2.52100	...	...
1	0.103636	0.0	0.0296065
2	0.0000341896	-69.6323	-113.29
3	0.00000465212	-86.9571	-91.241
4	0.000000507381	-106.204	139.228
5	0.00000000608212	-144.629	50.3252
6	0.00000000585538	-144.959	-77.962

the optical transmitter if every construct of Figure 4.1 is present. The adaptive optical transmitter must then include more than just a LD and pre-distorter. It must also have a second identical distortion system (positioned as a post-distorter), a comparison unit and the necessary output signal recovery circuitry. The function of the signal recovery circuitry is to monitor the transmitted optical power, converting a small portion of this to the electrical domain, removing the bias and amplifying or attenuating the recovered signal so that its waveform essentially matches that of the input signal current, i. This locally recovered signal is then fed into the post-distortion system so the comparison units are able to evaluate signal differences between corresponding points in both pre- and post-distorters. The ICAP/4 schematic of this adaptive transmitter system is shown in Figure 5.12.

If the initial pre-distorter could perfectly compensate for any distortion that the LD adds to the input signal, the second distortion system would be receiving a completely undistorted signal current, like the initial pre-distorter. In this case, comparison of the post- to pre-distorter would show no difference and no distortion adjustments would be made. However, such a situation is not possible due to the minor limitations that arise from the third-order design of the distortion system. As a result, the post-distorter receives a signal current that differs slightly from the transmitter system input.

In the optimal situation, the comparative differences between the distortion system inputs are minimal. When the LD characteristic parameters change, the adaptive compensation effect from the pre-distortion system is no longer optimal. The post-distortion system then receives a significantly different input signal, and this can be detected if comparisons between the two distortion systems are made.

By altering the branch weighting factors in both distortion systems so that the signal differences between them are again minimized, the LD output can remain in an optimal low distortion state. Each branch weighting factor effectively changes three distortion coefficients. The adaptation of the pre-distorter in this way is, therefore, critically dependent on the means of computing appropriate branch weighting values. In this work, those calculations use the differences observed during the comparison

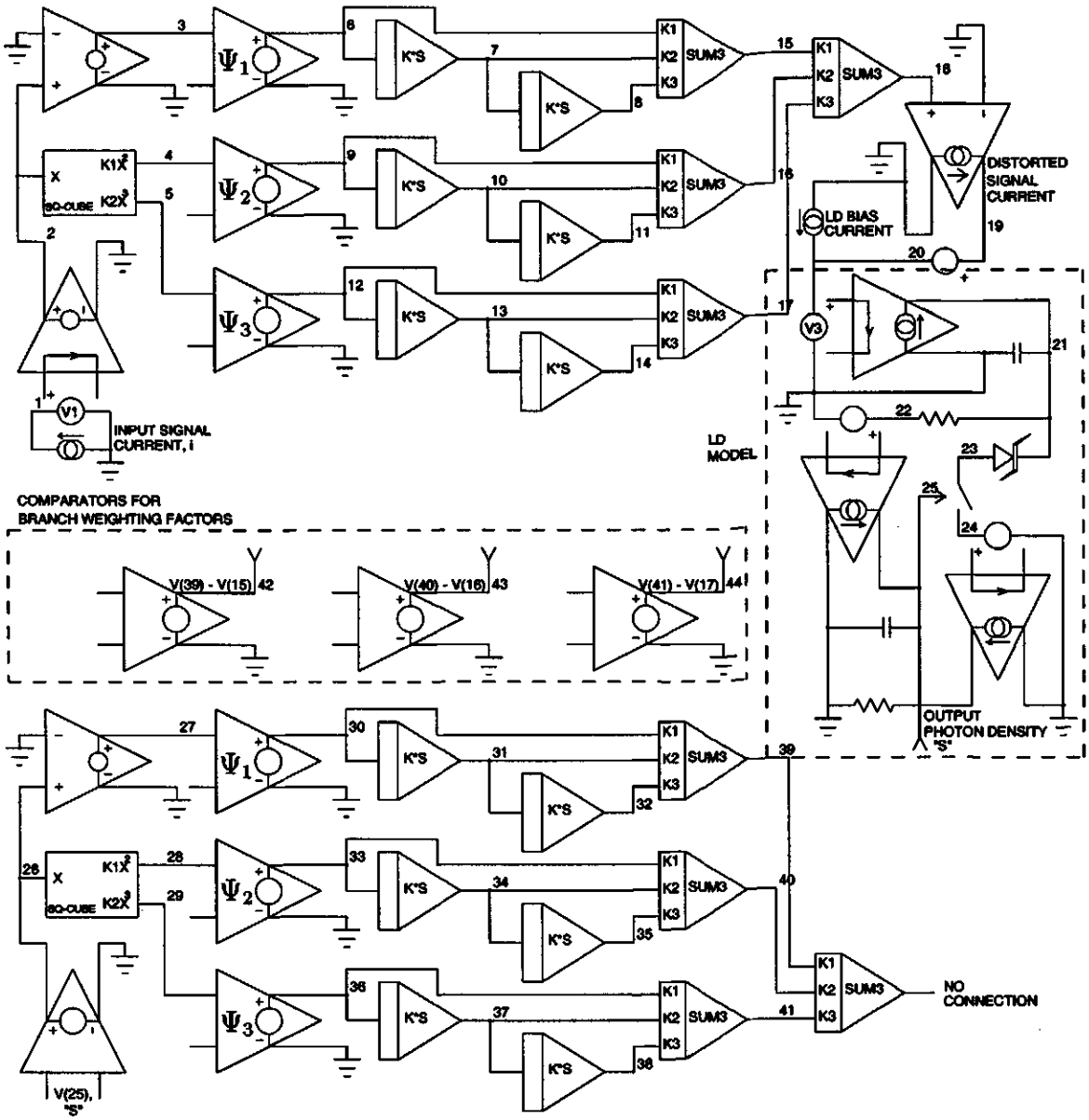

Figure 5.12: Schematic Construct of Adaptively Pre-distorted Laser 'A' in ICAP/4

of signals between the pre- and post-distortion systems. From the discussion of coefficient optimization in Appendix C, and the great accuracy and precision needed for each re-optimization during development, it was realized that the adaptive branch weighting calculations would be similarly sensitive.

In consideration of the small branch weighting changes from unity value, and while using observations from the Chapter 4 TOC, a linear scheme was proposed for the

comparison unit to compute the adjustments of Ψ_1, Ψ_2 and Ψ_3. Based on observations and the analysis of 'aged' and un-'aged' waveforms of comparative differences between nodes 15 and 39, nodes 16 and 40 and nodes 17 and 41, the following expressions were developed to compute the adaptive branch weighting values:

$$\Psi_1 = 1 \ , \tag{5.4}$$

$$\Psi_2 = 1 - 0.021 \left(\frac{340\text{E-}15 + \text{AVE}[y_{V43}]}{340\text{E-}15 - 329\text{E-}15} \right) \quad \text{and} \tag{5.5}$$

$$\Psi_3 = 1 - 0.007 \left(\frac{17.4\text{E-}12 - (\text{MAX}[y_{V44}] - \text{MIN}[y_{V44}])}{17.4\text{E-}12 - 15.9\text{E-}12} \right) \ . \tag{5.6}$$

Like the format used in a Chapter 4, the sub-scripts on the comparison output signals, y_{V43} and y_{V44}, indicate a node–voltage corresponding to the ICAP/4 schematic.

Different degrees of 'aging' were introduced to the LD so that the adapted branch weighting factors could be manually determined and 'plugged' into the simulated system. It was observed that Ψ_1 could remain unity. However, in recognizing that a time-invariant property of the comparative difference waveforms would be required in the expressions for Ψ_2 and Ψ_3, the average, minimum and maximum values were computed. Equations (5.5) and (5.6) were then created to compute the branch weighting factors from those properties of the appropriate difference waveforms. Constants in the numerator and denominator portions of the adaptive branch weighting expressions resulted from observations made at the limits of the explored 'aged' and un-'aged' conditions; during the 'aged' condition from Section 5.2, Equations (5.5) and (5.6) simplify to $1 - 0.021$ and $1 - 0.007$, which equal 0.979 and 0.993, respectively.

In each 'aged' case explored during the development and validation of Equations (5.4), (5.5) and (5.6), the application and computation of Ψ_1, Ψ_2 and Ψ_3 made a noticeable improvement to the HD_2 and HD_3 values. Also, optical signal distortion remained very near levels reported for the optimized un-'aged' case, not unlike that shown in Figures 5.10 and 5.11. The expressions were, therefore, found to be effective for the entire range of 'aging' considered.

5.4 Discussion of Results

The performance of pre-distortion to compensate for LD non-linearity is highly dependent on there being a complementary opposite match. An optimal design in this regard is difficult to determine, and may be difficult to maintain when slight system changes occur. Variations in temperature and aging will cause these kinds of change [16], and the optimized match condition to be lost.

When a third-order pre-distorter is used with a 1 GHz signal having a 30 % OMI, the optical output from the combined system shows reductions in HD_2 and HD_3 of 44.4 dB and 38.5 dB, respectively. If a CATV system using a per-channel OMI of 4 % is of interest, the distortion reductions were found to be 27.5 dB and 29.3 dB, respectively. These significant improvements are at the top end of the frequency range studied, were optical distortion often grows to system limiting levels. With and without the compensative benefit of a signal pre-distorting system, the increase in harmonic distortion with the frequency of the fundamental signal has been shown in the range up to 1 GHz. This frequency–sensitive increase agrees with expectations, since the inherent dynamic characteristic of any LD will have harmonic distortion levels that approach a maximum at the relaxation–oscillation frequency for the device.

As system bandwidths increase, higher order distortion products may require attention in SCM applications. Because a third-order pre-distorter contributes non-fundamental signal components to the drive current of the LD, it can be noticed that additional output distortion is created at frequencies the pre-distorter is not designed to address. The HD_4 and HD_5 results in Tables 3.2 and 5.1 provide hints of this potentially growing problem.

A Volterra structured pre-distorter was easily modified to provide an adaptive performance capable of maintaining the optimal compensative match between the pre-distorter and LD. A comparison of the initial input signal with that emitted from the LD was used indirectly to 'tune' the pre-distorter parameters so that changes to device characteristics within the control loop may be counteracted. Laser diode temperature and aging effects have been successfully avoided using this non-conventional feedback approach, showing that signal pre-distortion holds much promise in helping realize

robust optical system applications.

The adaptive pre-distortion system presented in Equations (5.1), (5.2), (5.3) and (5.4), (5.5), (5.6) effectively altered two of nine possible Volterra parameters in order to return the optical performance nearly to that before laser 'aging'. In an SCM-like system using a single channel OMI of 4 %, aging degradation that led to a 3 dB rise in second and third harmonic distortion levels was essentially eliminated.

The utilization of the adaptive pre-distortion concept may be valuable beyond the variation of system operating conditions. It may simplify the production and maintenance of LD modules. The performance of a pre-distorted LD relies on precise coefficient optimization for each distorter—LD pairing. But when an adaptive pre-distortion circuit is designed for a particular model of laser, it probably will not require the individualized pairing attention needed by a non-adaptive distortion circuit. The compensation provided by an adaptive pre-distorter will self–optimize to that of its LD. Because of this, the cost of producing light source modules containing pre-distortion technologies should be better controlled, giving this enhanced electro-optics approach even greater appeal.

Although the linear alteration of the pre-distorter using three branch weighting factors provided a high tolerance against the LD changes, other relationships may be more suitable in providing the adaptive control for specific, real applications. The concern in this regard, however, may not be very significant since 'aging' outside the study range was well compensated for using a proportional change to the branch weighting factors. (This 'aging' is shown in Table 5.7 using τ_s =2.88E-9, Γ =0.326, τ_p =1.92E-12 and bias at 538.897 μA. Table 5.8 shows the adaptively compensated results, using Ψ_1, Ψ_2 and Ψ_3 values of 1, 0.958 and 0.986, respectively.) Adaptation to this otherwise 6 dB HD_2 and HD_3 degradation appears very good, although recovery from this effect on HD_3 levels might suggest that Equation (5.6), in particular, might deserve further refinement.

This adaptive pre-distortion method involves control signals having particularly small amplitudes. Although the simulated operations computing the difference signals, y_{V42}, y_{V43} and y_{V44}, are capable of handling signals near 0.01 pV, it may be

Table 5.7: Harmonic Distortion from Pre-distorted Laser 'A' Operating at 1 GHz After Additional 'Aging' with a Single Channel OMI of 4 %

Frequency in GHz	Signal Amplitude in 1E20 photons/m^3	Signal Amplitude in dBc	Phase wrt sine-referenced Input in Degrees
0	2.52101	...	...
1	0.103636	0.0	0.0645622
2	0.0000653843	-64.0007	-113.34
3	0.00000783631	-82.4280	-88.822
4	0.000000568231	-105.220	147.049
5	0.00000000595544	-144.812	86.0286
6	0.00000000619871	-144.464	-77.956

Table 5.8: Harmonic Distortion from Adaptively Pre-distorted Laser 'A' Operating at 1 GHz After Additional 'Aging' with a Single Channel OMI of 4 %

Frequency in GHz	Signal Amplitude in 1E20 photons/m^3	Signal Amplitude in dBc	Phase wrt sine-referenced Input in Degrees
0	2.52101	...	...
1	0.103636	0.0	0.0645146
2	0.0000339284	-69.6989	-112.23
3	0.00000522260	-85.9525	-85.778
4	0.000000508562	-106.183	144.091
5	0.00000000615195	-144.530	61.7590
6	0.00000000555938	-145.410	-77.850

possible to avoid such low signal levels by designing the pre- and post-distortion systems differently. If the two distortion systems could accept, and operate on, signals significantly larger than a conventional μA–input, their signal differences could have magnitudes of nano- or, maybe, micro-volts. With such a design modification, the pre-distorter output would certainly also need attenuating for a return to the conventional signal levels supplied to the LD.

And finally, the results shown have all been acquired using simulated single–frequency scenarios. From this it can be suggested that, if the system is implemented,

the adaptive controls may be generated from a single pilot tone at the upper limit of the system bandwidth. This would allow the system to remain in an adapted, optimal state, and possibly simplify the operation of the branch weighting calculations when a complex, time–varying SCM signal is used. An out–of–band 'high–frequency' pilot tone could improve the assurance of operational system stability, since adding narrow–band filters to the pre-distortion coefficient controls would allow the isolation of the adaptive system features.

Chapter 6

Conclusions

6.1 Modeling Approach

The use of simulation in the completion of this work has been beneficial by improving analytical flexibility and by reducing future potential research costs. Although models may require some adaptation to the tools being used, the added research overhead can be offset by the ease of distributing a research effort and the fact that current computational abilities permit rapid evaluation and exploration. Simple models, the compatibility among simulation tools based on SPICE and standardized output data file formats have allowed abstract concepts to be shared and easily understood among researchers. In this work, where several detailed concepts may have an influence on an applied system, the benefit of passing along accurate models and information for personal exploration has been found very useful.

The recent structures and overall designs used in present day optical transmitters are rapidly evolving, and simulation tools will become even more important in application and device design work. It is, however, unfortunate that the future benefit of the research effort may be restricted due to the limited availability of published parameters and detailed device characterization reports having a material–physics perspective. Parameters for modeling the DFB laser used in this work are traceable to origins in a February, 1992 publication. Because of the date, the LD parameters are possibly not representative of devices presently in high–volume production. Without a close link to current fabrication and material sciences, the relevance of a specific modeled design becomes more questionable. On the other hand, the exploration of

general principles, like adaptive pre-distortion, may be found beneficial whether the application involves LDs or other broadband non-linear communication components.

6.2 Compensation Approach

A Volterra–based pre-distortion system is effective in compensating for the dynamic non-linear distortion produced by an intensity modulated LD operating at 'high' frequencies. A Volterra structure is limited, however, and this allows only a finite-order of distortion to be addressed. Based on findings from other optical system research [1], a third-order compensation approach should suit the needs of most realizable transmission applications, and support the demanding requirements of analogue–signal data systems.

By the nature of the LD, optical signal distortion increases significantly near the relaxation–oscillation frequency of the device. This distortion increase determines the upper limit to potential system bandwidth. In this work, it has been shown that a pre-distortion compensation approach can provide an appreciable benefit to broadband optical system applications that use inexpensive, low quality light sources.

The third-order Volterra pre-distortion system presented in this work is capable of lowering HD_2 and HD_3 by 27.5 dB and 29.3 dB, respectively, when used at 1 GHz with a single channel OMI of 4 %. This performance requires very specific pre-distorter coefficient settings in order to provide a nearly optimal complimentary opposite match to the LD non-linear characteristic. Also, different coefficient values may be chosen if a particular transmission application requires the reduction of one harmonic at the cost of another.

The improved light source capability presented indicates that sub-carrier multiplexed transmission/distribution systems, like that of CATV, can support the greater bandwidth demands caused by increasing choice of channels and changing baseband modulation formats. Although not discussed in detail, the optical transmitter linearity provided by the compensative approach should also permit digital systems to operate at higher data rates and/or lower bit–error rates.

An adaptive method of distortion compensation has been introduced so that per-

formance beyond that of a simple pre-distorter could be provided. Because the complimentary opposite signal distortion from the pre-distorter relies on precise coefficient settings that are specific to the corresponding LD parameters, changes due to temperature and device aging will diminish the complimentary match. With adaptation of the pre-distortion system, temperature and aging effects can be negated. This means that transmission systems requiring highly linear performance for the delivery of broadband services during otherwise prohibitive variations in operating conditions may be developed using adaptive coefficients.

The desired adjustments to the pre-distorter coefficients are conceptually simple and should not lead to system instabilities if the Volterra–based compensation method is constructed in the electrical domain. With some additional planning, a pilot signal located at the upper limit of the system bandwidth could ensure this reliably.

Unfortunately, reports [32],[9] indicate that some practical limitations prevent the widespread use of this electrical–based distortion compensation technique for the growing needs of broadband systems. Should there be affordable improvements made to the linearity of low power RF amplifiers, and to methods of performing squaring, cubing and derivative operations below 1 GHz, broadband pre-distortion would have greater commercial potential.

With these practical limitations addressed, it is possible that an electrical-based pre-distorter compensate for more than just signal altering effects within the light source. It may become possible to have an electrical pre-distorter compensate for optical signal distortion arising from other optical system components, like that of the optical waveguide or the opto-electronic receiver.

6.3 Thesis Contributions

The Volterra distortion system used in this work with the simulated model of a LD has been defined to allow rapid alteration for further investigative purposes. Its development makes available an explanation of the pre-distorter normalization and optimization requirements, and provides the coefficient values that produced the performance results presented. Structural modifications to the pre-distorter schematic

and redefinition of the derivative operations used in the SPICE representation were also made in this work. This will help the performance of simulations by easing the computational difficulty, and by handling a wider range of signal frequencies than would be otherwise possible using the simple library operations of common simulation programs.

An adaptive pre-distortion system structure was developed that could effectively compensate for parametric variations in the LD that can take place over time. Hypothetical changes to the semiconductor laser device were also simulated. By doing this, possible temperature and aging effects that will degrade the operation of a broadband optical system were shown to require very sensitive control circuitry within the suggested adaptive configuration.

While developing the system model, it was found that adaptive control voltages on the order of 1E-15 would be required. Although the adaptive system may be difficult to implement as simulated, the basic structure indicated that as much as 6 dB of HD may be compensated for by such highly sensitive control signals. For the hypothetical devices and scenarios examined, the adaptive pre-distorter maintained the performance of the optimally configured system before and after any changes to the LD.

Whatever the direction a more detailed hardware design might take, the adaptive system structure was designed to be very simple. Instead of adjusting all nine of the pre-distorter coefficients, the system was developed to become functionally adaptive using adjustments to only two. By using simplified controls, the pre-distorter could be 'tuned' to LD parametric changes, after having compared the original input signal with an electrical likeness of that being optically transmitted.

The adaptive pre-distortion system presented provides another significant advantage over a non-adaptive system. For demanding optical system applications, each non-adaptive pre-distorter would likely require careful construction and optimization with its individually paired LD. An adaptive system would prove this unnecessary, except when introducing the adaptive pre-distorter to a different model of LD. Since different devices of the same model LD have small parametric variations, each adap-

tive pre-distorter/LD pair could be expected to self–optimize when given 'ballpark' initial settings.

6.4 Suggested Future Work

Future work should include the integrated fabrication of an adjustable third-order distortion circuit. This would be a step toward the realization of a light source module containing a LD with adaptive pre-distortion circuitry. Presumably, an integrated–circuit approach would allow a second and identical distortion system — the post-distorter — to be placed in close proximity to both the pre-distortion system and LD so that the phase delays of the signals being compared would be minimal. Differences in pre-distorter performance might also be reduced through an integrated–circuit solution. The detailed design of the distortion circuit must also address the need for having a high resistance to temperature and aging variations, since it is in this ability that the adaptive pre-distortion structure becomes attractive for use with sensitive LD transmitters.

With the growing use of VCSEL devices for communication system applications, a simple method that achieves compensation for the strong temperature effects in these LDs will become highly desirable. However, due to application requirements for dense light source arrangements and the spatial–efficiency of VCSEL structures, the corresponding adaptive pre-distorters should be spatially efficient as well. This may mean that an even simpler adaptive pre-distortion structure should be considered, and that large or more complicated implementation should be avoided.

Bibliography

[1] J. A. Chiddix, H. Laor, D. M. Pangrac, L. D. Williamson, and R. W. Wolfe, "AM video on fiber in CATV systems: Need and implementation," *IEEE Journal on Selected Areas in Communications*, vol. 8, pp. 1229–1239, September 1990.

[2] Y.-K. Chen, C.-H. Chang, and C.-C. Lee, "Simultaneous transmission of 1.55–μm CATV video signal and 1.3–μm data signal over a multimode–fiber local area network," *IEEE Photonics Technology Letters*, vol. 10, pp. 1790–1792, December 1998.

[3] R. Sabella, M. Paciotti, and A. di Fonzo, "Impact of non-linear distortions on different modulation schemes in analog CATV distribution systems," *Conference Proceedings – LEOS Annual Meeting Proceedings of the 1996 9th Annual Meeting of IEEE LEOS*, vol. 2, pp. 406–407, November 18-21 1996.

[4] W. B. Jones, Jr., *Introduction to Optical Fiber Communication Systems.* Holt, Rinehart and Winston, Inc., 1988.

[5] B. Wilson, Z. Ghassemlooy, and I. Darwazeh, eds., *Analogue Optical Fibre Communications.* IEE Telecommunications Series 32, The Institution of Electrical Engineers, 1995.

[6] V. B. Gorfinkel and S. Luryi, "Fundamental limits for linearity of CATV lasers," *Journal of Lightwave Technology*, vol. 13, pp. 252–260, February 1995.

[7] J. L. Thomas, *Cable Television Proof–of–Performance.* Hewlett–Packard Professional Books Series, Prentice Hall PTR, 1995.

[8] R. Olshansky, V. A. Lanzisera, and P. M. Hill, "Subcarrier multiplexed lightwave systems for broad-band distribution," *Journal of Lightwave Technology*, vol. 7, pp. 1329–1342, September 1989.

[9] M. J. Sieben, "Semiconductor laser diode modeling and linearization by predistortion," Master's thesis, University of Saskatchewan, 1994.

[10] J. Hecht, *Laser Pioneers.* Academic Press, Inc., revised ed., 1985.

[11] D. Wood, *Optoelectronic Semiconductor Devices.* Prentice Hall International Series in Optoelectronics, Prentice Hall, 1994.

[12] L. Solymar and D. Walsh, *Lectures on the electrical properties of materials.* Oxford Science Publications, Oxford University Press, third ed., 1986.

[13] M. A. Karim, *Electro–Optical Devices and Systems.* The PWS–KENT Series in Electrical Engineering, PWS–KENT Publishing Company, 1990.

[14] B. G. Streetman, *Solid State Electronic Devices.* Prentice–Hall Series In Solid State Physical Electronics, Prentice–Hall, Inc., second ed., 1980.

[15] H. A. Haus, *Waves And Fields In Optoelectronics.* Prentice–Hall Series In Solid State Physical Electronics, Prentice–Hall, Inc., 1984.

[16] J.-W. Pan, M.-H. Chen, J.-I. Chyi, and T.-T. Shih, "Temperature–dependent characteristics of 1.3–μm AlGaInAs–InP lasers with multiquantum barriers at the guiding layers," *IEEE Photonics Technology Letters*, vol. 10, pp. 1700–1702, December 1998.

[17] S. J. Wang, A. B. Piccirilli, Y. J. Wang, and N. K. Dutta, "Temperature dependence of the second harmonic distortion of buried heterostructure distributed feedback lasers," *Electronics Letters*, vol. 26, pp. 1095–1097, July 1990.

[18] A. K. Dutta, H. Kosaka, K. Kurihara, Y. Sugimoto, and K. Kasahara, "High-speed VCSEL of modulation bandwidth over 7.0 GHz and its application to 100 m PCF datalink," *Journal of Lightwave Technology*, vol. 16, pp. 870–875, May 1998.

[19] P. V. Mena, J. J. Morikumi, S.-M. Kang, A. V. Harton, and K. W. Wyatt, "A comprehensive circuit-level model of vertical-cavity surface-emitting lasers," *Journal of Lightwave Technology*, vol. 17, pp. 2612–2632, December 1999.

[20] T. K. Biswas and W. F. McGee, "Volterra series analysis of semiconductor laser diode," *IEEE Photonics Technology Letters*, vol. 3, pp. 706–708, August 1991.

[21] C. Y. Kuo, "Fundamental second–order nonlinear distortions in analog AM CATV transport systems based on single frequency semiconductor lasers," *Journal of Lightwave Technology*, vol. 10, pp. 235–243, February 1992.

[22] W. I. Way, "Large signal nonlinear distortion prediction for a single–mode laser diode under microwave modulation," *Journal of Lightwave Technology*, vol. LT-5, pp. 305–315, March 1987.

[23] R. S. Tucker, "High–speed modulation of semiconductor lasers," *Journal of Lightwave Technology*, vol. LT-3, pp. 1180–1192, December 1985.

[24] R. S. Tucker and D. J. Pope, "Circuit modeling of the effect of diffusion on damping in a narrow-stripe semiconductor laser," *IEEE Journal of Quantum Electronics*, vol. QE-19, pp. 1179–1183, July 1983.

[25] P. Neusy and W. F. McGee, "Effects of laser nonlinearities on TV distribution using subcarrier multiplexing," *Proceedings of Canadian Conference on Electrical and Computer Engineering*, pp. 833–836, September 1989.

[26] P. V. Mena, S.-M. S. Kang, and T. A. DeTemple, "Rate-equation-based laser models with a single solution regime," *Journal of Lightwave Technology*, vol. 15, pp. 717–730, April 1997.

[27] Intusoft, *ICAP/4 version 7.0.* Personal Computer Circuit Design Tools: http://www.intusoft.com, Intusoft, San Pedro, California.

[28] D. E. Dodds and M. J. Sieben, "Fabry-perot laser diode modeling," *IEEE Photonics Technology Letters*, vol. 7, pp. 254–256, March 1995.

[29] K. Alameh and R. A. Minasian, "Ultimate limits of subcarrier multiplexed lightwave transmission," *Electronics Letters*, vol. 27, pp. 1260–1262, July 1991.

[30] C. J. Chung and I. Jacobs, "Simulation of the effects of laser clipping on the performance of AM SCM lightwave systems," *IEEE Photonics Technology Letters*, vol. 3, pp. 1034–1036, November 1991.

[31] C. J. Chung and I. Jacobs, "Practical TV channel capacity of lightwave multichannel AM SCM systems limited by the threshold nonlinearity of laser diodes," *IEEE Photonics Technology Letters*, vol. 4, pp. 289–292, March 1992.

[32] T. E. Darcie and G. E. Bodeep, "Lightwave subcarrier CATV transmission systems," *IEEE Transactions on Microwave Theory and Techniques*, vol. 38, pp. 524–533, May 1990.

[33] L. W. Couch, II, *Digital and Analog Communication Systems.* Macmillan Publishing Company, second ed., 1987.

[34] J. H. Angenent, "Simple model for calculation of distortion in an optical analogue subcarrier multiplexed CATV system," *Electronics Letters*, vol. 26, pp. 2049–2050, November 1990.

[35] G. E. Bodeep and T. E. Darcie, "Semiconductor lasers versus external modulators: A comparison of nonlinear distortion for lightwave subcarrier CATV applications," *IEEE Photonics Technology Letters*, vol. 1, pp. 401–403, November 1989.

[36] Microelectronics Group, Lucent Technologies, Inc., *A2300–Type Laser 2000 Analog DFB Laser Module.* Data Sheet: DS99-165LWP, Lucent Technologies, Inc., March 1999.

[37] P. W. Cornish and B. Duncan, *Predistortion Method and Apparatus for Laser Linearization.* Raynet Corporation, Menlo Park, California, US Patent Number 5321710, Filed: April 19, 1993, Issued: June 14, 1994.

[38] S. Narayanan, "Transistor distortion analysis using volterra series representation," *Bell Systems Technical Journal*, vol. 46, pp. 991–1024, May–June 1967.

[39] S. Narayanan, "Application of volterra series to intermodulation distortion analysis of transistor feedback amplifiers," *IEEE Transactions on Circuit Theory*, vol. 17, pp. 518–527, November 1970.

[40] M. Ghaderi, *Adaptive Linearization of Efficient High Power Amplifiers using Polynomial Predistortion with Global Optimization.* PhD thesis, University of Saskatchewan, 1995.

[41] D. Hassin and R. Vahldieck, "Feedforward linearization of analog modulated laser diodes–theoretical analysis and experimental verification," *IEEE Transactions on Microwave Theory and Techniques*, vol. 41, pp. 2376–2382, December 1993.

[42] M. Schetzen, *The Volterra and Wiener Theories of Nonlinear Systems.* John Wiley & Sons, Inc., 1980.

Appendix A

Derivations of Compensation Expression from LD Rate Equations

A compensation expression may be found for a LD by first deriving the complementary opposite expression. This means that an electrical current expression, in terms of optical power, or similar proportional parameter, serves this need. Photon density, S, being proportional to the output power of a LD, may be used as an input to a hypothetical system that works in reverse of the laser, producing an output current similar to that driving the LD. This hypothetical compensation system, expressed as a *post*-distorter, can later be placed ahead of the LD to function as a *pre*-distorter. Either way, it will contribute the complementary opposite signal distortion to that of the laser.

There are two well recognized rate equations that together express the interaction of electrical and optical systems within a LD. These equations permit the dynamic behavior of the device to be modeled. Dynamic behavior requires expression in this form, since time-varying currents with high frequency content do not create the linearly proportional optical powers indicated by static, or low frequency L-I characteristic curves when operating a LD in the 'linear' range. The equations are shown here as

$$\frac{dN}{dt} = \frac{I}{qV_c} - \frac{N}{\tau_s} - g(N - N_o)S \quad \text{and} \tag{A.1}$$

$$\frac{dS}{dt} = \Gamma g(N - N_o)S - \frac{S}{\tau_p} + \Gamma\beta\frac{N}{\tau_s} \quad . \tag{A.2}$$

The equations express the density of conduction band electrons, N, and density of photons, S, within an active cavity volume, relative directly and indirectly to the LD drive current, I. The device dependent parameters are: V_c, the volume of the active region; τ_s, the average electron or carrier lifetime before spontaneous emission; g, the optical power gain from the generation of stimulated emissions; N_o, the electron density at the lasing threshold; Γ, a measure of the useful photon–involvement called the optical confinement factor; τ_p, the average photon lifetime before absorption; and β, the fraction of spontaneously emitted photons that are in-phase with the lasing emissions.

A minor revision can be made to Equations (A.1) and (A.2) so that dynamic device behavior is even more accurately predicted for single mode LDs. Work by Kuo [21] showed that the following two rate equations are preferable to the earlier ones [23]. Results for Laser 'A' (Table 3.1) are, therefore, based on the modified equations, containing ε, the power gain compression parameter. The equations used are shown here as

$$\frac{dN}{dt} = \frac{I}{qV_c} - \frac{N}{\tau_s} - g(N - N_o)(1 - \varepsilon S)S \quad \text{and} \tag{A.3}$$

$$\frac{dS}{dt} = \Gamma g(N - N_o)(1 - \varepsilon S)S - \frac{S}{\tau_p} + \Gamma\beta\frac{N}{\tau_s} \quad . \tag{A.4}$$

To begin development of a compensation expression for a LD, Equation (A.4) can be expanded and rearranged to give

$$\frac{dS}{dt} = \left[\Gamma g(1 - \varepsilon S)S + \frac{\Gamma\beta}{\tau_s}\right] N - \Gamma g(1 - \varepsilon S)SN_o - \frac{S}{\tau_p} \quad . \tag{A.5}$$

Further manipulation of Equation (A.5) provides this expression for the electrical carrier density:

$$N = \frac{\frac{dS}{dt} + \frac{S}{\tau_p} + \Gamma g(1 - \varepsilon S)SN_o}{\Gamma g(1 - \varepsilon S)S + \frac{\Gamma\beta}{\tau_s}} \quad . \tag{A.6}$$

If a substitution is made in Equation (A.6), based on $S = S(t) = S_b + s$ where S_b is

the bias photon density and s is the time-varying signal component, and numerator and denominator terms are arranged according to s, the carrier density becomes

$$N = \frac{\frac{d(S_b+s)}{dt} + \left[\frac{1}{\tau_p} + \Gamma g N_o - 2S_b\Gamma g N_o\varepsilon\right]s + \left[-\Gamma g N_o\varepsilon\right]s^2}{\left[-\Gamma g\varepsilon\right]s^2 + \left[\Gamma g - 2\Gamma g\varepsilon S_b\right]s + \left[\Gamma g S_b - \Gamma g\varepsilon S_b^2 + \frac{\Gamma\beta}{\tau_s}\right]}$$

$$+ \frac{\left[\frac{S_b}{\tau_p} + S_b\Gamma g N_o - S_b^2\Gamma g N_o\varepsilon\right]}{\left[-\Gamma g\varepsilon\right]s^2 + \left[\Gamma g - 2\Gamma g\varepsilon S_b\right]s + \left[\Gamma g S_b - \Gamma g\varepsilon S_b^2 + \frac{\Gamma\beta}{\tau_s}\right]} \quad . \qquad (A.7)$$

For simplification of the denominator in Equation (A.7), the following third-order mathematical relation can be applied:

$$\frac{1}{\rho s^2 + \upsilon s + \varphi} = A + Bs + Cs^2 + Ds^3 \quad , \qquad (A.8)$$

where $\rho = -\Gamma g\varepsilon$,

$\upsilon = \Gamma g - 2\Gamma g\varepsilon S_b$,

$\varphi = \Gamma g S_b - \Gamma g\varepsilon S_b^2 + \frac{\Gamma\beta}{\tau_s}$,

$A = \frac{1}{\varphi}$,

$B = -\frac{\upsilon}{\varphi^2}$,

$C = \frac{\upsilon^2}{\varphi^3} - \frac{\rho}{\varphi^2}$ and

$D = \frac{2\rho\upsilon}{\varphi^3} - \frac{\upsilon^3}{\varphi^4}$.

The third-order expression of Equation (A.8) will be suitable for use, since the need for compensation of higher orders of non-linearity in a LD is virtually non-existent. Its substitution into Equation (A.7) allows the carrier density expression to become

$$N = \left[A + Bs + Cs^2 + Ds^3\right]\left[s' + Es + Fs^2 + G\right] \quad , \qquad (A.9)$$

where $s' = \frac{d(S_b+s)}{dt} = \frac{ds}{dt}$,

$E = \frac{1}{\tau_p} + \Gamma g N_o - 2S_b\Gamma g N_o\varepsilon$,

$F = -\Gamma g N_o\varepsilon$ and

$G = \frac{S_b}{\tau_p} + S_b\Gamma g N_o - S_b^2\Gamma g N_o\varepsilon$.

Equation (A.3) can now be manipulated, preparing the signal current to be expressed in terms of s. Expansion and rearrangement of Equation (A.3) gives

$$\frac{I}{qV_c} = \frac{dN}{dt} + \frac{N}{\tau_s} + gNS - gN\epsilon S^2 - gN_oS + gN_o\epsilon S^2 \quad . \tag{A.10}$$

Again, a substitution based on $S = S(t) = S_b + s$ can be made. Equation (A.10) becomes

$$\frac{I}{qV_c} = \frac{dN}{dt} + \left[\frac{1}{\tau_s} + gS_b + gs - g\epsilon S_b^2 - 2g\epsilon S_b s - g\epsilon s^2\right] N$$

$$- gN_oS_b - gN_os + gN_o\epsilon S_b^2 + 2gN_o\epsilon S_b s + gN_o\epsilon s^2 \quad , \tag{A.11}$$

and simplifies to

$$\frac{I}{qV_c} = \frac{dN}{dt} + \left[H + Js + Ks^2\right] N + Ls^2 + Ms + P \quad , \tag{A.12}$$

where $H = \frac{1}{\tau_s} + gS_b - g\epsilon S_b^2$,

$J = g - 2g\epsilon S_b$,

$K = -g\epsilon$,

$L = gN_o\epsilon$,

$M = 2gN_o\epsilon S_b - gN_o$ and

$P = gN_o\epsilon S_b^2 - gN_oS_b$.

The carrier density, N, can be substituted for using its equivalent expression from Equation (A.9). This will permit Equation (A.12) to become

$$\frac{I}{qV_c} = \frac{d}{dt}\Big(\left[A + Bs + Cs^2 + Ds^3\right]\left[s' + Es + Fs^2 + G\right]\Big)$$

$$+ \left[H + Js + Ks^2\right]\Big(\left[A + Bs + Cs^2 + Ds^3\right]\left[s' + Es + Fs^2 + G\right]\Big)$$

$$+ Ls^2 + Ms + P \quad . \tag{A.13}$$

A substitution should be made, based on $I = I(t) = I_b + i$ where I_b is the bias current and i is the time-varying signal component, and the derivative operation carried out. This changes Equation (A.13) to

$$\begin{aligned}\frac{I_b+i}{qV_c} &= \left[Bs' + 2Css' + 3Ds^2s'\right]\left[s' + Es + Fs^2 + G\right] \\ &\quad + \left[A + Bs + Cs^2 + Ds^3\right]\left[s'' + Es' + 2Fss'\right] \\ &\quad + \left[H + Js + Ks^2\right]\left[A + Bs + Cs^2 + Ds^3\right]\left[s' + Es + Fs^2 + G\right] \\ &\quad + Ls^2 + Ms + P \quad . \end{aligned} \tag{A.14}$$

Next, expansion of the products in Equation (A.14) and some rearranging leads to

$$\begin{aligned} I_b + i &= qV_c\Big[Bs's' + BEss' + BFs^2s' + BGs' + 2Css's' + 2CEs^2s' + 2CFs^3s' \\ &\quad + 2CGss' + 3Ds^2s's' + 3DEs^3s' + 3DFs^4s' + 3DGs^2s' + As'' + AEs' \\ &\quad + 2AFss' + Bss'' + BEss' + 2BFs^2s' + Cs^2s'' + CEs^2s' + 2CFs^3s' \\ &\quad + Ds^3s'' + DEs^3s' + 2DFs^4s' + AHs' + AEHs + AFHs^2 + AGH \\ &\quad + BHss' + BEHs^2 + BFHs^3 + BGHs + CHs^2s' + CEHs^3 + CFHs^4 \\ &\quad + CGHs^2 + DHs^3s' + DEHs^4 + DFHs^5 + DGHs^3 + AJss' + AEJs^2 \\ &\quad + AFJs^3 + AGJs + BJs^2s' + BEJs^3 + BFJs^4 + BGJs^2 + CJs^3s' \\ &\quad + CEJs^4 + CFJs^5 + CGJs^3 + DJs^4s' + DEJs^5 + DFJs^6 + DGJs^4 \end{aligned}$$

$$+ AKs^2s' + AEKs^3 + AFKs^4 + AGKs^2 + BKs^3s' + BEKs^4 + BFKs^5$$

$$+ BGKs^3 + CKs^4s' + CEKs^5 + CFKs^6 + CGKs^4 + DKs^5s'$$

$$+ DEKs^6 + DFKs^7 + DGKs^5 + Ls^2 + Ms + P\Big] \quad . \tag{A.15}$$

Equation (A.15) can be rearranged to finally show signal current in terms of the time-varying photon density. The third-order complementary opposite compensation expression will become

$$\begin{aligned} i \;=\; & AGHqV_c + PqV_c - I_b + [AEHqV_c + BGHqV_c + AGJqV_c + MqV_c]s + [BGqV_c \\ & + AEqV_c + AHqV_c]s' + [AqV_c]s'' + [AFHqV_c + BEHqV_c + CGHqV_c \\ & + AEJqV_c + BGJqV_c + AGKqV_c + LqV_c]s^2 + [BEqV_c + 2CGqV_c + 2AFqV_c \\ & + BEqV_c + BHqV_c + AJqV_c]ss' + [BqV_c]ss'' + [BqV_c]s's' + [BFHqV_c \\ & + CEHqV_c + DGHqV_c + AFJqV_c + BEJqV_c + CGJqV_c + AEKqV_c \\ & + BGKqV_c]s^3 + [BFqV_c + 2CEqV_c + 3DGqV_c + 2BFqV_c + CEqV_c + CHqV_c \\ & + BJqV_c + AKqV_c]s^2s' + [CqV_c]s^2s'' + [2CqV_c]ss's' \quad . \end{aligned} \tag{A.16}$$

Simplification of Equation (A.16) leads to

$$\begin{aligned} i \;=\; & a + bs + cs' + ds'' + es^2 + fss' + gss'' + hs's' \\ & + ks^3 + ls^2s' + ms^2s'' + nss's' \quad , \end{aligned} \tag{A.17}$$

where $a = AGHqV_c + PqV_c - I_b$,

$$b = AEHqV_c + BGHqV_c + AGJqV_c + MqV_c \quad ,$$

$$c = BGqV_c + AEqV_c + AHqV_c \quad ,$$

$$d = AqV_c \quad ,$$

$$e = AFHqV_c + BEHqV_c + CGHqV_c + AEJqV_c + BGJqV_c + AGKqV_c + LqV_c \, ,$$

$$f = BEqV_c + 2CGqV_c + 2AFqV_c + BEqV_c + BHqV_c + AJqV_c \quad ,$$

$$g = BqV_c \quad ,$$

$$h = BqV_c \quad ,$$

$$k = BFHqV_c + CEHqV_c + DGHqV_c + AFJqV_c + BEJqV_c + CGJqV_c + AEKqV_c + BGKqV_c \quad ,$$

$$l = BFqV_c + 2CEqV_c + 3DGqV_c + 2BFqV_c + CEqV_c + CHqV_c + BJqV_c + AKqV_c \quad ,$$

$m = CqV_c$ and

$n = 2CqV_c$.

It should be noted that the coefficients g and h in Equation (A.17) are equal.

Appendix B

Volterra Analysis Leading to Third-order Distortion System

B.1 Derivation Of Volterra Transfer Functions

Having an expression for the signal distortion required to compensate for LD dynamic non-linearity, the transfer function(s) for a compensation system can now be determined.

For an arbitrary, ideal linear system or device, the output, $y(t)$, may be expressed as the convolution of the system impulse response, $h(t)$, with the input signal, $x(t)$. This is shown as

$$y(t) = \int_{-\infty}^{\infty} h(\tau)x(t-\tau)d\tau \quad . \tag{B.1}$$

However, for a non-linear system, such as the complementary opposite distorter for a LD, Equation (B.1) only applies in part. As discussed thoroughly by Schetzen [42], a Volterra series representation of the system would be far more appropriate. Such a representation is a generalization of a power series that is capable of handling frequency dependent systems. A Volterra series could take the form

$$y(t) = \int_{-\infty}^{\infty} h_1(\tau_1)x(t-\tau_1)d\tau_1 + \int_{-\infty}^{\infty}\int_{-\infty}^{\infty} h_2(\tau_1,\tau_2)x(t-\tau_1)x(t-\tau_2)d\tau_1 d\tau_2$$

$$+\sum_{u=3}^{n}\left[\int_{-\infty}^{\infty}\cdots\int_{-\infty}^{\infty} h_u(\tau_1,\cdots\tau_u)x(t-\tau_1)\cdots x(t-\tau_u)d\tau_1\cdots d\tau_u\right] \quad . \tag{B.2}$$

Volterra analysis is used on a system to determine the n^{th}-order non-linear transfer functions, $H_n(j\omega_1,\cdots j\omega_n)$, where n is a positive integer. These transfer functions

are the n-dimensional Fourier transforms of $h_n(t_1, \cdots t_n)$. The transform-domain representation then brings into focus the frequency behavior of the system. When a transfer function is known, it is important to note that the n^{th}-order non-linear impulse response, also known as the n^{th}-order Volterra kernel, may be determined by using the expression

$$h_n(t_1, \cdots t_n) = \frac{1}{(2\pi)^n} \int_{-\infty}^{\infty} \cdots \int_{-\infty}^{\infty} H_n(j\omega_1, \cdots j\omega_n) e^{j(\omega_1 t_1 + \cdots + \omega_n t_n)} d\omega_1 \cdots d\omega_n \quad . \tag{B.3}$$

Because the expression in Equation (A.17) is capable of compensating for no more than third-order non-linearities, due to earlier design considerations, the Volterra analysis applied here need be no more than third-order, too. This analytical approach permits Equation (A.17) to be thought of in a form similar to Equation (B.2), represented by the block diagram of the distortion system shown in Figure 3.9 and rewritten as $i(t) - a = \boldsymbol{D}_1[s(t)] + \boldsymbol{D}_2[s(t)] + \boldsymbol{D}_3[s(t)]$, where $\boldsymbol{D}_1[\cdot]$, $\boldsymbol{D}_2[\cdot]$ and $\boldsymbol{D}_3[\cdot]$ are the respective first-, second- and third-order Volterra operators for a LD complementary opposite distortion system. Since the distortion system operators each have a representative transfer function, three functions should be produced.

Starting the analysis of Equation (A.17) by defining the first-order Volterra transfer function, $D_1(j\omega_1)$, the post-distortion system can be 'probed' by applying $s = s(t) = s_{pk}e^{j\omega_1 t}$ in Equation (A.17), giving

$$\begin{aligned} i(t) = {} & a + bs_{pk}e^{j\omega_1 t} + c\frac{d}{dt}\left[s_{pk}e^{j\omega_1 t}\right] + d\frac{d^2}{dt^2}\left[s_{pk}e^{j\omega_1 t}\right] + e\left[s_{pk}e^{j\omega_1 t}\right]^2 \\ & + fs_{pk}e^{j\omega_1 t}\frac{d}{dt}\left[s_{pk}e^{j\omega_1 t}\right] + gs_{pk}e^{j\omega_1 t}\frac{d^2}{dt^2}\left[s_{pk}e^{j\omega_1 t}\right] \\ & + h\frac{d}{dt}\left[s_{pk}e^{j\omega_1 t}\right]\frac{d}{dt}\left[s_{pk}e^{j\omega_1 t}\right] + k\left[s_{pk}e^{j\omega_1 t}\right]^3 + l\left[s_{pk}e^{j\omega_1 t}\right]^2\frac{d}{dt}\left[s_{pk}e^{j\omega_1 t}\right] \\ & + m\left[s_{pk}e^{j\omega_1 t}\right]^2\frac{d^2}{dt^2}\left[s_{pk}e^{j\omega_1 t}\right] + ns_{pk}e^{j\omega_1 t}\frac{d}{dt}\left[s_{pk}e^{j\omega_1 t}\right]\frac{d}{dt}\left[s_{pk}e^{j\omega_1 t}\right] \quad , \end{aligned} \tag{B.4}$$

where s_{pk} is the peak amplitude of s, and ω_1 is a sinusoidal signal frequency. Equation (B.4) can then be expanded and rearranged so that $D_1(j\omega_1)e^{j\omega_1 t}$ can be found and $D_1(j\omega_1)$ identified. The result of this becomes

$$\begin{aligned} i(t) &= a + bs_{pk}e^{j\omega_1 t} + jcs_{pk}\omega_1 e^{j\omega_1 t} - ds_{pk}\omega_1^2 e^{j\omega_1 t} + es_{pk}^2 e^{j2\omega_1 t} + jfs_{pk}^2\omega_1 e^{j2\omega_1 t} \\ &\quad - jgs_{pk}^2\omega_1^2 e^{j2\omega_1 t} - hs_{pk}^2\omega_1^2 e^{j2\omega_1 t} + ks_{pk}^3 e^{j3\omega_1 t} + jls_{pk}^3\omega_1 e^{j3\omega_1 t} - ms_{pk}^3\omega_1^2 e^{j3\omega_1 t} \\ &\quad - ns_{pk}^3\omega_1^2 e^{j3\omega_1 t} \quad . \end{aligned} \tag{B.5}$$

Since the second, third and fourth terms on the right are the only ones containing $e^{j\omega_1 t}$, the first-order transfer function can be identified as $D_1(j\omega_1) = s_{pk}(b + jc\omega_1 - d\omega_1^2)$.

Next, $D_2(j\omega_1, j\omega_2)$ can be similarly found by 'probing' Equation (A.17) with $s = s(t) = s_{pk}(e^{j\omega_1 t} + e^{j\omega_2 t})$ and noting the coefficients of the terms containing $e^{j(\omega_1+\omega_2)t}$. First, the substitution gives

$$\begin{aligned} i(t) &= a + b\left[s_{pk}(e^{j\omega_1 t} + e^{j\omega_2 t})\right] + c\frac{d}{dt}\left[s_{pk}(e^{j\omega_1 t} + e^{j\omega_2 t})\right] + d\frac{d^2}{dt^2}\left[s_{pk}(e^{j\omega_1 t} + e^{j\omega_2 t})\right] \\ &\quad + e\left[s_{pk}(e^{j\omega_1 t} + e^{j\omega_2 t})\right]^2 + fs_{pk}(e^{j\omega_1 t} + e^{j\omega_2 t})\frac{d}{dt}\left[s_{pk}(e^{j\omega_1 t} + e^{j\omega_2 t})\right] \\ &\quad + gs_{pk}(e^{j\omega_1 t} + e^{j\omega_2 t})\frac{d^2}{dt^2}\left[s_{pk}(e^{j\omega_1 t} + e^{j\omega_2 t})\right] \\ &\quad + h\frac{d}{dt}\left[s_{pk}(e^{j\omega_1 t} + e^{j\omega_2 t})\right]\frac{d}{dt}\left[s_{pk}(e^{j\omega_1 t} + e^{j\omega_2 t})\right] + k\left[s_{pk}(e^{j\omega_1 t} + e^{j\omega_2 t})\right]^3 \\ &\quad + l\left[s_{pk}(e^{j\omega_1 t} + e^{j\omega_2 t})\right]^2\frac{d}{dt}\left[s_{pk}(e^{j\omega_1 t} + e^{j\omega_2 t})\right] \\ &\quad + m\left[s_{pk}(e^{j\omega_1 t} + e^{j\omega_2 t})\right]^2\frac{d^2}{dt^2}\left[s_{pk}(e^{j\omega_1 t} + e^{j\omega_2 t})\right] \end{aligned}$$

$$+ ns_{pk}(e^{j\omega_1 t} + e^{j\omega_2 t})\frac{d}{dt}\left[s_{pk}(e^{j\omega_1 t} + e^{j\omega_2 t})\right]\frac{d}{dt}\left[s_{pk}(e^{j\omega_1 t} + e^{j\omega_2 t})\right] \quad . \qquad \text{(B.6)}$$

Equation (B.6) can be expanded and rearranged so that $D_2(j\omega_1, j\omega_2)e^{j(\omega_1+\omega_2)t}$ can be apparent and $D_2(j\omega_1, j\omega_2)$ identified. This results in

$$\begin{aligned}
i(t) = a &+ bs_{pk}\left[e^{j\omega_1 t} + e^{j\omega_2 t}\right] + jcs_{pk}\left[\omega_1 e^{j\omega_1 t} + \omega_2 e^{j\omega_2 t}\right] - ds_{pk}\left[\omega_1^2 e^{j\omega_1 t} + \omega_2^2 e^{j\omega_2 t}\right] \\
&+ es_{pk}^2\left[e^{j2\omega_1 t} + 2e^{j(\omega_1+\omega_2)t} + e^{j2\omega_2 t}\right] \\
&+ jfs_{pk}^2\left[\omega_1 e^{j2\omega_1 t} + \omega_1 e^{j(\omega_1+\omega_2)t} + \omega_2 e^{j(\omega_1+\omega_2)t} + \omega_2 e^{j2\omega_2 t}\right] \\
&- gs_{pk}^2\left[\omega_1^2 e^{j2\omega_1 t} + \omega_1^2 e^{j(\omega_1+\omega_2)t} + \omega_2^2 e^{j(\omega_1+\omega_2)t} + \omega_2^2 e^{j2\omega_2 t}\right] \\
&- hs_{pk}^2\left[\omega_1^2 e^{j2\omega_1 t} + \omega_1\omega_2 e^{j(\omega_1+\omega_2)t} + \omega_2^2 e^{j2\omega_2 t}\right] \\
&+ ks_{pk}^3\left[e^{j3\omega_1 t} + 2e^{j(2\omega_1+\omega_2)t} + e^{j(\omega_1+2\omega_2)t} + e^{j(2\omega_1+\omega_2)t} + 2e^{j(\omega_1+2\omega_2)t} + e^{j3\omega_2 t}\right] \\
&+ jls_{pk}^3\left[\omega_1 e^{j3\omega_1 t} + 2\omega_1 e^{j(2\omega_1+\omega_2)t} + \omega_1 e^{j(\omega_1+2\omega_2)t} + \omega_2 e^{j(2\omega_1+\omega_2)t}\right. \\
&\left. + 2\omega_2 e^{j(\omega_1+2\omega_2)t} + \omega_2 e^{j3\omega_2 t}\right] - ms_{pk}^3\left[\omega_1^2 e^{j3\omega_1 t} + 2\omega_1^2 e^{j(2\omega_1+\omega_2)t}\right. \\
&\left. + \omega_1^2 e^{j(\omega_1+2\omega_2)t} + \omega_2^2 e^{j(2\omega_1+\omega_2)t} + 2\omega_2^2 e^{j(\omega_1+2\omega_2)t} + \omega_2^2 e^{j3\omega_2 t}\right] \\
&- ns_{pk}^3\left[\omega_1^2 e^{j3\omega_1 t} + \omega_1\omega_2 e^{j(2\omega_1+\omega_2)t} + \omega_2^2 e^{j(\omega_1+2\omega_2)t} + \omega_1^2 e^{j(2\omega_1+\omega_2)t}\right. \\
&\left. + \omega_1\omega_2 e^{j(\omega_1+2\omega_2)t} + \omega_2^2 e^{j3\omega_2 t}\right] \quad . \qquad \text{(B.7)}
\end{aligned}$$

The second-order transfer function can then be found to be $D_2(j\omega_1, j\omega_2) = s_{pk}^2(2e + jf\omega_1 + jf\omega_2 - g\omega_1^2 - g\omega_2^2 - 2h\omega_1\omega_2)$, and simplified to $D_2(j\omega_1, j\omega_2) = s_{pk}^2(2e + jf(\omega_1 + \omega_2) - h(\omega_1 + \omega_2)^2)$, since we know from Equation (A.17) $h = g$.

And finally, $s = s(t) = s_{pk}(e^{j\omega_1 t} + e^{j\omega_2 t} + e^{j\omega_3 t})$ can be used in Equation (A.17) so that $D_3(j\omega_1, j\omega_2, j\omega_3)$ may be equated to coefficients of terms containing $e^{j(\omega_1+\omega_2+\omega_3)t}$. However, the mathematical derivation would be similar to those already shown and will not be shown here due to its length.

The three Volterra transfer functions for the pre-distortion system are summarized as

$$D_1(j\omega_1) = s_{pk}\left(b + jc\omega_1 - d\omega_1^2\right) , \tag{B.8}$$

$$D_2(j\omega_1, j\omega_2) = s_{pk}^2\left(2e + jf(\omega_1+\omega_2) - h(\omega_1+\omega_2)^2\right) \text{ and} \tag{B.9}$$

$$D_3(j\omega_1, j\omega_2, j\omega_3) = s_{pk}^3\left(6k + j2l(\omega_1+\omega_2+\omega_3) - 2m(\omega_1+\omega_2+\omega_3)^2\right) . \tag{B.10}$$

B.2 Realization Of Volterra Transfer Functions In Practical Constructs

So that a simple time–based representation can be made, each of the three transfer function can be translated from the Fourier form to a Laplacian form and then decomposed into a combination of linear operations. This is done by first replacing $j\omega$ with $\sigma + j\omega$. Since $\sigma = 0$ in stable systems, this results in the following when letting the Laplacian variable s equal $\sigma + j\omega$ in Equations (B.8), (B.9) and (B.10):

$$D_1(s_1) = s_{pk}\left(b + cs_1 + ds_1^2\right) , \tag{B.11}$$

$$D_2(s_1, s_2) = s_{pk}^2\left(2e + f(s_1+s_2) + h(s_1+s_2)^2\right) \text{ and} \tag{B.12}$$

$$D_3(s_1, s_2, s_3) = s_{pk}^3\left(6k + 2l(s_1+s_2+s_3) + 2m(s_1+s_2+s_3)^2\right) . \tag{B.13}$$

The third-order generic version of Equation (B.2) may now be thought of as

$$y(t) = \boldsymbol{H}_1[x(t)] + \boldsymbol{H}_2[x(t)] + \boldsymbol{H}_3[x(t)] , \tag{B.14}$$

where $\boldsymbol{H_u}[x(t)] = \int_{-\infty}^{\infty} \cdots \int_{-\infty}^{\infty} h_u(\tau_1, \cdots \tau_u) x(t-\tau_1) \cdots x(t-\tau_u) d\tau_1 \cdots d\tau_u$. Converting to the Laplace domain, operator $\boldsymbol{H_1}[\cdot]$ becomes function $H_1(s_1)$, operator $\boldsymbol{H_2}[\cdot]$ becomes function $H_2(s_1, s_2)$ and operator $\boldsymbol{H_3}[\cdot]$ becomes function $H_3(s_1, s_2, s_3)$.

Because

$$H_2(s_1, s_2) = \int_{-\infty}^{\infty} \int_{-\infty}^{\infty} h_2(\tau_1, \tau_2) e^{-(s_1\tau_1 + s_2\tau_2)} d\tau_1 d\tau_2 \quad , \tag{B.15}$$

and in general

$$h_2(\tau_1, \tau_2) = \int_{-\infty}^{\infty} h_c(t) h_a(\tau_1 - t) h_b(\tau_2 - t) dt \quad , \tag{B.16}$$

a second-order system in time domain form may look like Figure B.1. Recognizing from the general fact that

$$H_2(s_1, s_2) = H_a(s_1) H_b(s_2) H_c(s_1 + s_2) \quad , \tag{B.17}$$

Equation (B.12) equates to a system operating only on the square of the input signal (since $D_2(s_1, s_2) = D_c(s_1 + s_2)$). Also, and similarly, because

$$H_3(s_1, s_2, s_3) = H_a(s_1) H_b(s_2) H_c(s_1 + s_2) H_d(s_3) H_e(s_1 + s_2 + s_3) \quad , \tag{B.18}$$

Equation (B.13) equates to a system operating only on the cubed value of the input signal.

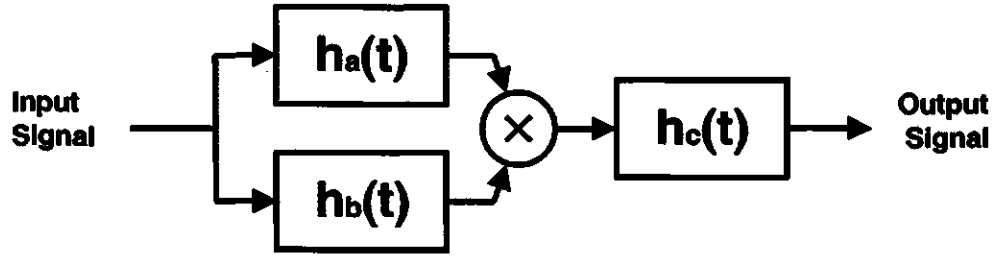

Figure B.1: General Second-order System Structure

If s_{1+2} is used in place of $s_1 + s_2$ in Equation (B.12), and s_{1+2+3} is used in place of $s_1 + s_2 + s_3$ in Equation (B.13), these new, independent expressions can be seen to

have the same three–term linear form as Equation (B.11):

$$D_{2'}(s_{1+2}) = s_{pk}^2\left(2e + fs_{1+2} + hs_{1+2}^2\right) \text{ and} \tag{B.19}$$

$$D_{3'}(s_{1+2+3}) = s_{pk}^3\left(6k + 2ls_{1+2+3} + 2ms_{1+2+3}^2\right) . \tag{B.20}$$

Because a derivative operation in the time domain is represented by s in its Laplace form, Equations (B.11), (B.12) and (B.13) each represent a system performing the summation of the results from a simple amplifier operation, an amplifier and derivative with respect to time operation and an amplifier and double–derivative with respect to time operation, as shown in Figure B.2. The values of X, Y and Z in Figure B.2 would correspond to the three coefficients in the transfer function expression of choice. Overall, Equations (B.8), (B.9) and (B.10) can be realized by using the system structures shown in Figures 3.10 and 5.1.

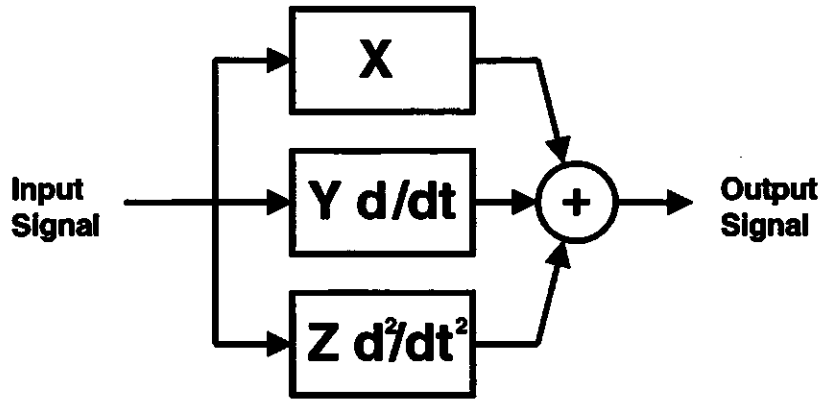

Figure B.2: Common System Structure in Volterra Pre-distorter

Appendix C

Approach for Normalization/Optimization of Pre-distortion System Coefficients

Because a LD pre-distortion system uses an appropriate current magnitude for its input, the coefficients in the Volterra transfer functions found earlier must be normalized in order to produce the appropriate current magnitude required by the LD model. The concept for the distortion system described by Equations (B.8), (B.9) and (B.10) expects an input signal magnitude at photon density levels and produces an output signal having LD modulating current levels. If the distortion system is to be electrically implemented as a signal pre-distorter, then both the system input and output levels must deal in magnitudes of current, not photon density.

The LD L-I characteristic has a slope at the bias point equal to the inverse of the post-distortion system gain. For this work with Laser 'A' the slope at 500 μA is 11758.8695E20 photons m^{-3} A^{-1}. The complimentary opposite post-distortion system produces the inverse of this 'translation gain'; $b = 1 \div 11758.8695E20$ A (photons $m^{-3})^{-1}$, represented as 8.5042189E-25 when ignoring proper units. As such, it is apparent that the 'translation gain' of the distortion system must be negated if it is to be applied as a pre-distorter.

The mathematical way of realizing a pre-distortion system from Equation (A.17) or Equations (B.8), (B.9) and (B.10) is to let $s = i \div b$ and $s_{pk} = i_{pk} \div b$. The pre-distortion system would then have the following transfer function representations:

$$i_{distorted} = a + \frac{b}{b}i + \frac{c}{b}i' + \frac{d}{b}i'' + \frac{e}{b^2}i^2 + \frac{f}{b^2}ii' + \frac{g}{b^2}ii'' + \frac{h}{b^2}i'i'$$

$$+\frac{k}{b^3}i^3+\frac{l}{b^3}i^2i'+\frac{m}{b^3}i^2i''+\frac{n}{b^3}ii'i' \quad \text{, or} \tag{C.1}$$

$$D_1(j\omega_1) = i_{pk}\left(b_n+jc_n\omega_1-d_n\omega_1^2\right) \quad , \tag{C.2}$$

$$D_2(j\omega_1,j\omega_2) = i_{pk}^2\left(2e_n+jf_n(\omega_1+\omega_2)-h_n(\omega_1+\omega_2)^2\right) \quad \text{and} \tag{C.3}$$

$$D_3(j\omega_1,j\omega_2,j\omega_3) = i_{pk}^3\left(6k_n+j2l_n(\omega_1+\omega_2+\omega_3)-2m_n(\omega_1+\omega_2+\omega_3)^3\right) \quad , \tag{C.4}$$

where $i'=\frac{di}{dt}$, $i''=\frac{d}{dt}(\frac{di}{dt})$, $g=h$, $b_n=b\div b$, $c_n=c\div b$, $d_n=d\div b$, $e_n=e\div b^2$, $f_n=f\div b^2$, $h_n=h\div b^2$, $k_n=k\div b^3$, $l_n=l\div b^3$ and $m_n=m\div b^3$.

The LD pre-distortion system suitable for use with Laser 'A' has, according to Appendixes A and B and the normalization above, the following coefficient values:

$b_n = 1$ $\quad (b_n = 1)$,
$c_n = 1.475105\text{E-}11$ $\quad (\frac{c_n}{b_n} = 1.475105\text{E-}11)$,
$d_n = 2.652802\text{E-}21$ $\quad (\frac{d_n}{c_n} = 1.798382\text{E-}10)$,
$e_n = -2.617203$ $\quad (2e_n = -5.234406)$,
$f_n = -1.980601\text{E-}8$ $\quad (\frac{f_n}{2e_n} = 3.783812\text{E-}9)$,
$h_n = -1.227349\text{E-}17$ $\quad (\frac{h_n}{f_n} = 6.196850\text{E-}10)$,
$k_n = 1.276412\text{E}4$ $\quad (6k_n = 7.658475\text{E}4)$,
$l_n = 1.340478\text{E-}4$ $\quad (\frac{2l_n}{6k_n} = 3.500639\text{E-}9)$ and
$m_n = 5.722427\text{E-}14$ $\quad (\frac{2m_n}{2l_n} = 4.268945\text{E-}10)$.

The values have been calculated based on the device parameters shown in Table 3.1, and are for use when I_b equals 500 μA. (The values in parentheses can be applied to the system structure shown in Figure 5.1.)

These calculated coefficients do not produce remarkable results. This may be due to the fact that simplifications that limited derivations of the post-distorter to no more than the third-order overlook other complexities of the dynamic LD behavior. If the distortion system were to use the coefficients as determined above, the pre-distorted laser would perform as shown in Figures C.1 and C.2 for single channel OMIs of 30 and 4 percent, respectively.

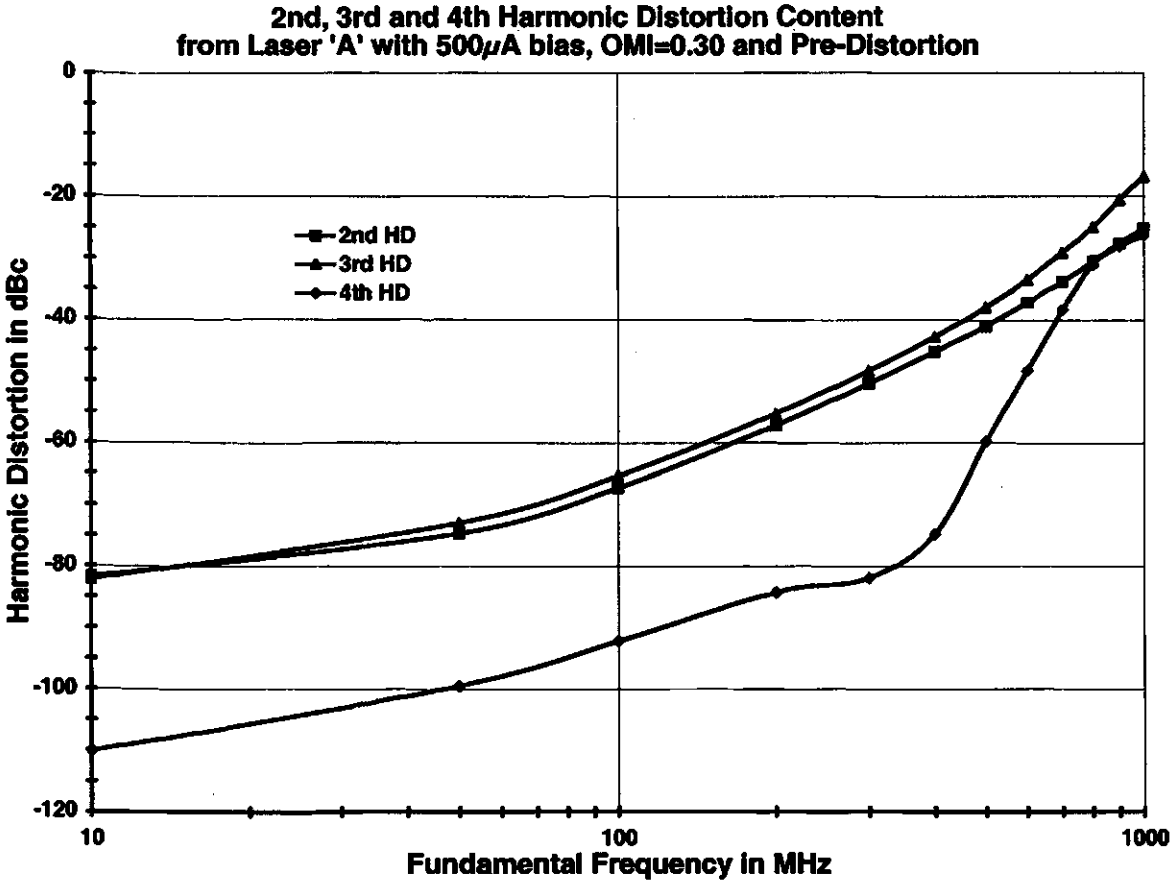

Figure C.1: Harmonic Distortion Content for Simulated Laser 'A' with Non-optimized Pre-distortion (OMI = 30 %)

Through the examination of the harmonic content contributed by the pre-distortion system, as well as that of the modeled LD, it was determined that some optimization of the pre-distorter coefficients would bring about a significant overall performance improvement. After optimizing, the preferred coefficient values became

$$
\begin{aligned}
b_p &= 1.00025 && (b_p = 1.00025)\ , \\
c_p &= 1.475105\text{E-}11 && (\tfrac{c_p}{b_p} = 1.475067\text{E-}11)\ , \\
d_p &= 2.652802\text{E-}21 && (\tfrac{d_p}{c_p} = 1.798268\text{E-}10)\ , \\
e_p &= -1.37380 && (2e_p = -2.7476)\ , \\
f_p &= -1.980601\text{E-}8 && (\tfrac{f_p}{2e_p} = 3.783892\text{E-}9)\ , \\
h_p &= -1.227349\text{E-}17 && (\tfrac{h_p}{f_p} = 6.197352\text{E-}10)\ ,
\end{aligned}
$$

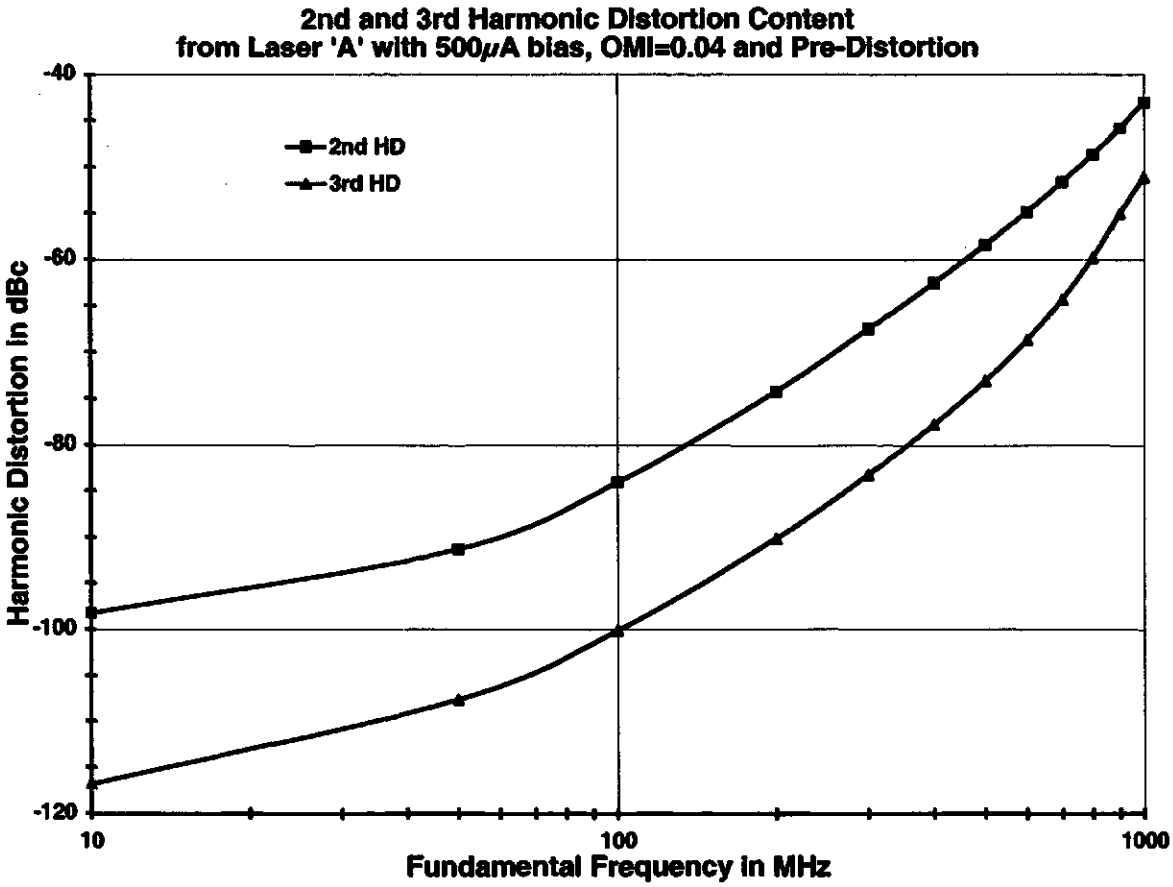

Figure C.2: Harmonic Distortion Content for Simulated Laser 'A' with Non-optimized Pre-distortion (OMI = 4 %)

$$k_p = 0.22153\text{E}4 \qquad (6k_p = 1.3292\text{E}4)\ ,$$
$$l_p = 1.340478\text{E-}4 \qquad (\tfrac{2l_p}{6k_p} = 3.500684\text{E-}9) \ \text{ and}$$
$$m_p = 5.722427\text{E-}14 \quad (\tfrac{2m_p}{2l_p} = 4.269273\text{E-}10)\ .$$

The values of e_p, f_p and h_p are, simply, the calculated normalized values reduced by a common factor. Similarly, the values of k_p, l_p and m_p have also been reduced. This optimized pre-distortion system was used with Laser 'A' to obtain all of the results reported in this document, with the exception of Figures C.1 and C.2. Also, unless denoted otherwise, a coefficient without its subscript 'p' will still imply a reference to the preferred normalized *and* optimized value.

Although the preferred coefficients could not be analytically explained, their dif-

ference from the calculated normalized values is relatively small. The preferred coefficients are more easily accepted when one notes that both the second- and third-order Volterra transfer functions must be weighted differently in order to provide complimentary opposite distortion for the LD; each order of the system transfer function behaves independently. Results from Sieben's work [9, p.74] support the use of the preferred coefficients, since good agreement exists with Figure 5.5, and not Figure C.1.

Appendix D

Listing of Simulation Files

D.1 Laser Diode Simulation

In order to investigate current signals in ICAP/4 [27], the simulation tool must have an object through which it can observe the travel–through parameter. This can be done using a monitor or 'dummy' voltage source (having no applied voltage value), and designating it as a current monitoring point. In Figure 3.2, the voltage source and probe between node 1 and ground are one example of the reporting method for a 'current' signal within the LD model.

The LD circuit–equivalent model is not fundamentally an electrical circuit. It is a model based on the electrical–charge carriers and photons in a single mode semiconductor laser cavity. Because of this, certain parameters of the laser cavity system, that have magnitudes far beyond any true electrical circuit parameter, dictate that the LD model interpret values in the simulation tool with a notably different perspective. The magnitude of the carrier density at node 2 in Figure 3.2 can not be successfully simulated with ICAP/4 if it remains of an order beyond ±32. The model and its simulated results have accommodated this by scaling down the volume of the modeled cavity by 1E20, without affecting the interaction between the carriers and photons. So when ICAP/4 reports 2.521084 volts at node 6, it is important to note that with this model that value is properly interpreted as 2.521084E20 photons m^{-3}.

One last important note about the LD model, titled `LaserDiode`, is that the two–variable polynomial expression (`POLY(2)`) is an essential function necessary for investigating the LD using a SPICE–based modeling tool. Its syntax in ICAP/4 is as follows:

$$\texttt{POLY}(u)\ \text{node}_1^+\ \text{node}_1^-\ \cdots\ \text{node}_u^+\ \text{node}_u^-\ \text{constant}_1\ \text{constant}_2\ \cdots\ .$$

The expression $y = 5.0 + 6.0x_{1wrt2} + 7.0x_{3wrt4} + 8.0x_{1wrt2}^2 + 9.0x_{1wrt2}x_{3wrt4} + 10.0x_{3wrt4}^2 + 11.0x_{1wrt2}^3 + 12.0x_{1wrt2}^2x_{3wrt4} + 13.0x_{1wrt2}x_{3wrt4}^2 + 14.0x_{3wrt4}^3$ may be shown as

```
POLY(2) 1 2 3 4 5.0 6.0 7.0 8.0 9.0 10.0 11.0 12.0 13.0 14.0 .
```

The voltage–controlled resistance needed for a LD circuit–equivalent representation uses a `POLY(2)` expression in its sub-circuit definition, `VCNTRLDR`. This can be found in the `.cir` file, and is conceptually illustrated by Figure D.1.

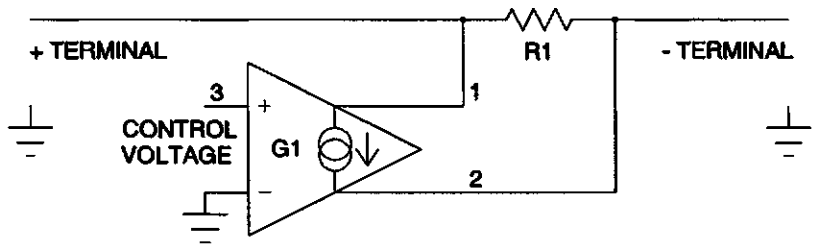

Figure D.1: Schematic Construct of a Voltage–controlled Resistance

Below is the netlist from the ICAP/4 `LaserDiode.cir` file.

```
LaserDiode
*SPICE_NET
.SUBCKT ZENER 1 2
D1 1 2 DZEN
.MODEL DZEN D(CJO=1E-32 IS=1E-32 TT=1E-32
+ BV={ZV} IBV=1E32 N=2 RS=0)
.ENDS
.SUBCKT VCNTRLDR 1 2 3
R1 1 2 1E32
G1 1 2 POLY(2) 1 2 3 0
+ 0 0 0 0 3E-12*1E20 0
+ 0 0 -1*3E-12*1E20*3E-23*1E20 0
.ENDS
;.TRAN 0.2P 5N 0N 0.2P
.TRAN 0.5P 102N 100N 0.2P UIC
;INIT CONS FOR 500UA BIAS FOLLOW
.IC V(2)=14934.179V V(4)=4932.690V V(6)=2.521084V
.OPTIONS RELTOL=0.001 METHOD=GEAR
.FOUR 1000MEGHZ I(V1)
```

```
.FOUR 1000MEGHZ V(6)
.PRINT TRAN I(V1) V(6)
V1 1 0
F1 0 2 V1 0 1/5.76E-17
C1 2 0 1
R1 2 3 3E-9
V2 3 0
X1 4 2 ZENER {ZV=1E4 }
X2 4 5 6 VCNTRLDR
V3 5 0
F2 0 6 V2 0 0.001*0.34
F3 0 6 V3 0 0.34
C2 6 0 1
R2 6 0 2E-12
I2 0 1 SIN 0 8.8U 1000MEG 0
I1 0 1 PULSE 0 500U 0
.END
```

D.2 Concept Trial for Adaptive Pre-distorter

The pre-distortion system in the TOC has been constructed so that voltage–controlled voltage sources (B1, B2, B4 and B5) are used to simplify adaptive changes in both the pre- and post-distortion systems. Because both of the distortion systems are intended to operate identically, both systems should rely on the same control voltages for performing any needed adaptive changes to initial design coefficients.

A SPICE–based simulation tool can not produce a transient analysis while a network control loop having a non-traditional structure undergoes change. In order to investigate the adaptive nature of the pre-distortion system (shown in Figure 4.2), the control loop that combats long–term changes in the non-linear 'device' is left open at the point of computing a new control voltage for the distortion systems. The computation of the adaptive control voltage is done outside the scope of the simulation tool.

Below is the netlist from the ICAP/4 `Concept.cir` file.

```
Concept
*SPICE_NET
*INCLUDE SYS.LIB
```

```
.TRAN 0.5P 2N 0 0.1P
.FOUR 1000MEGHZ V(7)
.PRINT TRAN V(15) V(14) V(13) V(9) V(8)
.PRINT TRAN V(7) V(4) V(3) V(2) V(1)
X1 1 5 6 SQ-CUBE {K1=1 K2=1 }
B1 2 0 V=V(5)*V(16)
B2 3 0 V=V(6)*V(17)
X2 1 2 3 4 SUM3 {K1=1 K2=1 K3=1 }
B3 7 0 V=V(4)+0.1*V(4)*V(4)
X3 7 10 11 SQ-CUBE {K1=1 K2=1 }
B4 8 0 V=V(10)*V(16)
B5 9 0 V=V(11)*V(17)
X4 7 8 9 12 SUM3 {K1=1 K2=1 K3=1 }
B6 13 0 V=V(7)-V(1)
B7 14 0 V=V(8)-V(2)
B8 15 0 V=V(9)-V(3)
V1 1 0 SIN 0 1 1000MEG ON
V2 16 0 -0.105521
V3 17 0 0.021804
.END
```

D.3 Laser Diode with Pre-distorter Simulation

The ICAP/4 `.cir` file below defines a system were the pre-distortion structure from Figure 5.1 precedes the modeled LD as shown in Figure 5.3. The pre-distorter was given the structure shown in Figure 5.1 instead of Figure 3.10 so that the nine multipliers would all have values less likely to cause a problem with the ICAP/4 5-bit exponent limitation ($32 = 2^5$). For instance, when 8.8 μA is cubed, its magnitude after being multiplied by $2m_p$ would be very small, and almost un-resolvable.

The ICAP/4 library function, SDIFF, performs a derivative operation, but unfortunately does not work well at high frequencies due to its underlying sub-circuit definition. Because the Volterra pre-distortion system depends on effective derivative operations for signals that may contain 3 GHz content, a new sub-circuit definition, called `DIFF`, was created for this work. It is illustrated in Figure D.2, and its definition appears within the `VolterraLD` netlist below.

Below is the netlist from the ICAP/4 `VolterraLD.cir` file.

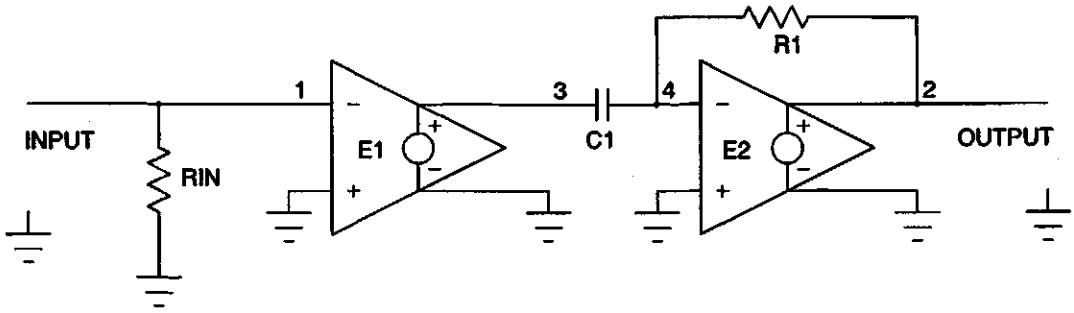

Figure D.2: Schematic Construct of Signal Differentiator

```
VolterraLD
*SPICE_NET
.SUBCKT DIFF 1 2
RIN 1 0 1E30
E1 3 0 0 1 0 {K}
C1 3 4 0.001F IC=0
R1 2 4 1E18
E2 2 0 0 4 1E18
.ENDS
*INCLUDE SYS.LIB
.SUBCKT VCNTRLDR 1 2 3
R1 1 2 1E32
G1 1 2 POLY(2) 1 2 3 0
+ 0 0 0 0 3E8 0 0 0 -9E5
.ENDS
.SUBCKT ZENER 1 2
D1 1 2 DZEN
.MODEL DZEN D(CJO=1E-30 IS=1E-30 TT=1E-30
+ BV={ZV} IBV=1E30 N=2 RS=0)
.ENDS
.TRAN 0.5P 102N 100N 0.1P UIC
;INIT CONS FOR 1.0MA BIAS FOLLOWS
;.IC V(21)=15027.4V V(23)=5026.686V V(25)=8.40276V
;INIT CONS FOR 500UA BIAS FOLLOWS
.IC V(21)=14936.179V V(23)=4933.69V V(25)=2.521084V
;INIT CONS FOR 0.5MA BIAS & 0.02 AGING FOLLOWS
;.IC V(21)=15140.7V V(23)=5139.21V V(25)=2.521V
.OPTION RELTOL=0.0001 METHOD=GEAR
.FOUR 1000MEGHZ V(25)
.PRINT TRAN V(25) I(V2) I(V1)
```

```
*ALIAS I(V1)="i"
*ALIAS V(25)="S"
I5 0 1 SIN 0 8.8U 1000MEG 0N
V1 1 0
H1 2 0 V1 0 1
E1 3 0 2 0 0 1.00025
X1 2 4 5 SQ-CUBE {K1=-2.7476 K2=13292 }
B1 6 0 V=1*V(3)
X19 6 7 DIFF {K=1.475067E-11 }
X21 7 8 DIFF {K=1.798268E-10 }
X3 6 7 8 15 SUM3 {K1=1 K2=1 K3=1 }
B2 9 0 V=1*V(4)
X22 9 10 DIFF {K=3.783892E-9 }
X24 10 11 DIFF {K=6.197352E-10 }
X4 9 10 11 16 SUM3 {K1=1 K2=1 K3=1 }
B3 12 0 V=1*V(5)
X25 12 13 DIFF {K=3.500684E-9 }
X27 13 14 DIFF {K=4.269273E-10 }
X5 12 13 14 17 SUM3 {K1=1 K2=1 K3=1 }
X6 15 16 17 18 SUM3 {K1=1 K2=1 K3=1 }
G1 0 19 18 0 0 2.521084/2.51746
V2 19 20
I4 0 20 PULSE 0 500U 0N
V3 20 0
F1 0 21 V3 0 1/5.76E-17
C1 21 0 1
R5 21 22 3E-9
V4 22 0
X28 23 21 ZENER {ZV=1E4 }
X29 23 24 25 VCNTRLDR
V5 24 0
F2 0 25 V4 0 0.34*0.001
F3 0 25 V5 0 0.34
C2 25 0 1
R6 25 0 2E-12
.END
```

D.4 Laser Diode with Adaptive Pre-distorter Simulation

The adaptive version of the pre-distorter and LD system contains the addition of the second, identical distortion system, a simplified optical output recovery and

signal conversion operation, and the three comparison operations that compute the difference between the distortion systems.

Below is the netlist from the ICAP/4 `AdaptiveVolterraLD.cir` file.

```
AdaptiveVolterraLD
*SPICE_NET
.SUBCKT DIFF 1 2
RIN 1 0 1E30
E1 3 0 0 1 0 {K}
C1 3 4 0.001F IC=0
R1 4 2 1E18
E2 2 0 0 4 1E18
.ENDS
*INCLUDE SYS.LIB
.SUBCKT VCNTRLDR 1 2 3
R1 1 2 1E32
G1 1 2 POLY(2) 1 2 3 0
+ 0 0 0 0 3E8 0 0 0 -9E5
.ENDS
.SUBCKT ZENER 1 2
D1 1 2 DZEN
.MODEL DZEN D(CJO=1E-30 IS=1E-30 TT=1E-30
+ BV={ZV} IBV=1E30 N=2 RS=0)
.ENDS
.TRAN 0.5P 12N 10N 0.1P UIC
;INIT CONS FOR 500UA BIAS FOLLOWS
.IC V(21)=14936.179V V(23)=4933.69V V(25)=2.521084V
;.INIT CONS FOR 0.5MA BIAS & 0.02 AGING FOLLOWS
;.IC V(21)=15140.7V V(23)=5139.21V V(25)=2.521V
.OPTION RELTOL=0.0001
.OPTION METHOD=GEAR
.FOUR 1000MEGHZ V(25)
.PRINT TRAN V(25) I(V2) I(V1)
*ALIAS I(V1)="i"
*ALIAS V(25)="S"
I5 0 1 SIN 0 8.8U 1000MEG 0N
V1 1 0
H1 2 0 V1 0 1
X1 2 4 5 SQ-CUBE {K1=-2.7476 K2=13292 }
X3 6 7 8 15 SUM3 {K1=1 K2=1 K3=1 }
X4 9 10 11 12 SUM3 {K1=1 K2=1 K3=1 }
X5 12 13 14 17 SUM3 {K1=1 K2=1 K3=1 }
```

```
X6 15 16 17 18 SUM3 {K1=1 K2=1 K3=1 }
X19 6 7 DIFF {K=1.475067E-11 }
X21 7 8 DIFF {K=1.798268E-10 }
X22 9 10 DIFF {K=3.783892E-9 }
X24 10 11 DIFF {K=6.197352E-10 }
X25 12 13 DIFF {K=3.500684E-9 }
X27 13 14 DIFF {K=4.269273E-10 }
E1 3 0 2 0 0 1.00025
V3 20 0
G1 0 19 18 0 0 2.521084/2.51746
V2 19 20
I4 0 20 PULSE 0 500U 0N
F1 0 21 V3 0 1/5.76E-17
C1 21 0 1
V4 22 0
R5 21 22 3E-9
X28 23 21 ZENER {ZV=1E4 }
X29 23 24 25 VCNTRLDR
V5 24 0
F2 0 25 V4 0 0.34*0.001
F3 0 25 V5 0 0.34
C2 25 0 1
R6 25 0 2E-12
B1 26 0 V=(V(25)-2.521084)/11761
E3 27 0 26 0 0 1.00025
X30 26 28 29 SQ-CUBE {K1=-2.7476 K2=13292 }
B2 6 0 V=V(3)*V(45)
B4 9 0 V=V(4)*V(46)
B5 12 0 V=V(5)*V(47)
B6 30 0 V=V(27)*V(45)
B7 33 0 V=V(28)*V(46)
B8 36 0 V=V(37)*V(47)
X31 30 31 DIFF {K=1.475067E-11 }
X32 31 32 DIFF {K=1.798268E-10 }
X33 33 34 DIFF {K=3.783892E-9 }
X34 34 35 DIFF {K=6.197352E-10 }
X35 36 37 DIFF {K=3.500684E-9 }
X36 37 38 DIFF {K=4.269273E-10 }
X37 30 31 32 39 SUM3 {K1=1 K2=1 K3=1 }
X38 33 34 35 40 SUM3 {K1=1 K2=1 K3=1 }
X39 36 37 38 41 SUM3 {K1=1 K2=1 K3=1 }
B9 42 0 V=1*(V(39)-V(15))
```

```
B10 43 0 V=1*(V(40)-V(16))
B11 44 0 V=1*(V(41)-V(17))
V6 45 0 1
V7 46 0 1
V8 47 0 1
.END
```